Pedeciba - Universidad de la República

Tesis de Maestría

Coding of Multichannel Signals with Irregular Sampling Rates and Data Gaps (Appendix)

Autor:
Pablo Cerveñansky

Supervisores:
Álvaro Martín
Gadiel Seroussi

Núcleo de Teoría de la Información
Facultad de Ingeniería

Introduction

This document includes each plot figure generated from the experimental results obtained in our work. In **Appendix A** we present the figures corresponding to Section 4.2 (Comparison of Masking and Non-Masking Variants). In **Appendix B** we present the figures corresponding to Section 4.3 (Window Size Parameter). Finally, in **Appendix C** we present the figures corresponding to Section 4.4 (Algorithm Compression Performance).

Table of Contents

List of Figures

Appendix A

Figures: Comparison of Masking and Non-Masking Variants

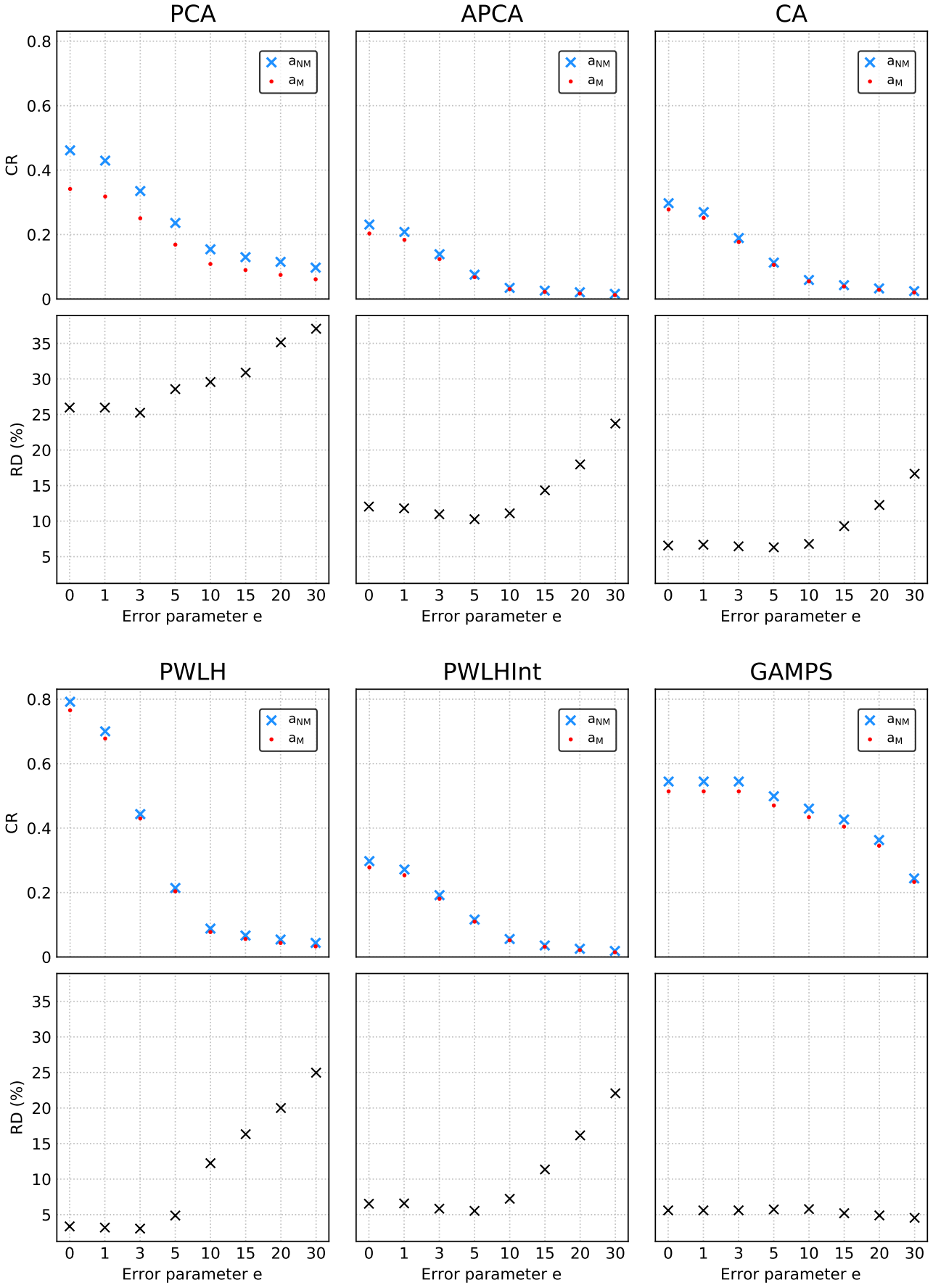

FIGURE A.1: CR and RD plots for variants a_M and a_{NM}, for each algorithm $a \in A_M$, for the data type "VWC" of the dataset IRKIS.

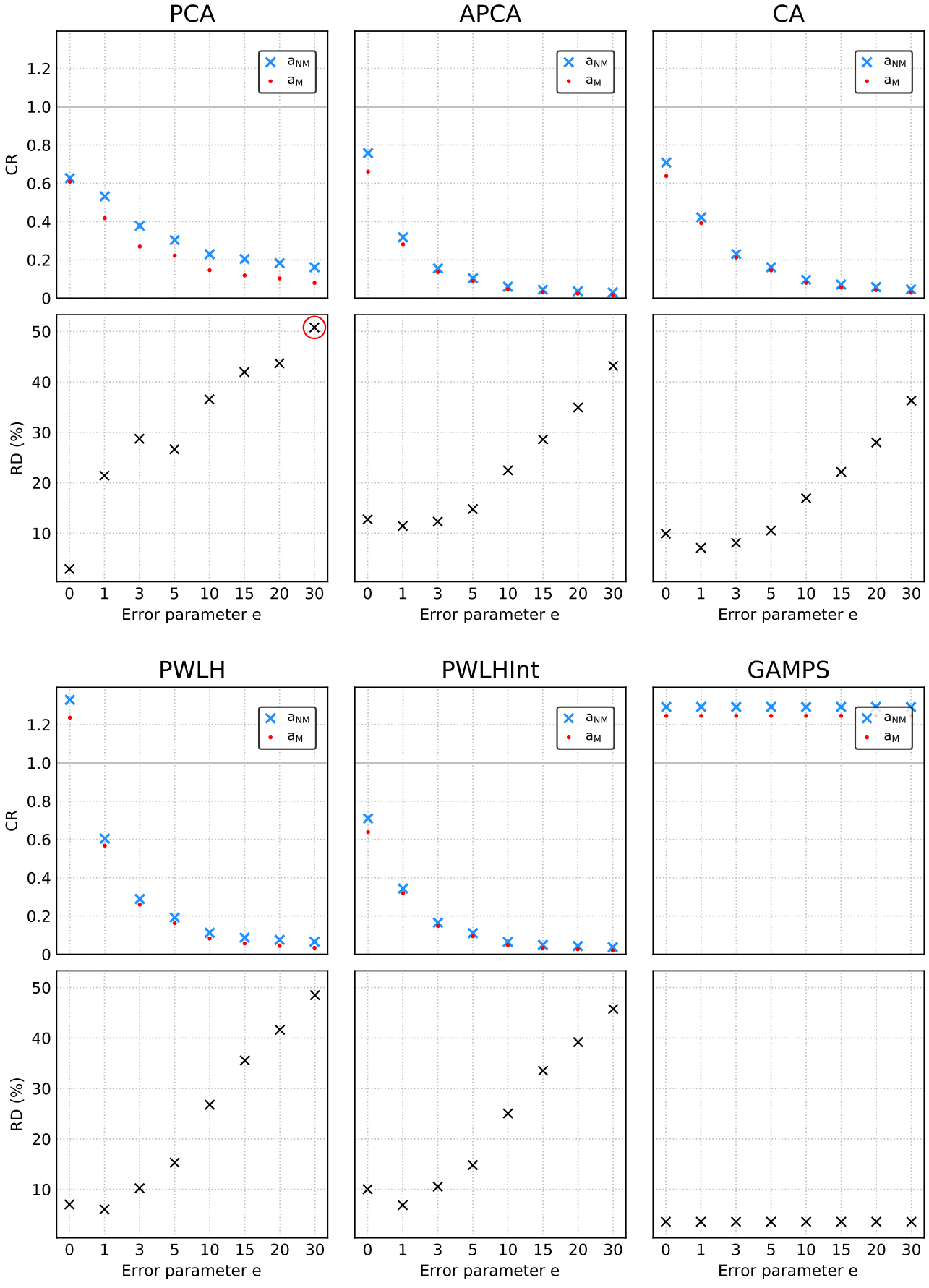

FIGURE A.2: CR and RD plots for variants a_M and a_{NM}, for each algorithm $a \in A_M$, for the data type "SST" of the dataset SST. In the RD plot for algorithm PCA we highlight with a red circle the marker for the maximum value (50.78%) obtained for all the tested CAIs.

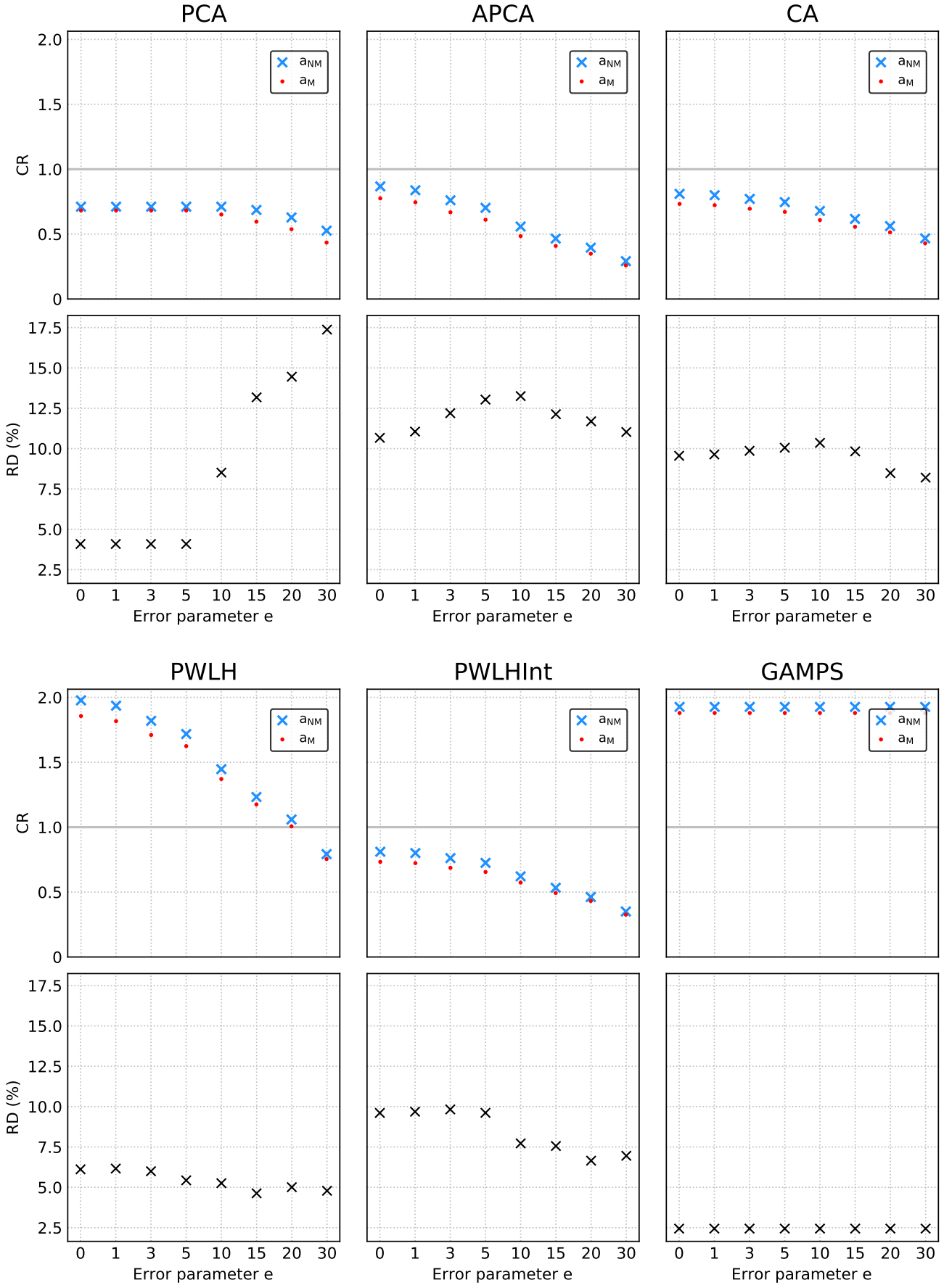

FIGURE A.3: CR and RD plots for variants a_M and a_{NM}, for each algorithm $a \in A_M$, for the data type "Velocity" of the dataset ADCP.

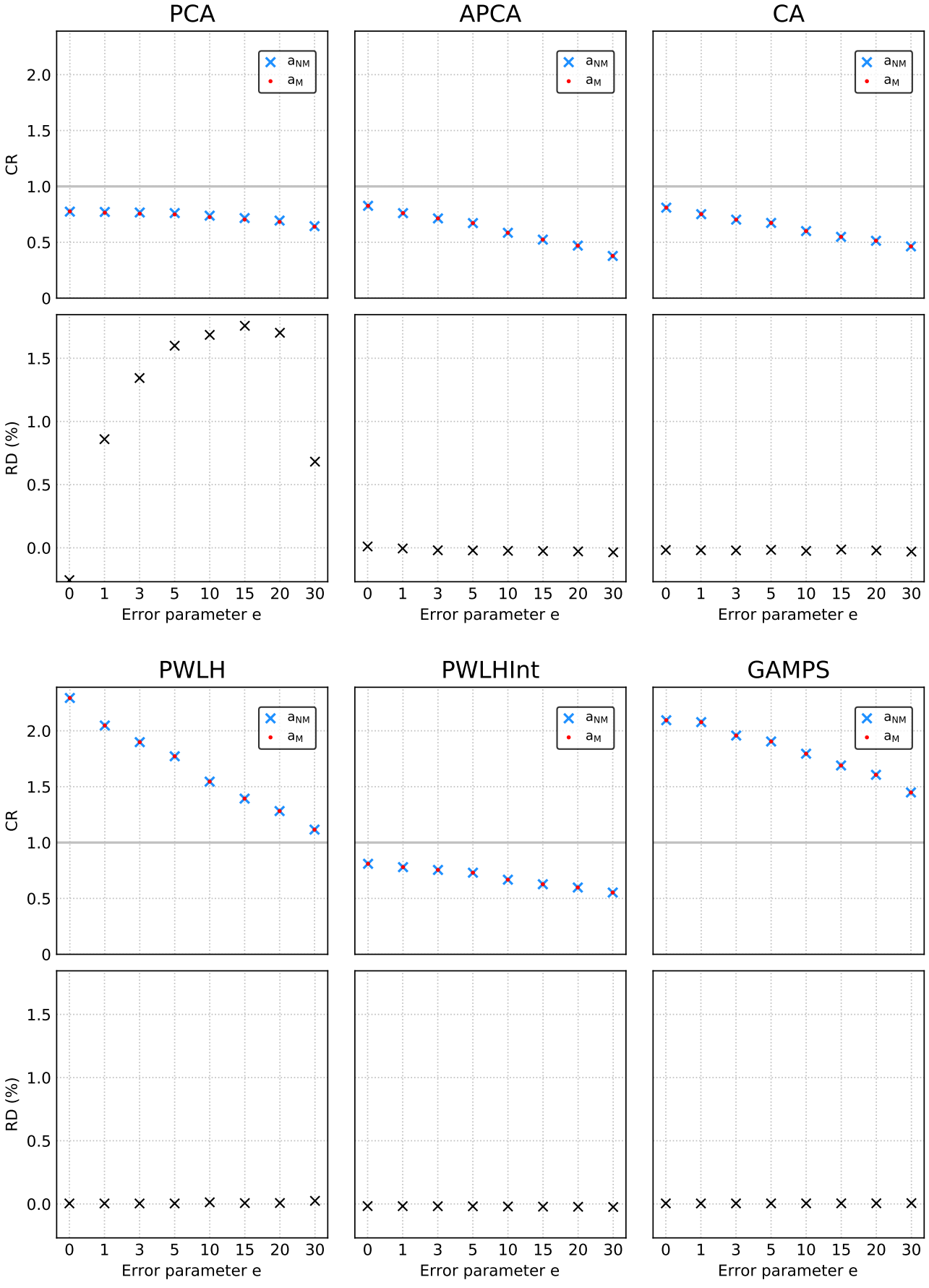

FIGURE A.4: CR and RD plots for variants a_M and a_{NM}, for each algorithm $a \in A_M$, for the data type "GHI" of the dataset Solar.

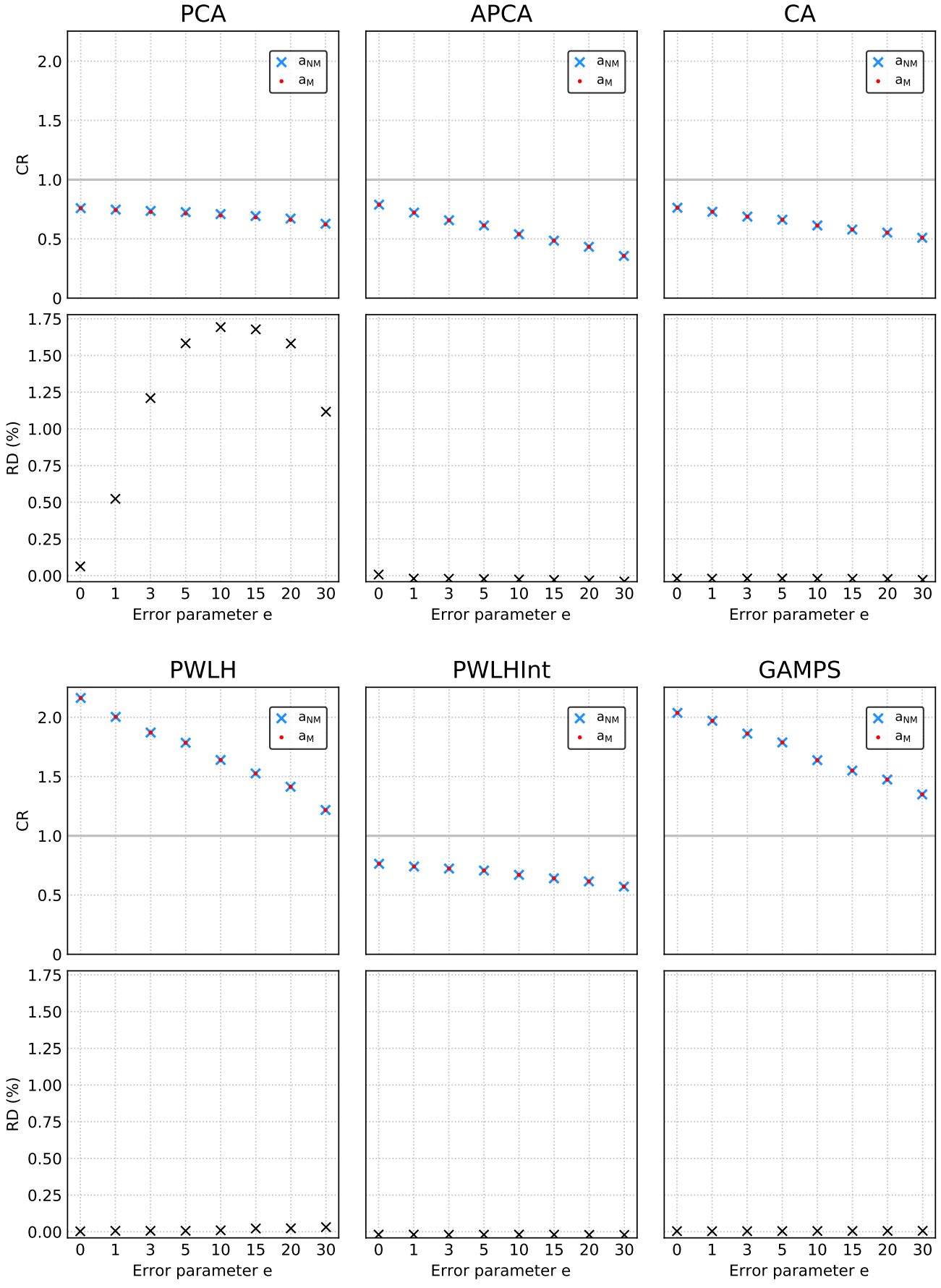

FIGURE A.5: CR and RD plots for variants a_M and a_{NM}, for each algorithm $a \in A_M$, for the data type "DNI" of the dataset Solar.

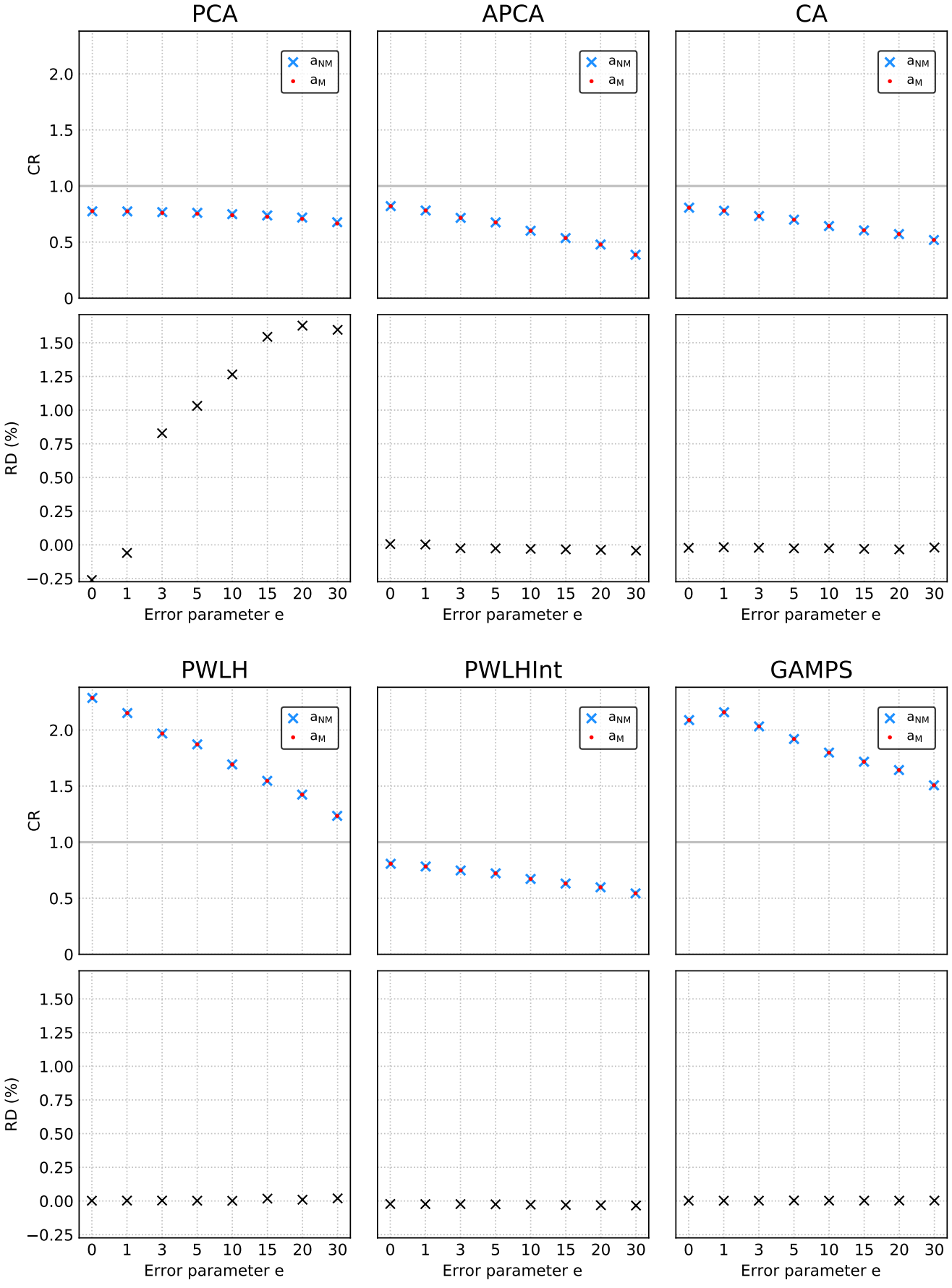

FIGURE A.6: CR and RD plots for variants a_M and a_{NM}, for each algorithm $a \in A_M$, for the data type "DHI" of the dataset Solar.

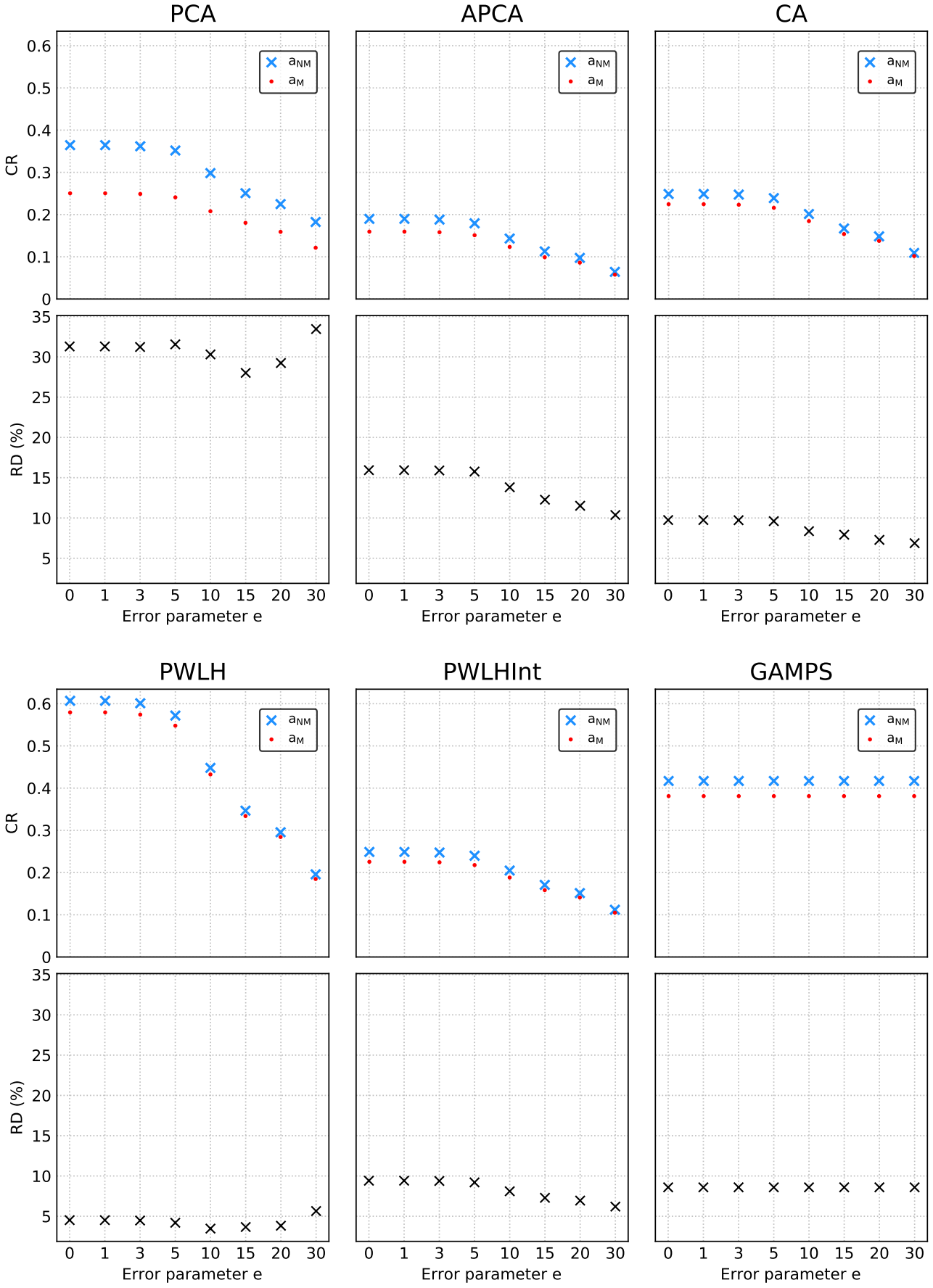

FIGURE A.7: CR and RD plots for variants a_M and a_{NM}, for each algorithm $a \in A_M$, for the data type "Latitude" of the dataset ElNino.

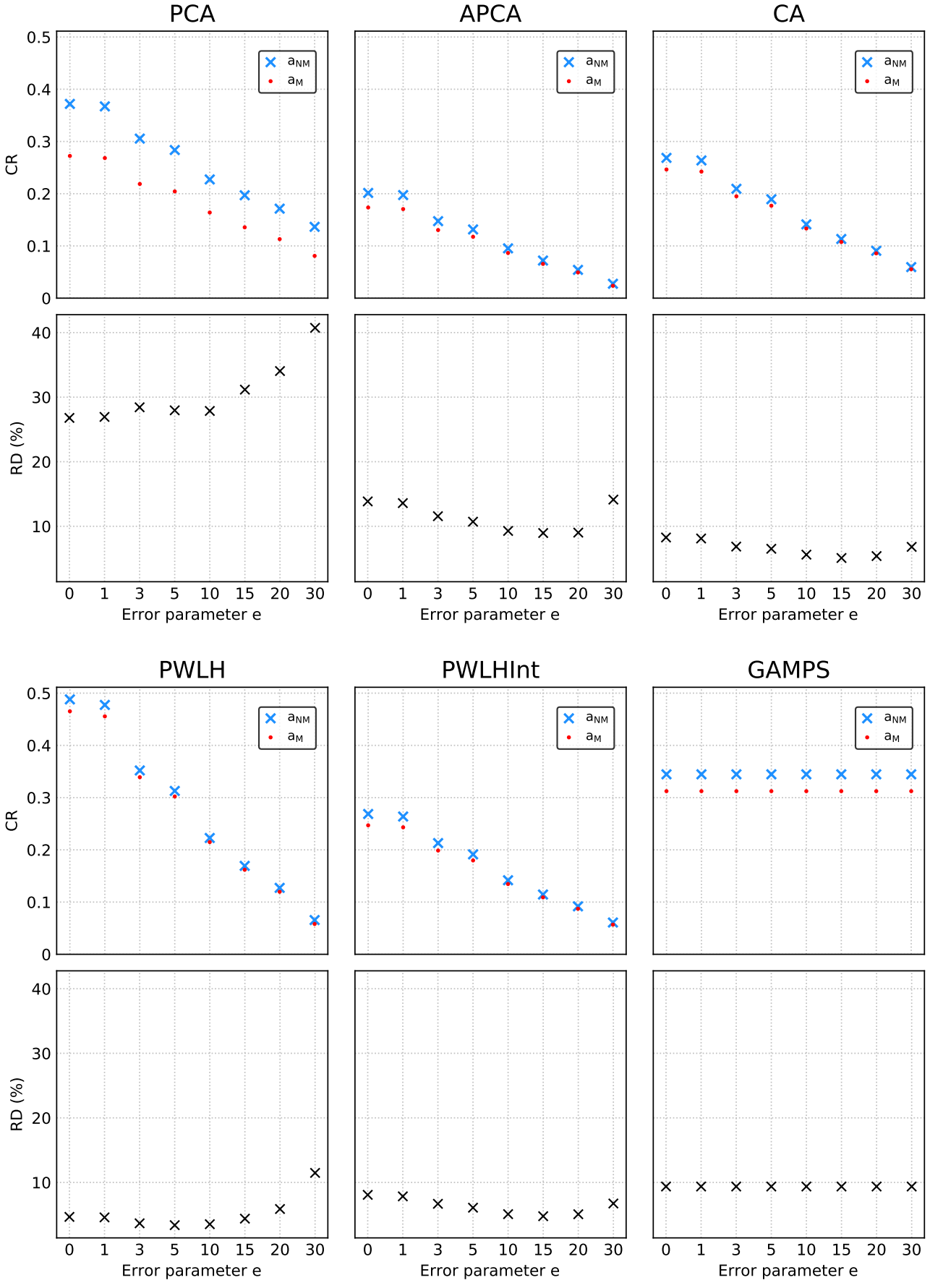

FIGURE A.8: CR and RD plots for variants a_M and a_{NM}, for each algorithm $a \in A_M$, for the data type "Longitude" of the dataset ElNino.

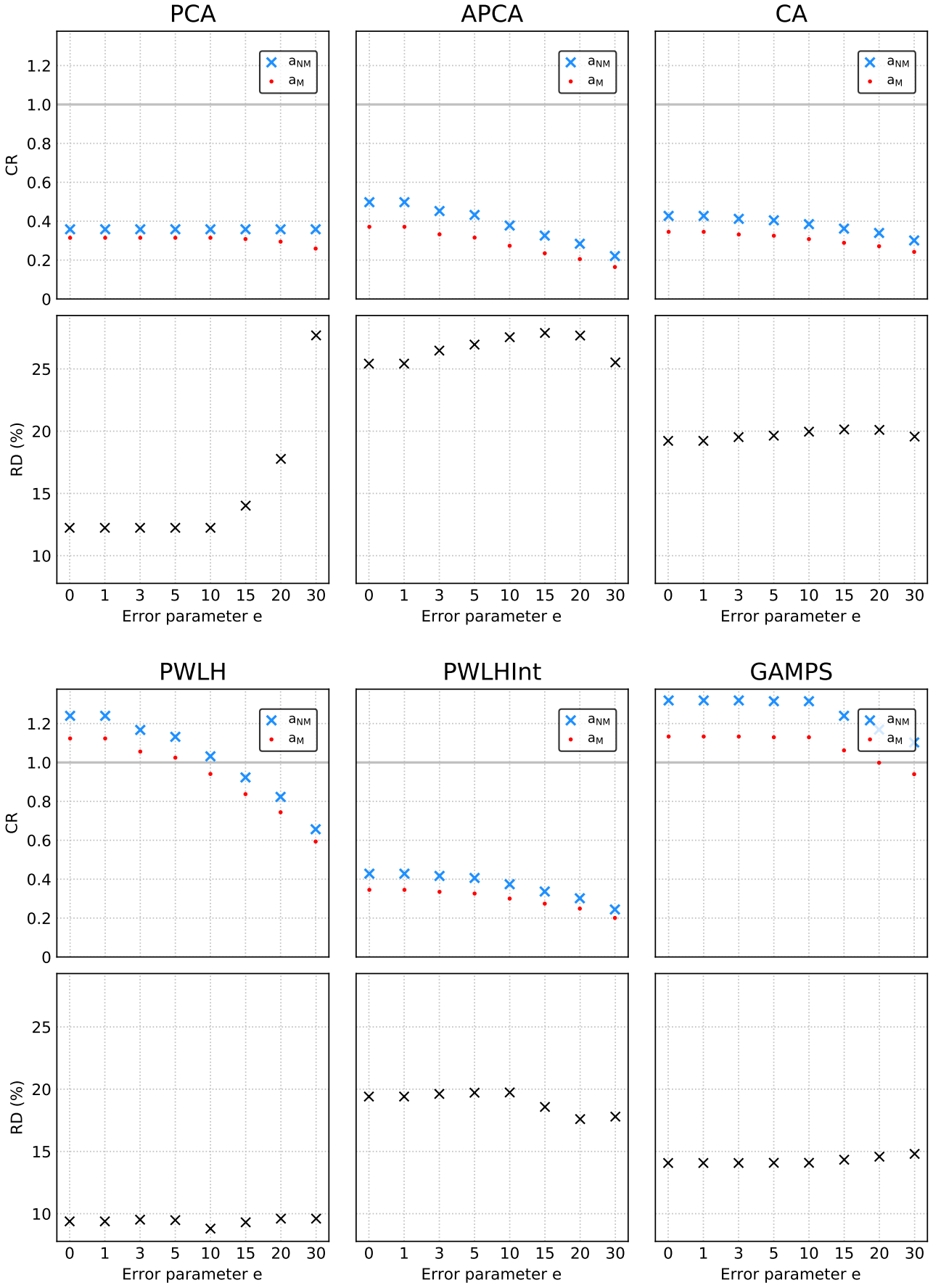

FIGURE A.9: CR and RD plots for variants a_M and a_{NM}, for each algorithm $a \in A_M$, for the data type "Zon. Wind" of the dataset ElNino.

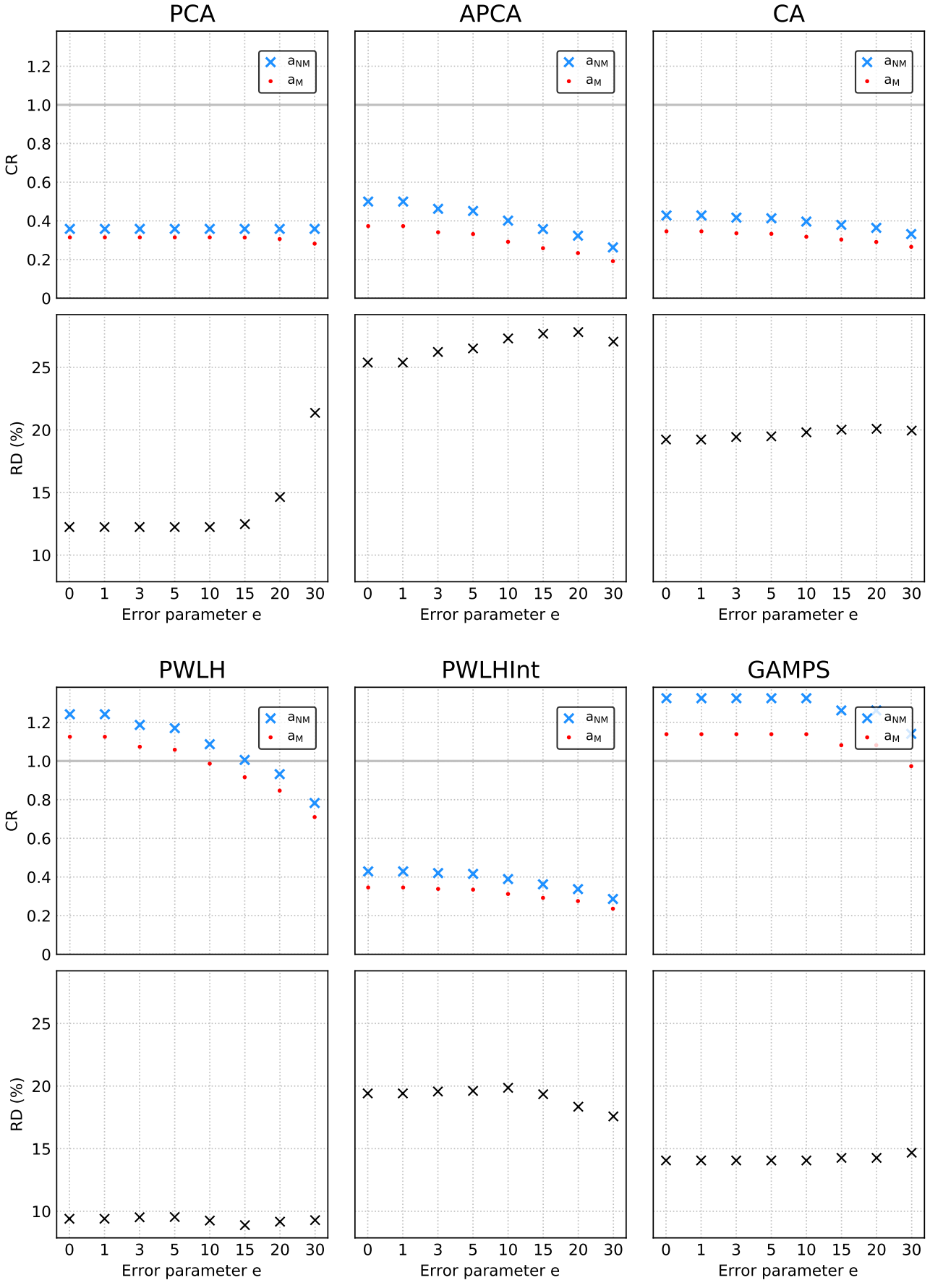

FIGURE A.10: CR and RD plots for variants a_M and a_{NM}, for each algorithm $a \in A_M$, for the data type "Mer. Wind" of the dataset ElNino.

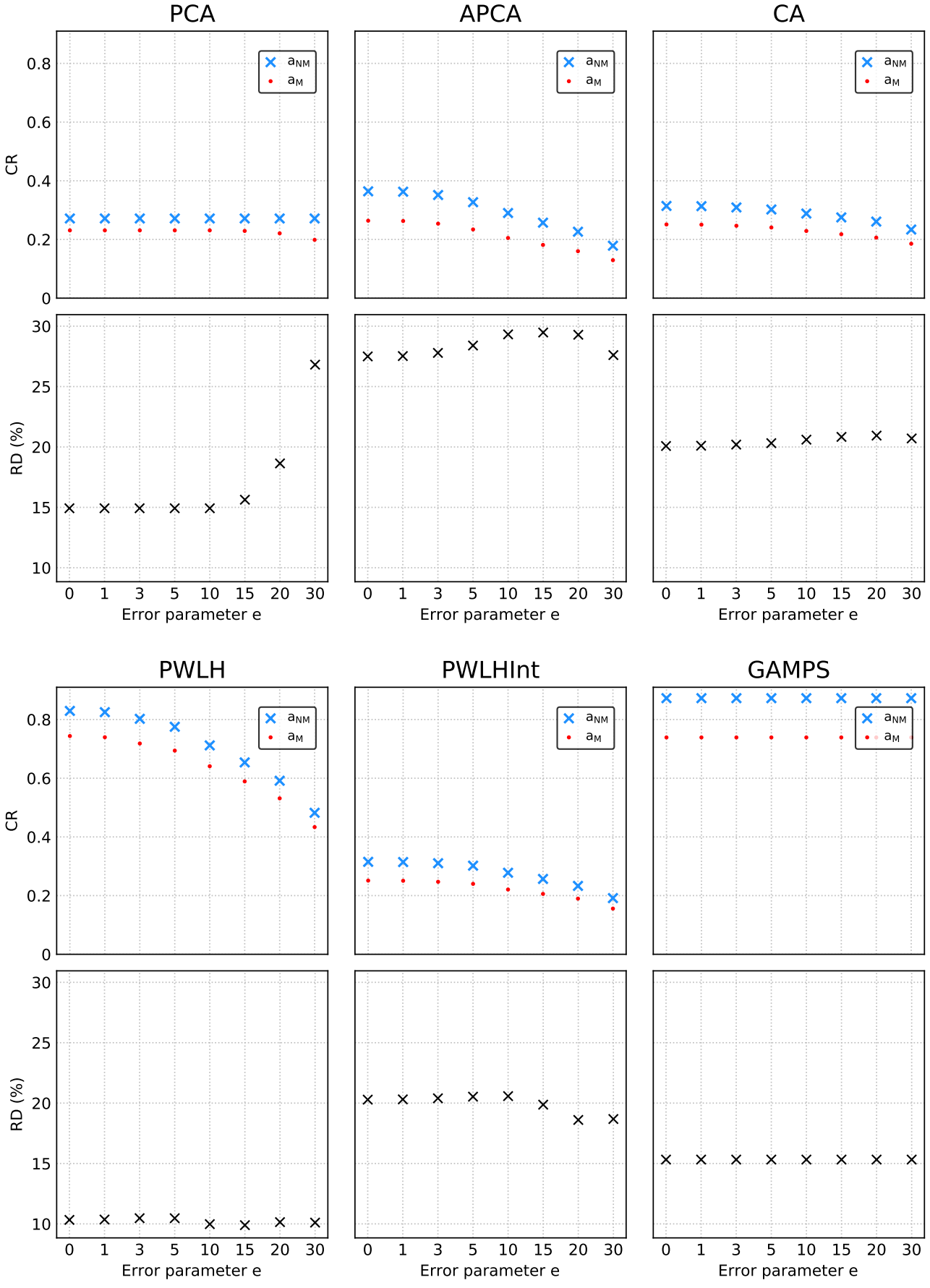

FIGURE A.11: CR and RD plots for variants a_M and a_{NM}, for each algorithm $a \in A_M$, for the data type "Humidity" of the dataset ElNino.

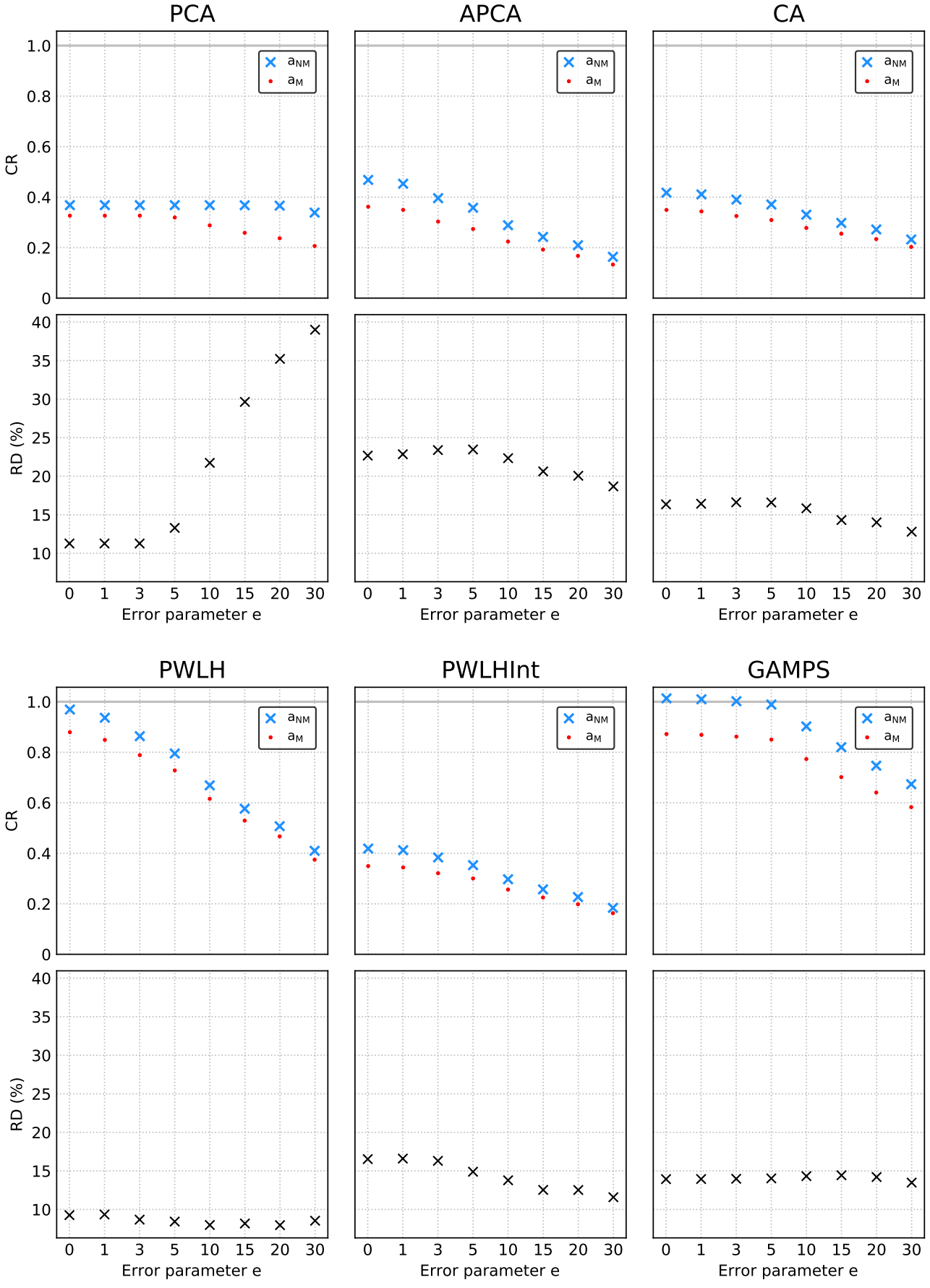

FIGURE A.12: CR and RD plots for variants a_M and a_{NM}, for each algorithm $a \in A_M$, for the data type "Air Temp." of the dataset ElNino.

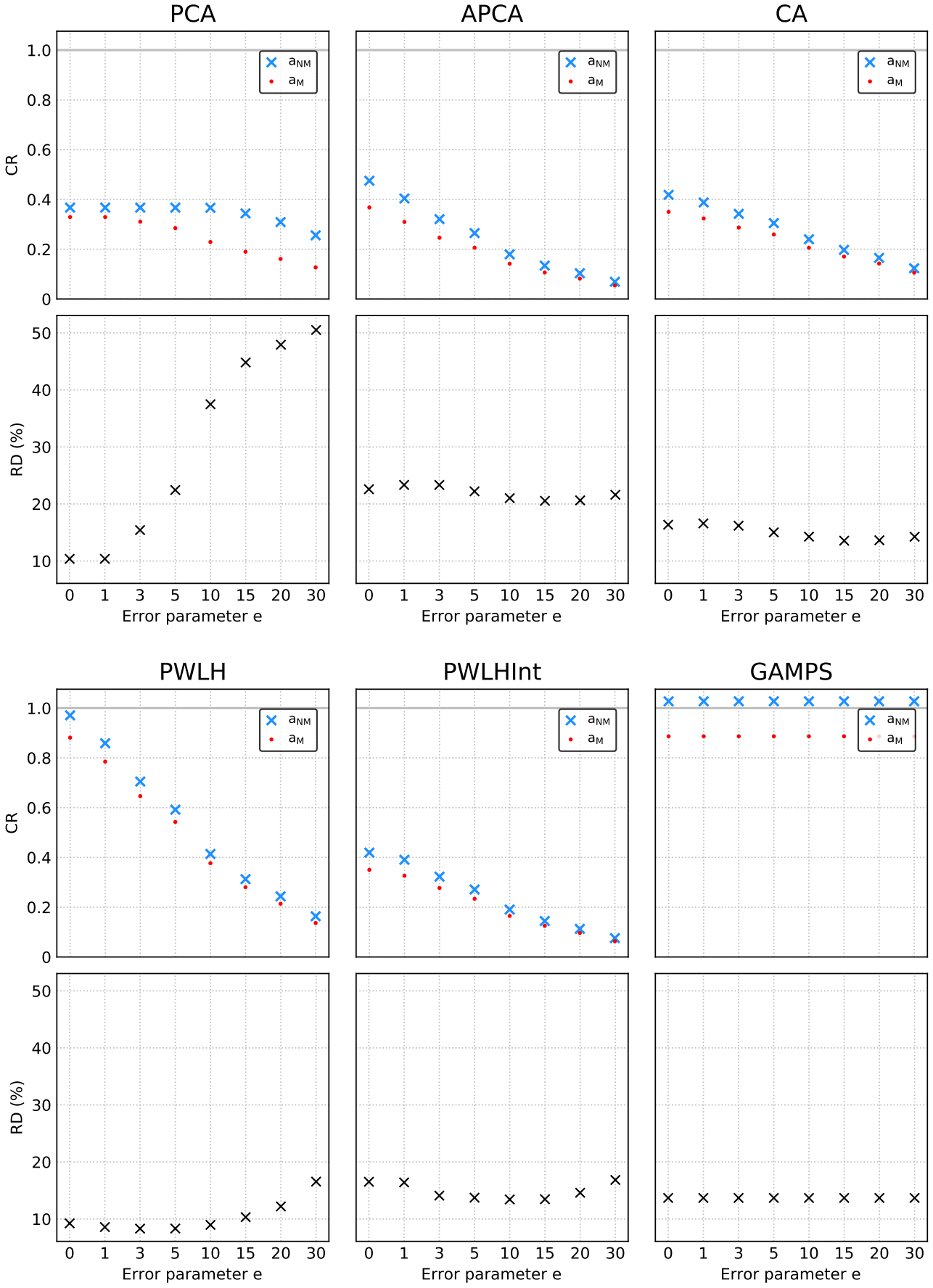

FIGURE A.13: CR and RD plots for variants a_M and a_{NM}, for each algorithm $a \in A_M$, for the data type "Sea Temp." of the dataset ElNino.

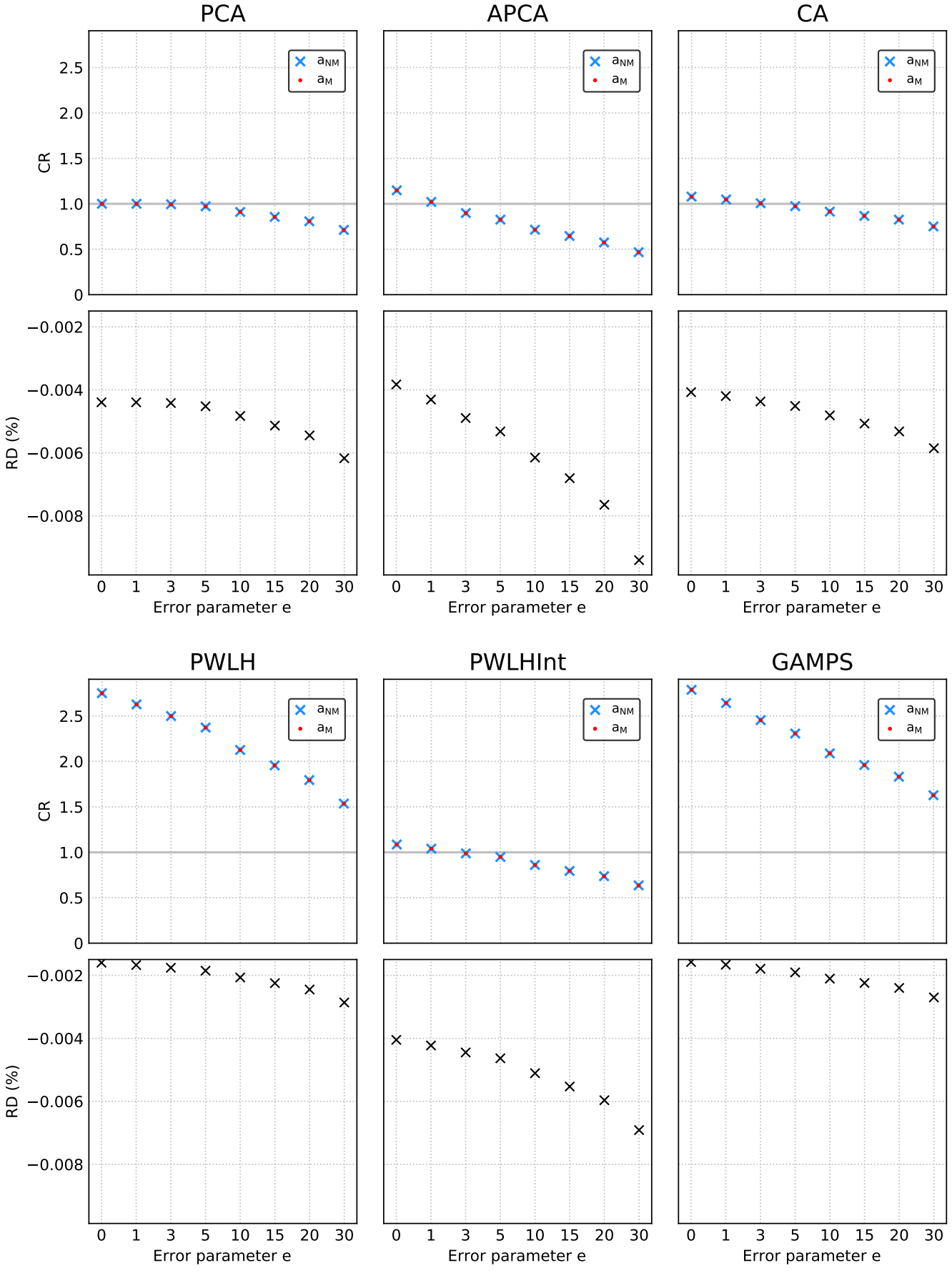

FIGURE A.14: CR and RD plots for variants a_M and a_{NM}, for each algorithm $a \in A_M$, for the data type "Latitude" of the dataset Hail.

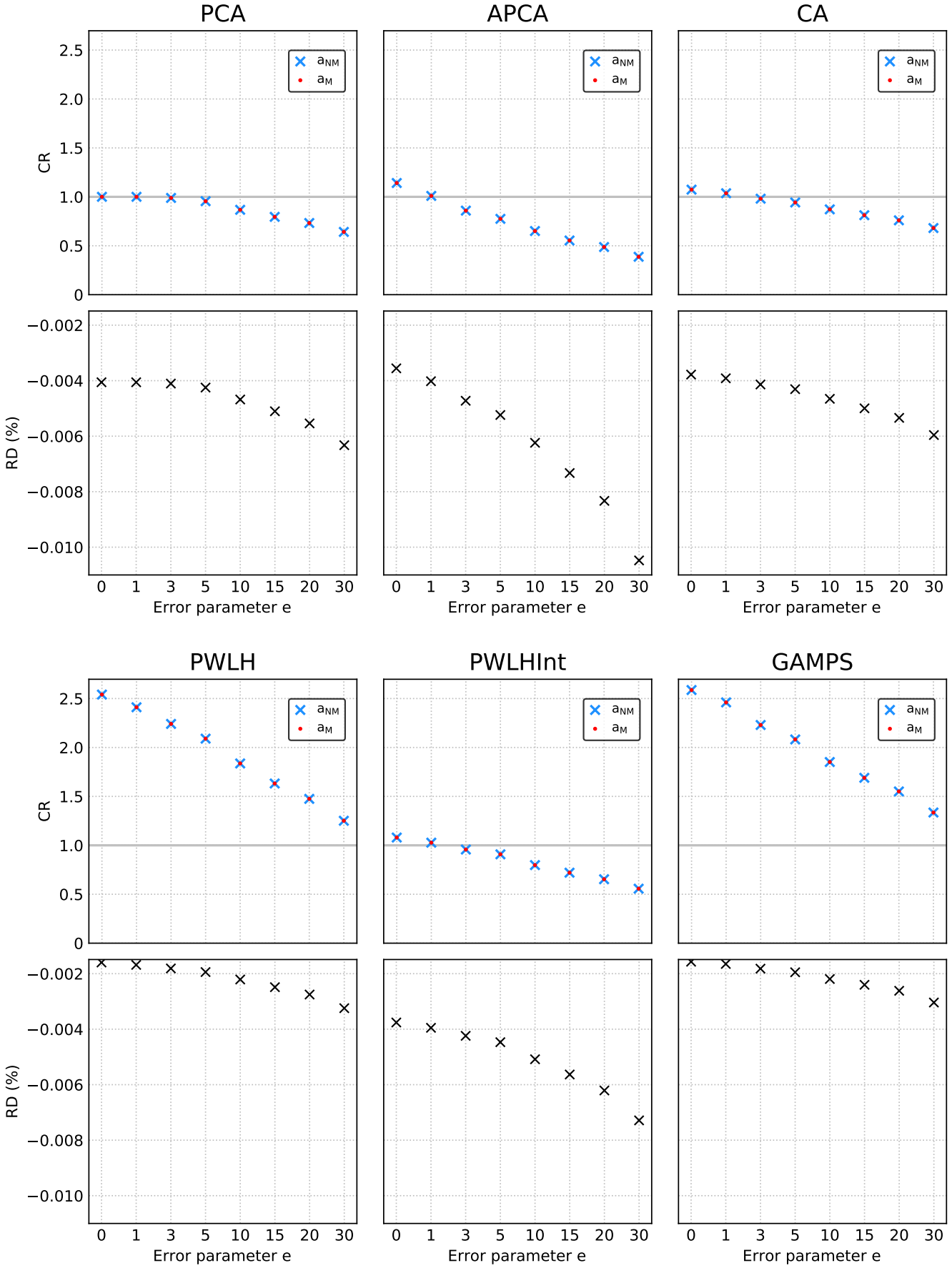

FIGURE A.15: CR and RD plots for variants a_M and a_{NM}, for each algorithm $a \in A_M$, for the data type "Longitude" of the dataset Hail.

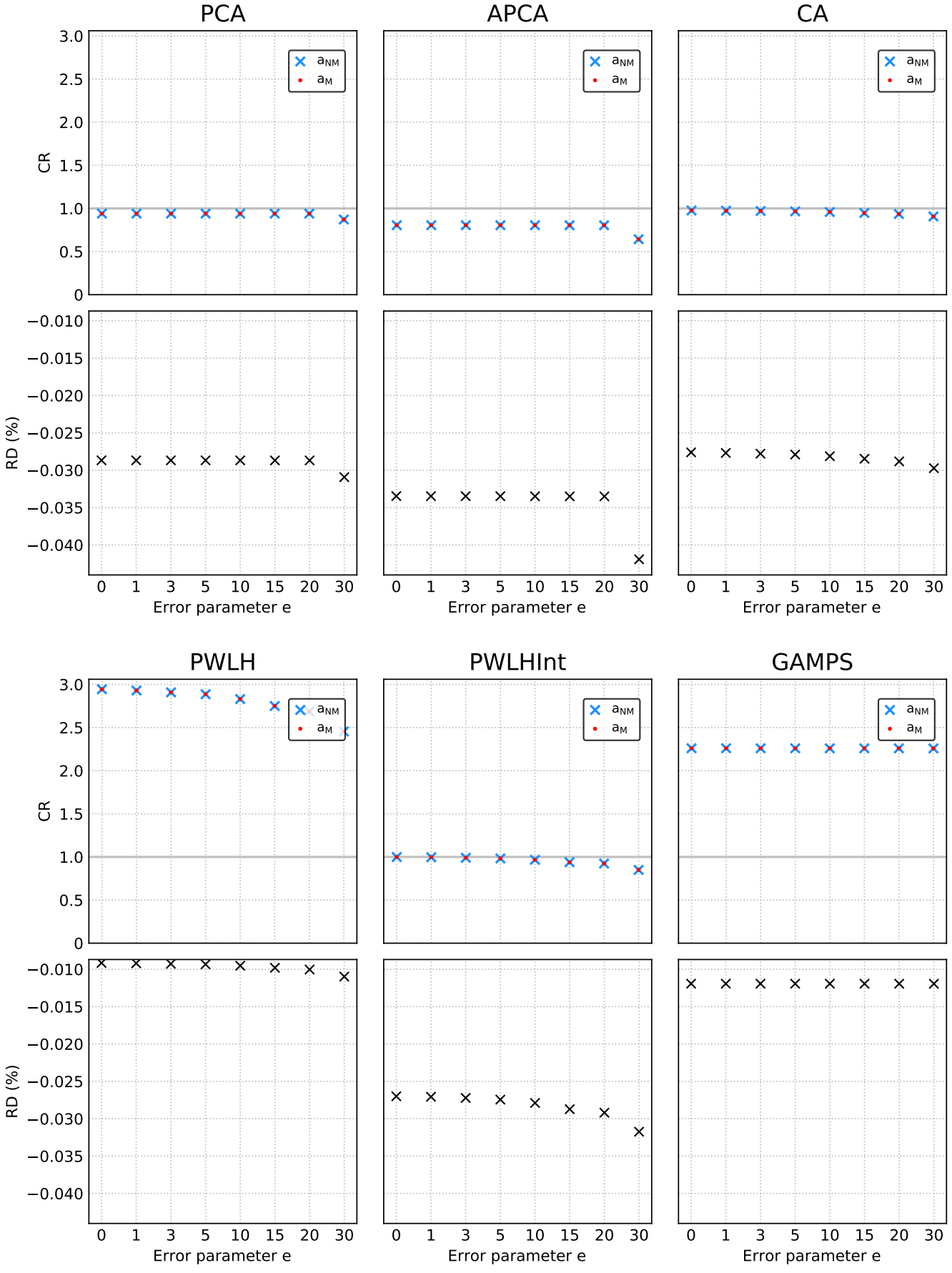

FIGURE A.16: CR and RD plots for variants a_M and a_{NM}, for each algorithm $a \in A_M$, for the data type "Size" of the dataset Hail.

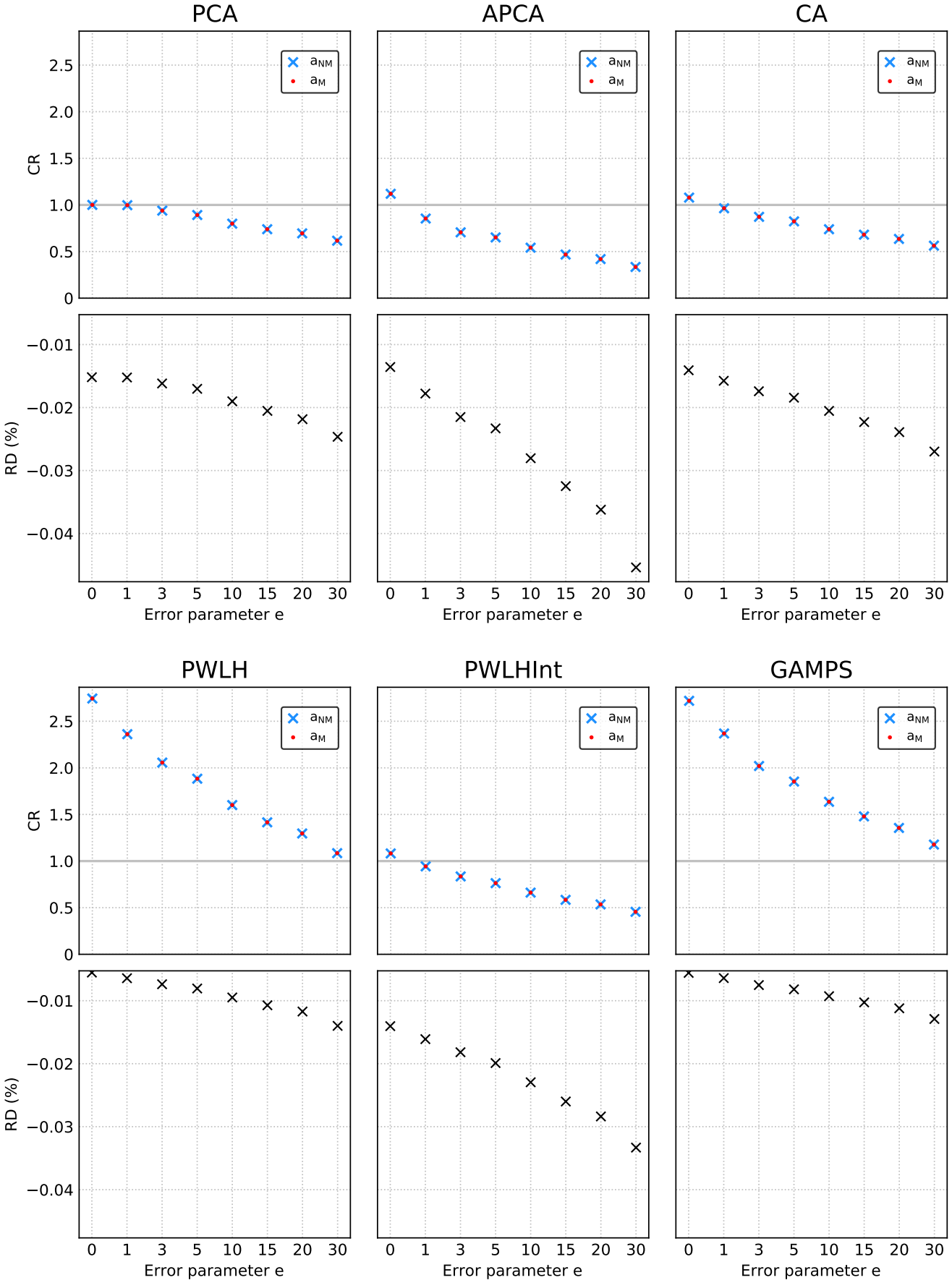

FIGURE A.17: CR and RD plots for variants a_M and a_{NM}, for each algorithm $a \in A_M$, for the data type "Latitude" of the dataset Tornado.

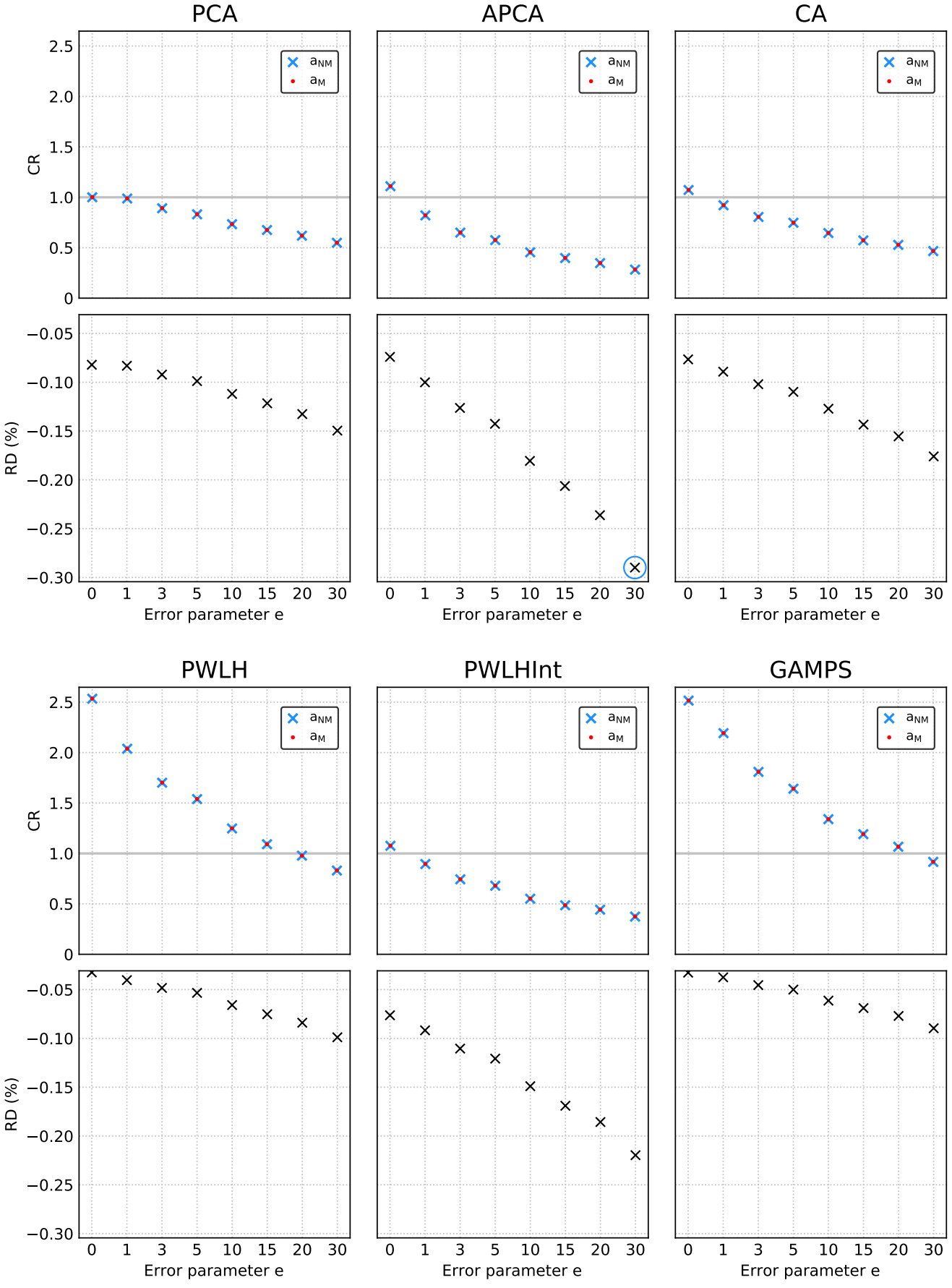

FIGURE A.18: CR and RD plots for variants a_M and a_{NM}, for each algorithm $a \in A_M$, for the data type "Longitude" of the dataset Tornado. In the RD plot for algorithm APCA we highlight with a blue circle the marker for the minimum value (-0.29%) obtained for all the tested CAIs.

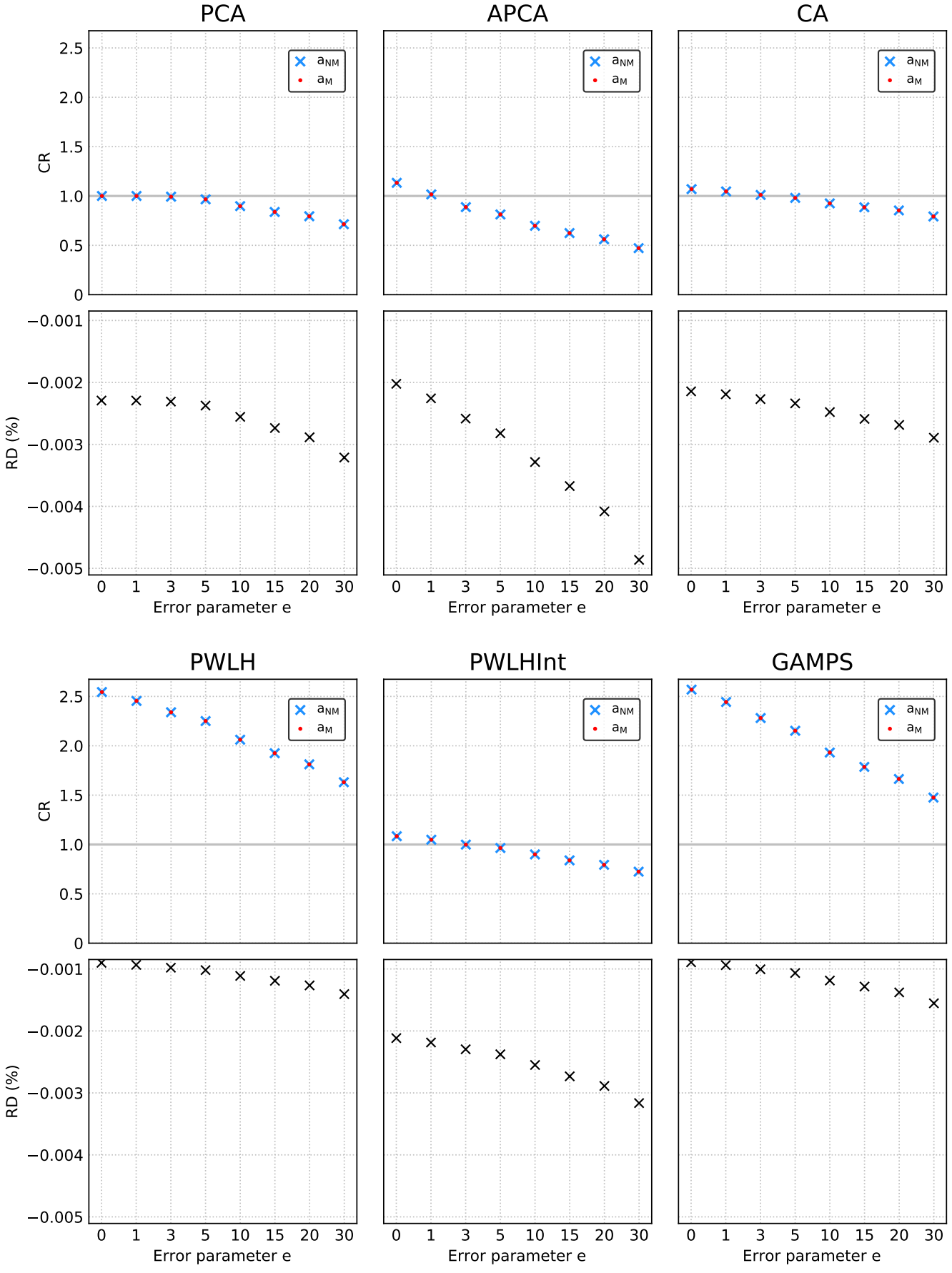

FIGURE A.19: CR and RD plots for variants a_M and a_{NM}, for each algorithm $a \in A_M$, for the data type "Latitude" of the dataset Wind.

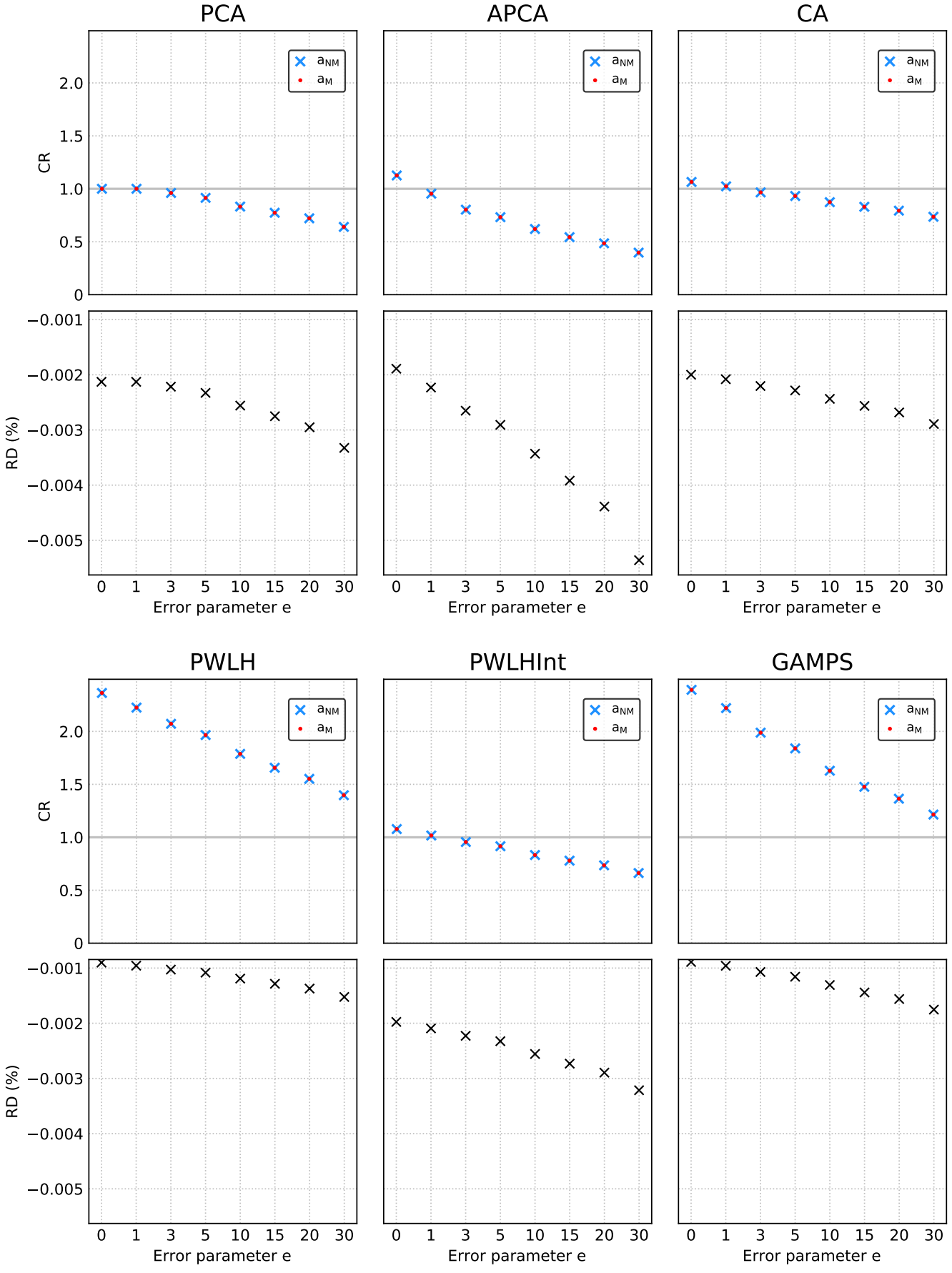

FIGURE A.20: CR and RD plots for variants a_M and a_{NM}, for each algorithm $a \in A_M$, for the data type "Longitude" of the dataset Wind.

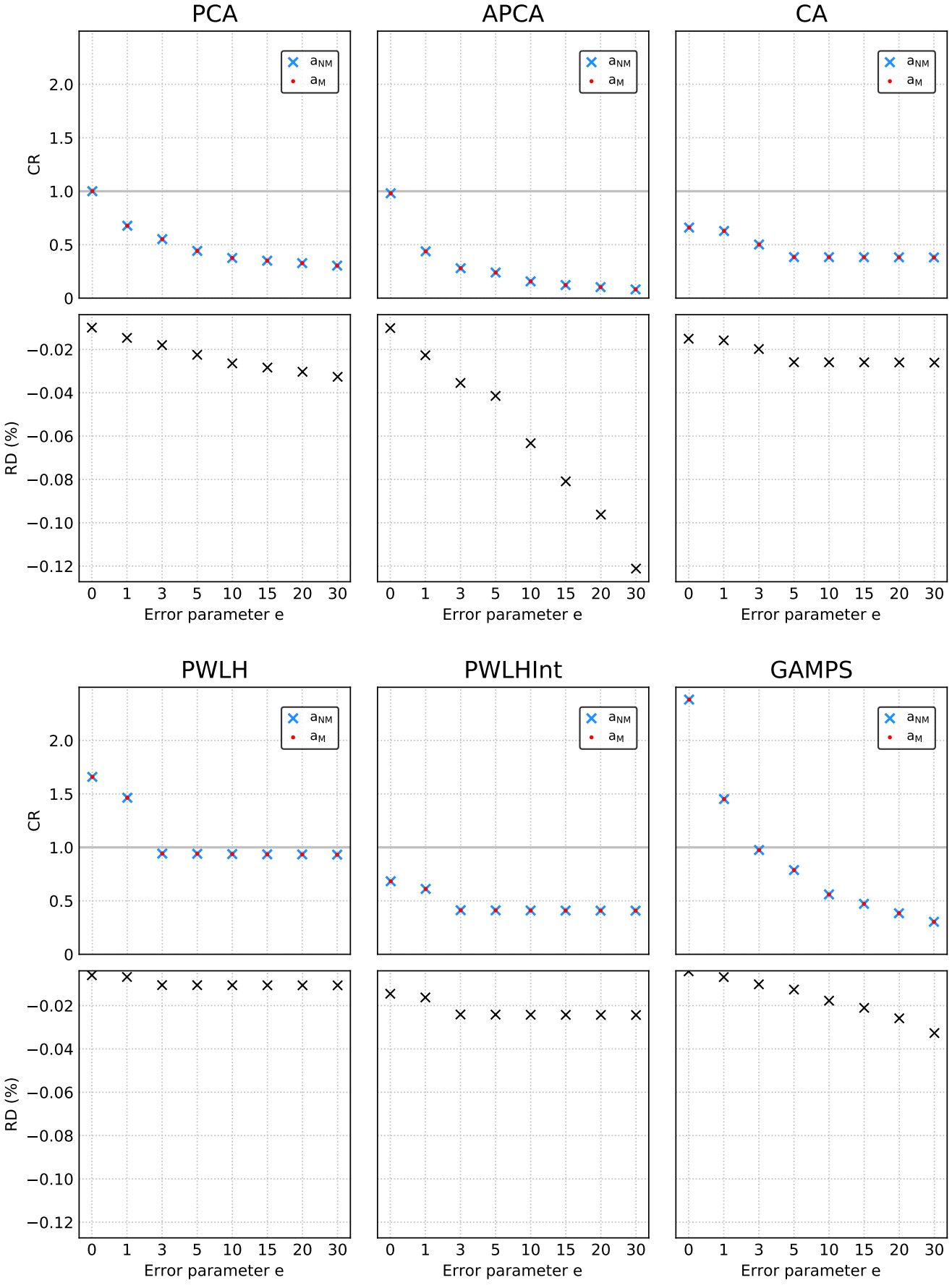

FIGURE A.21: CR and RD plots for variants a_M and a_{NM}, for each algorithm $a \in A_M$, for the data type "Speed" of the dataset Wind.

Appendix B

Figures: Window Size Parameter

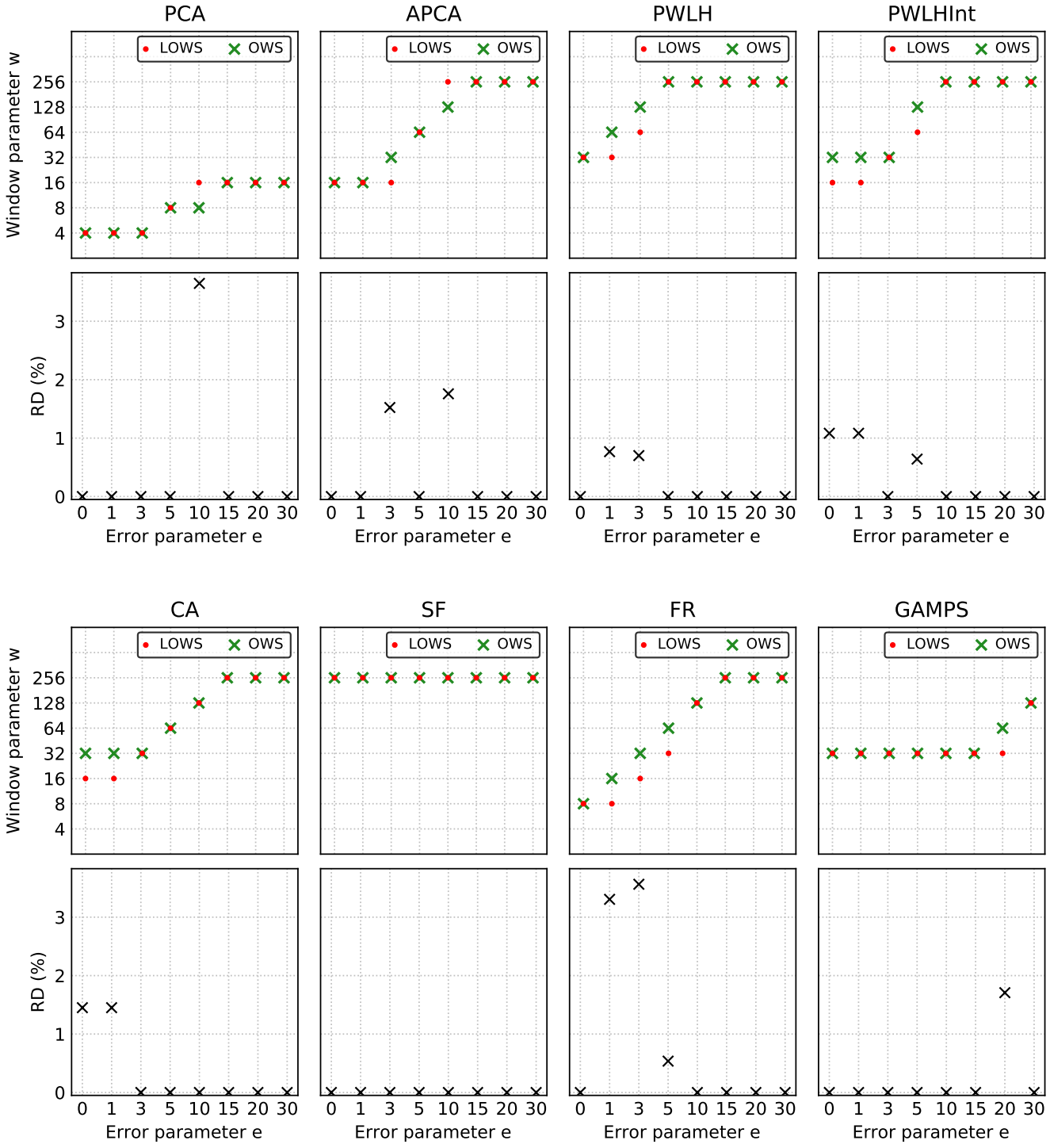

FIGURE B.1: Plots of w^*_{global}, w^*_{local}, and the RD between $c_{<a_v,w^*_{global},e>}$ and $c_{<a_v,w^*_{local},e>}$, as a function of the error parameter e, obtained for the data type "VWC" of the file "irkis-1202.csv" of the dataset IRKIS.

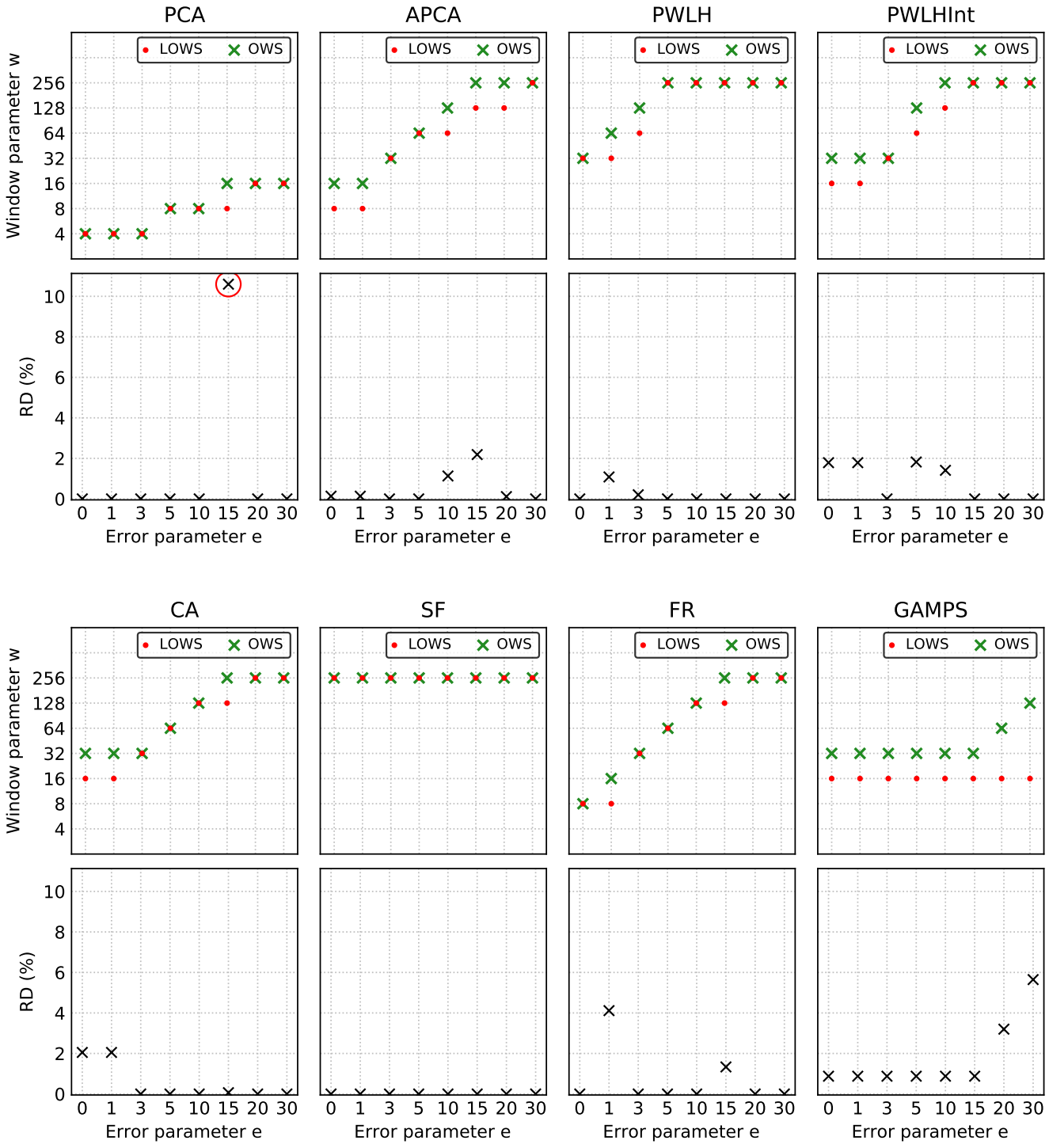

FIGURE B.2: Plots of w^*_{global}, w^*_{local}, and the RD between $c_{<a_v,w^*_{global},e>}$ and $c_{<a_v,w^*_{local},e>}$, as a function of the error parameter e, obtained for the data type "VWC" of the file "irkis-1203.csv" of the dataset IRKIS. In the RD plot for variant PCA_M we highlight with a red circle the marker for the maximum value (10.6%) obtained for all the tested CAIs.

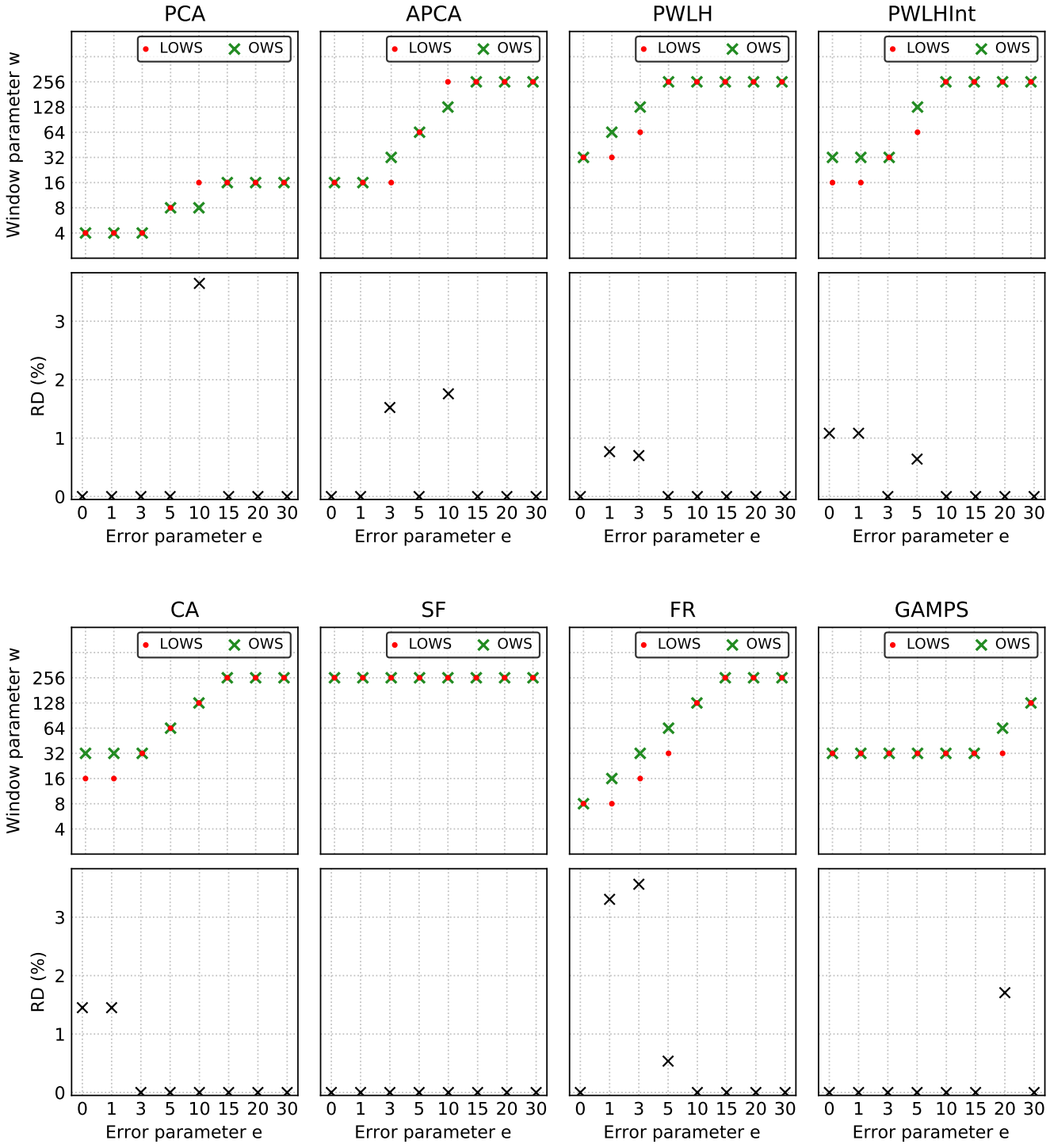

FIGURE B.3: Plots of w^*_{global}, w^*_{local}, and the RD between $c_{<a_v,w^*_{global},e>}$ and $c_{<a_v,w^*_{local},e>}$, as a function of the error parameter e, obtained for the data type "VWC" of the file "irkis-1204.csv" of the dataset IRKIS.

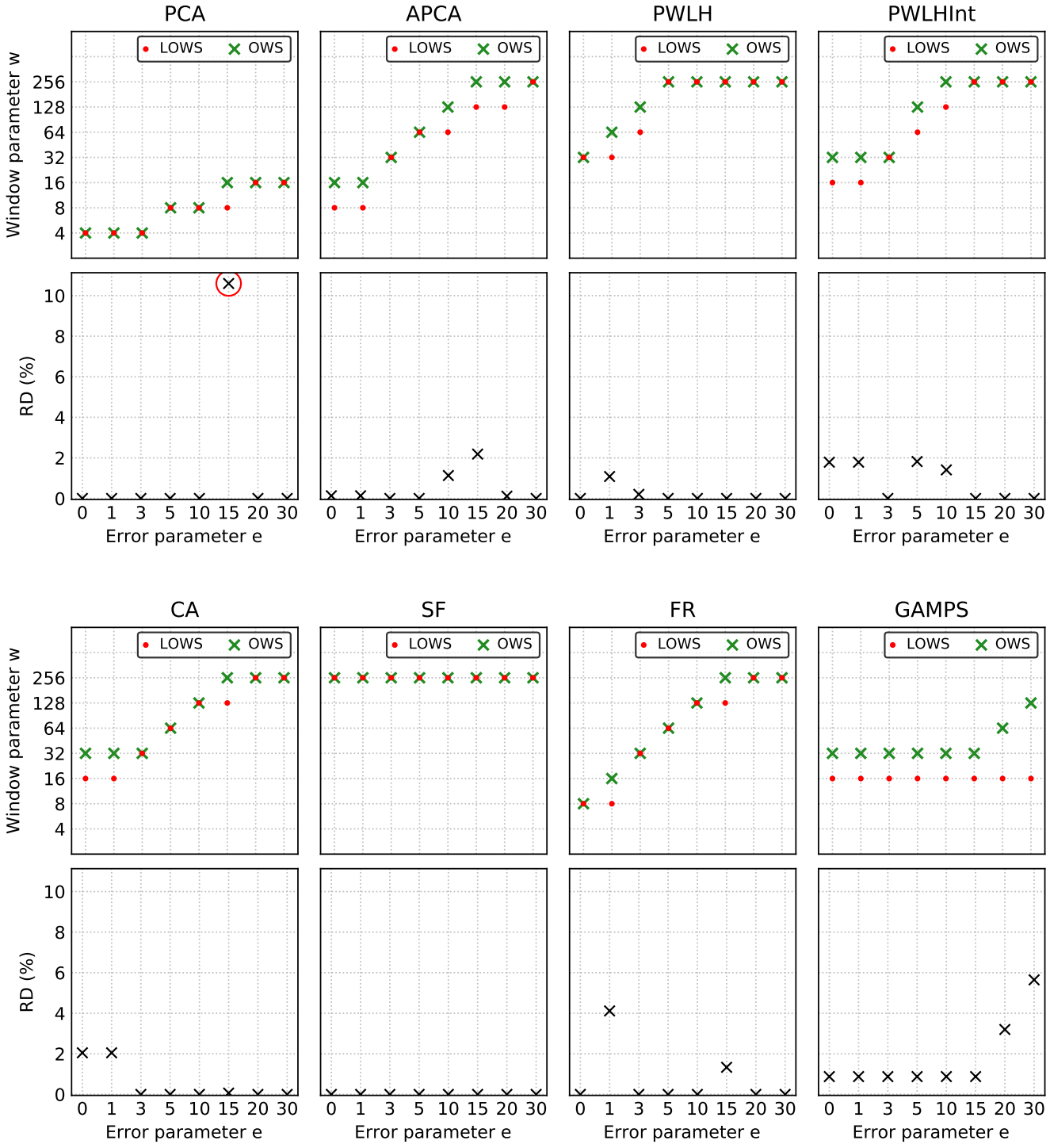

FIGURE B.4: Plots of w^*_{global}, w^*_{local}, and the RD between $c_{<a_v,w^*_{global},e>}$ and $c_{<a_v,w^*_{local},e>}$, as a function of the error parameter e, obtained for the data type "VWC" of the file "irkis-1205.csv" of the dataset IRKIS.

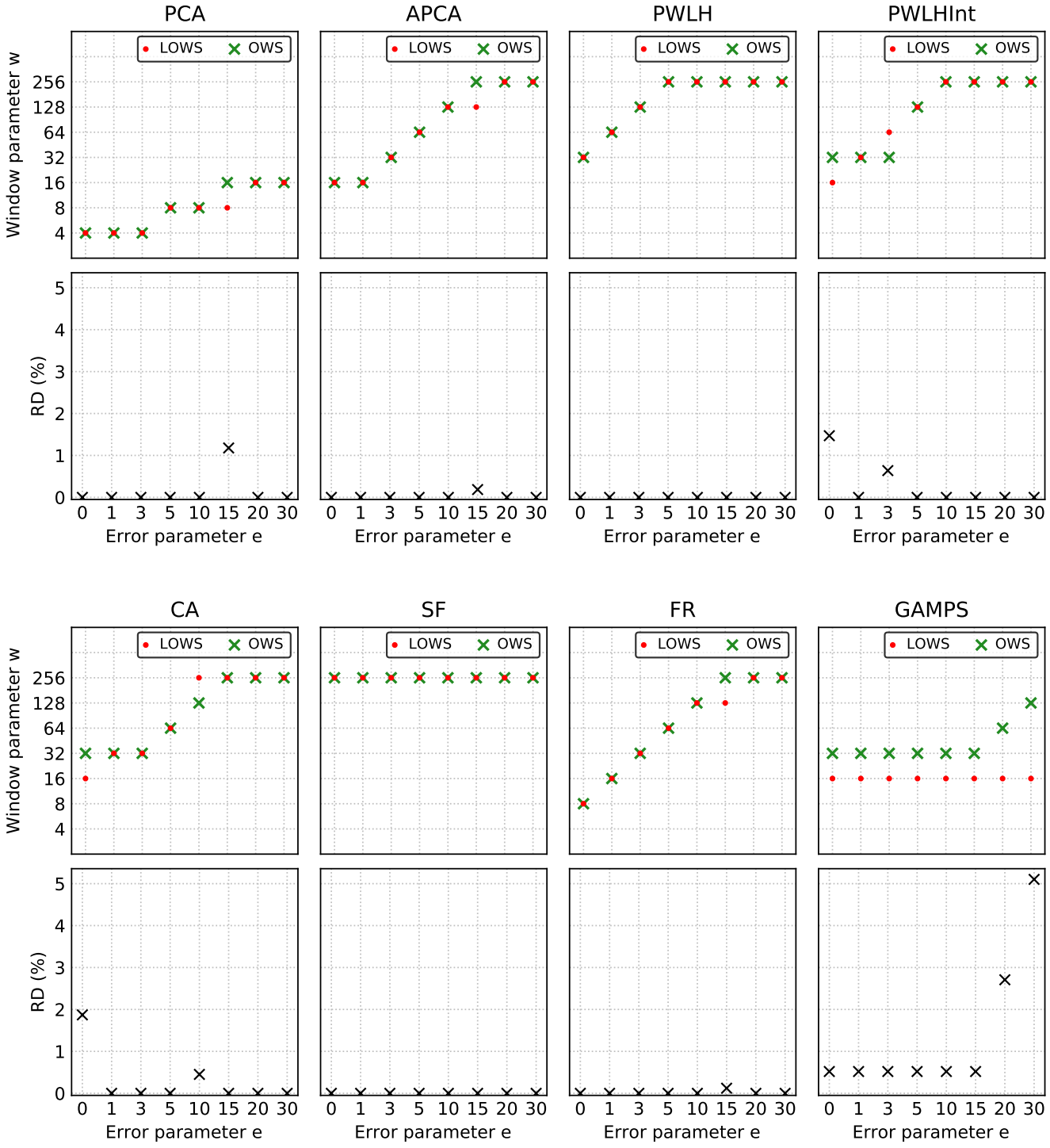

FIGURE B.5: Plots of w^*_{global}, w^*_{local}, and the RD between $c_{<a_v,w^*_{global},e>}$ and $c_{<a_v,w^*_{local},e>}$, as a function of the error parameter e, obtained for the data type "VWC" of the file "irkis-222.csv" of the dataset IRKIS.

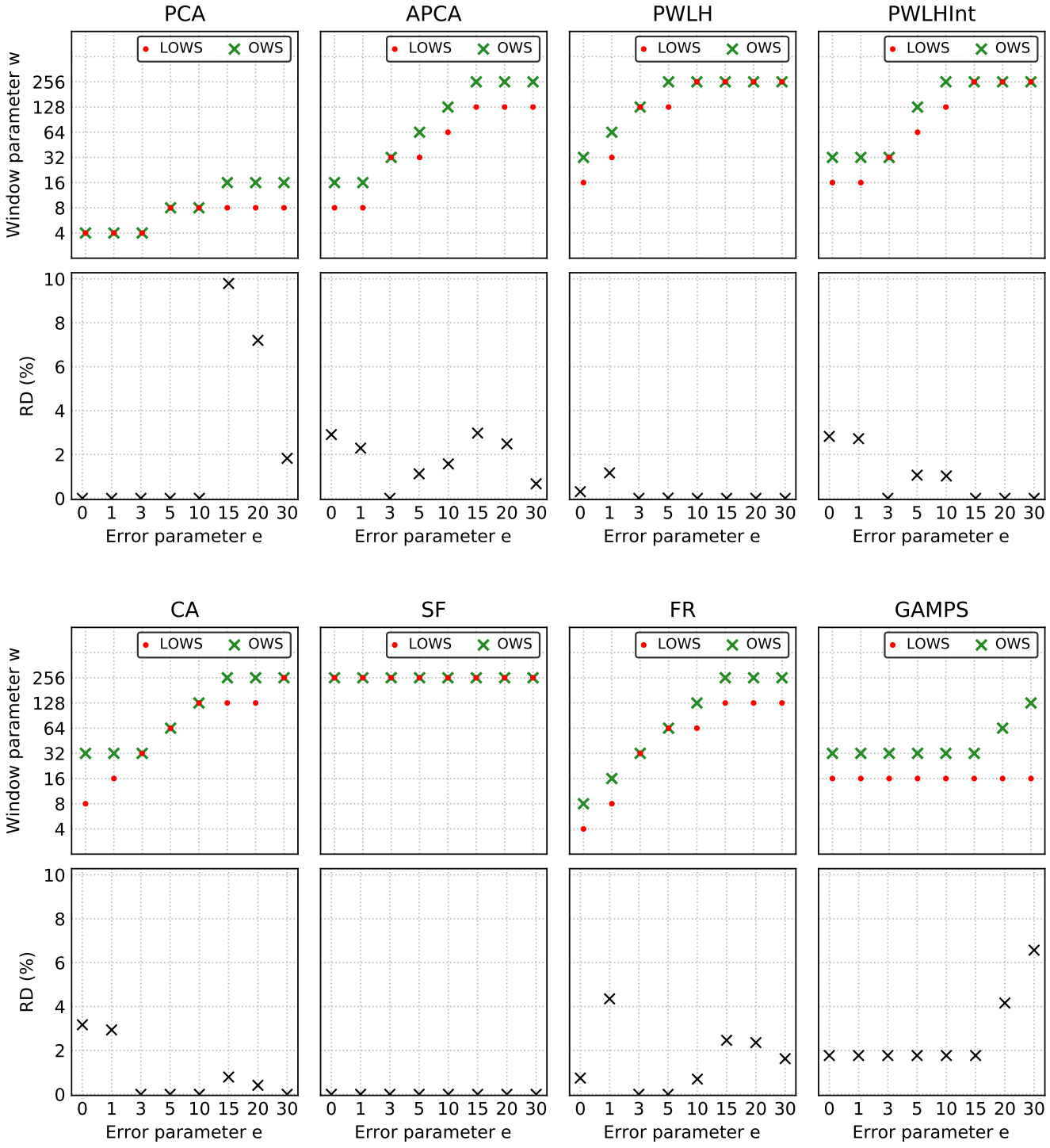

FIGURE B.6: Plots of w^*_{global}, w^*_{local}, and the RD between $c_{<a_v,w^*_{global},e>}$ and $c_{<a_v,w^*_{local},e>}$, as a function of the error parameter e, obtained for the data type "VWC" of the file "irkis-333.csv" of the dataset IRKIS.

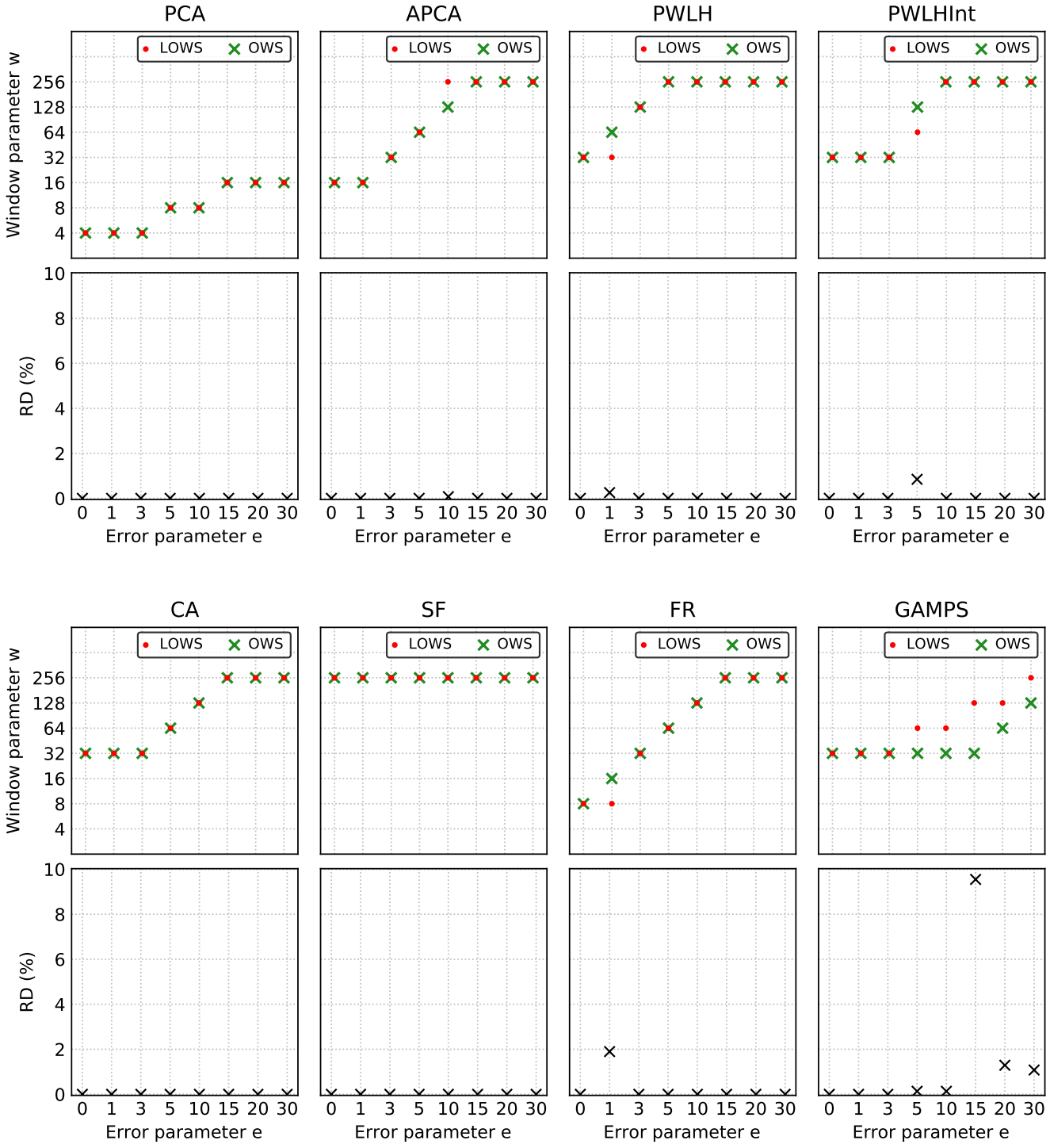

FIGURE B.7: Plots of w^*_{global}, w^*_{local}, and the RD between $c_{<a_v,w^*_{global},e>}$ and $c_{<a_v,w^*_{local},e>}$, as a function of the error parameter e, obtained for the data type "VWC" of the file "irkis-SLF2.csv" of the dataset IRKIS.

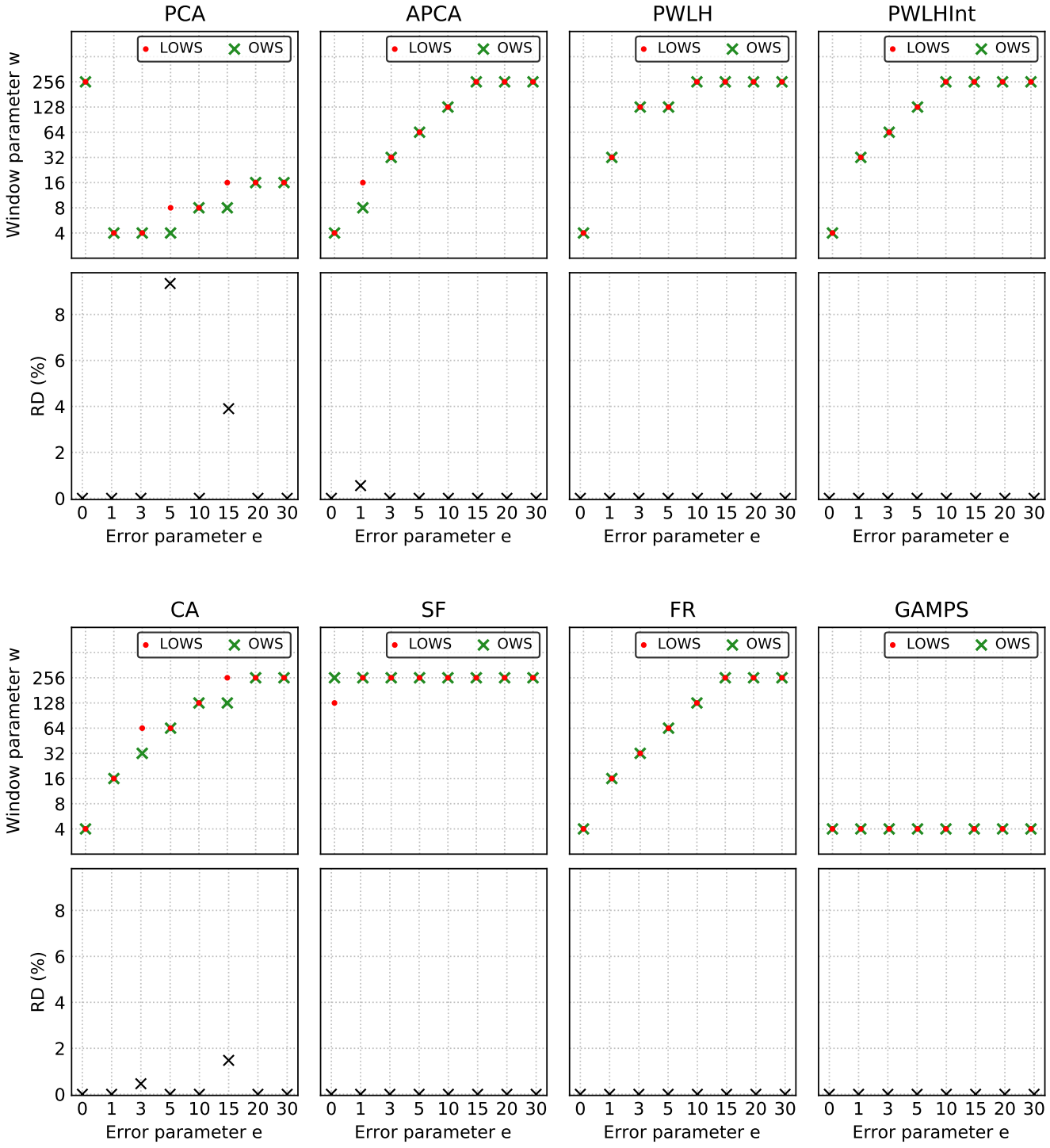

FIGURE B.8: Plots of w^*_{global}, w^*_{local}, and the RD between $c_{<a_v,w^*_{global},e>}$ and $c_{<a_v,w^*_{local},e>}$, as a function of the error parameter e, obtained for the data type "SST" of the file "sst-01-2017.csv" of the dataset SST.

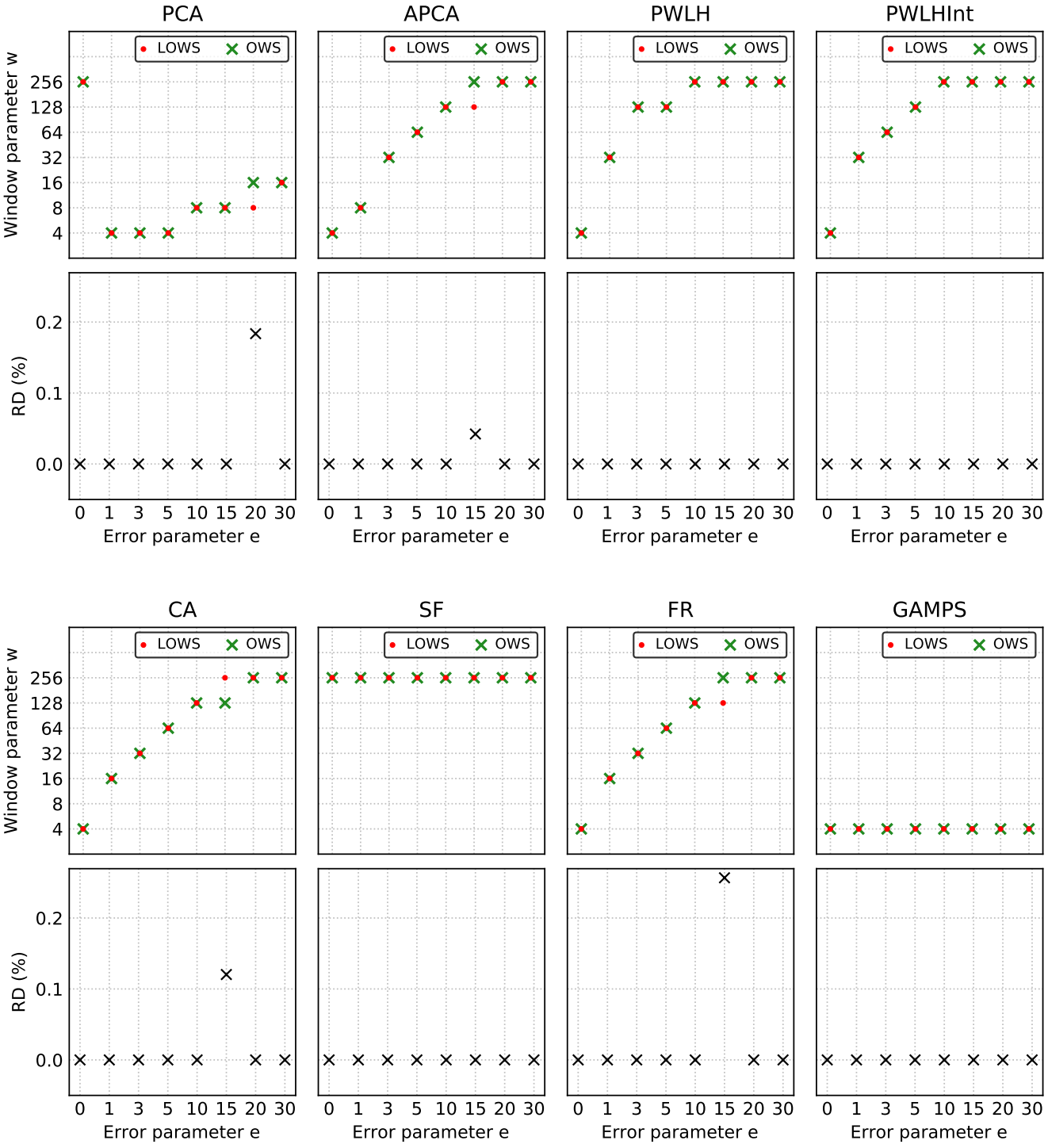

FIGURE B.9: Plots of w^*_{global}, w^*_{local}, and the RD between $c_{<a_v,w^*_{global},e>}$ and $c_{<a_v,w^*_{local},e>}$, as a function of the error parameter e, obtained for the data type "SST" of the file "sst-02-2017.csv" of the dataset SST.

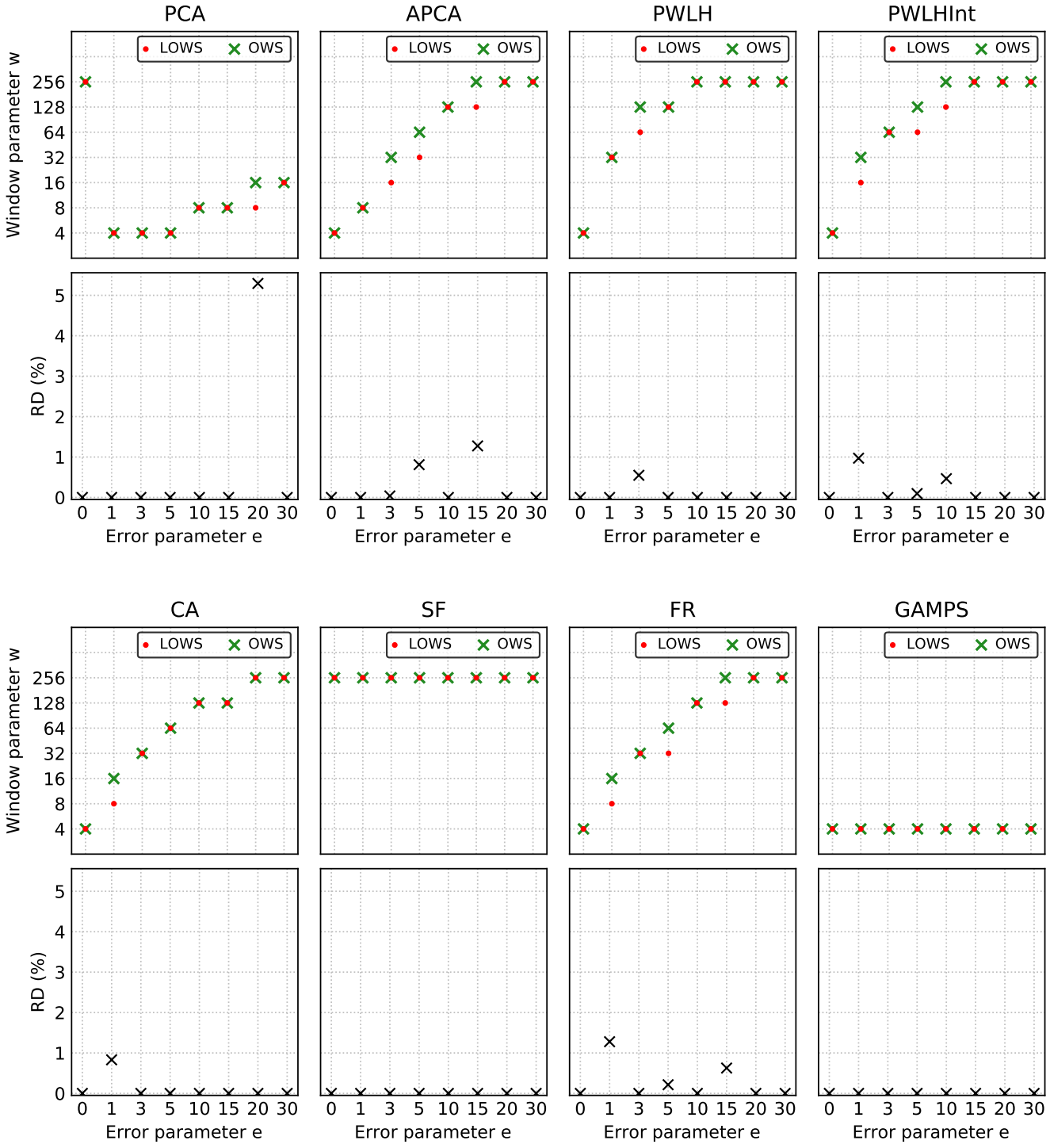

FIGURE B.10: Plots of w^*_{global}, w^*_{local}, and the RD between $c_{<a_v,w^*_{global},e>}$ and $c_{<a_v,w^*_{local},e>}$, as a function of the error parameter e, obtained for the data type "SST" of the file "sst-03-2017.csv" of the dataset SST.

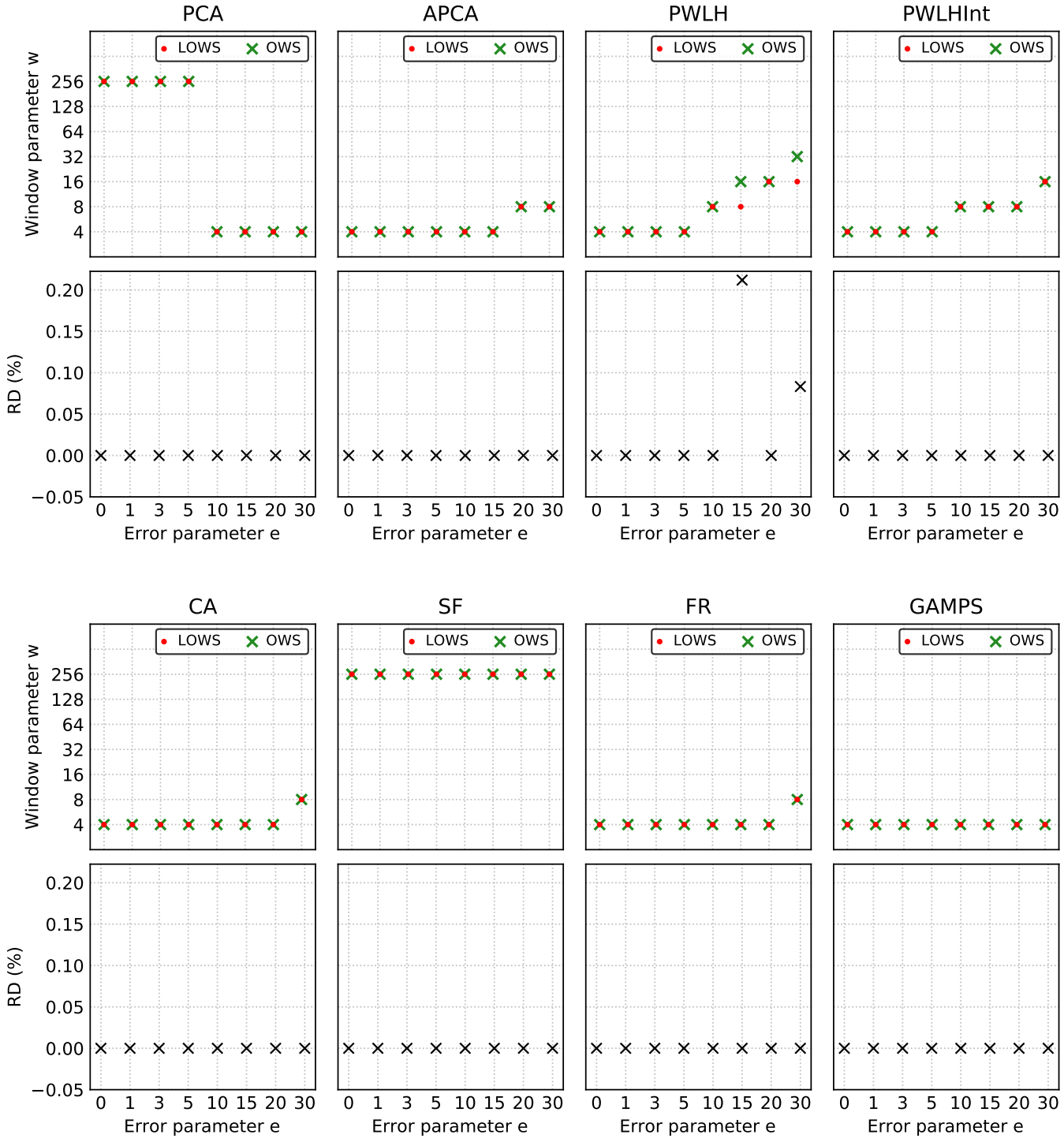

FIGURE B.11: Plots of w^*_{global}, w^*_{local}, and the RD between $c_{<a_v,w^*_{global},e>}$ and $c_{<a_v,w^*_{local},e>}$, as a function of the error parameter e, obtained for the data type "Velocity" of the file "adcp-01-2015.csv" of the dataset SST.

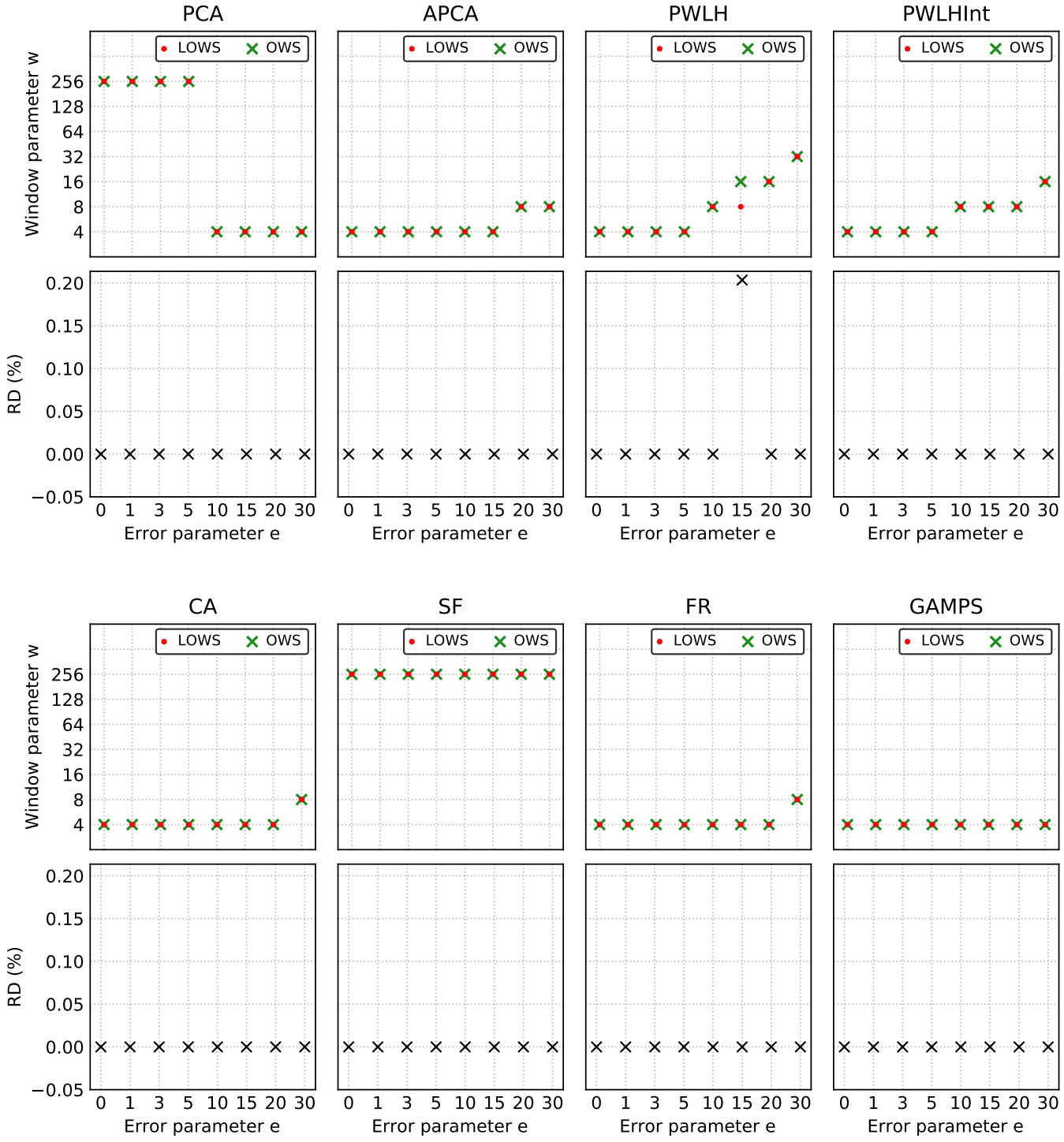

FIGURE B.12: Plots of w^*_{global}, w^*_{local}, and the RD between $c_{<a_v,w^*_{global},e>}$ and $c_{<a_v,w^*_{local},e>}$, as a function of the error parameter e, obtained for the data type "Velocity" of the file "adcp-02-2015.csv" of the dataset SST.

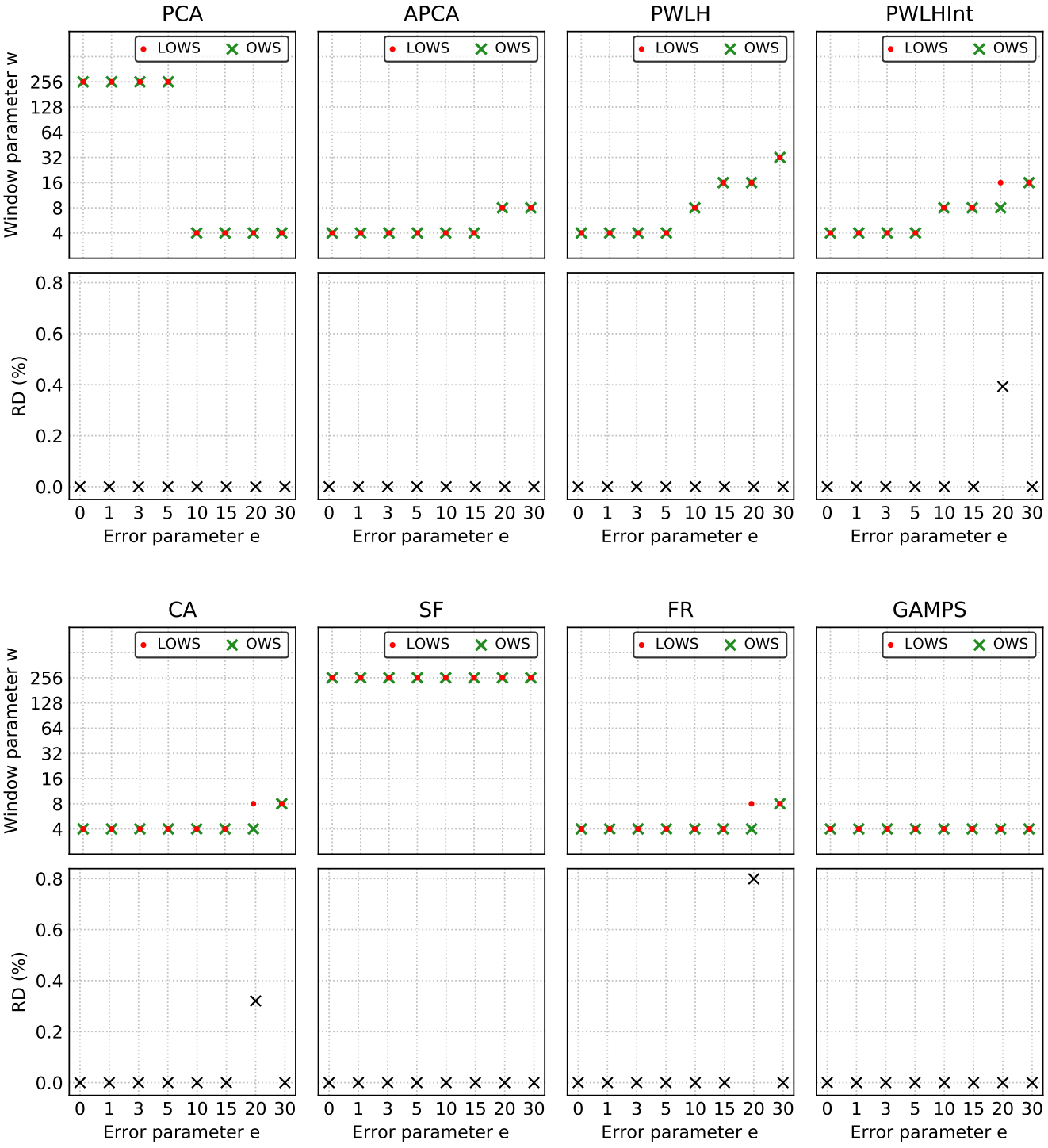

FIGURE B.13: Plots of w^*_{global}, w^*_{local}, and the RD between $c_{<a_v,w^*_{global},e>}$ and $c_{<a_v,w^*_{local},e>}$, as a function of the error parameter e, obtained for the data type "Velocity" of the file "adcp-03-2015.csv" of the dataset SST.

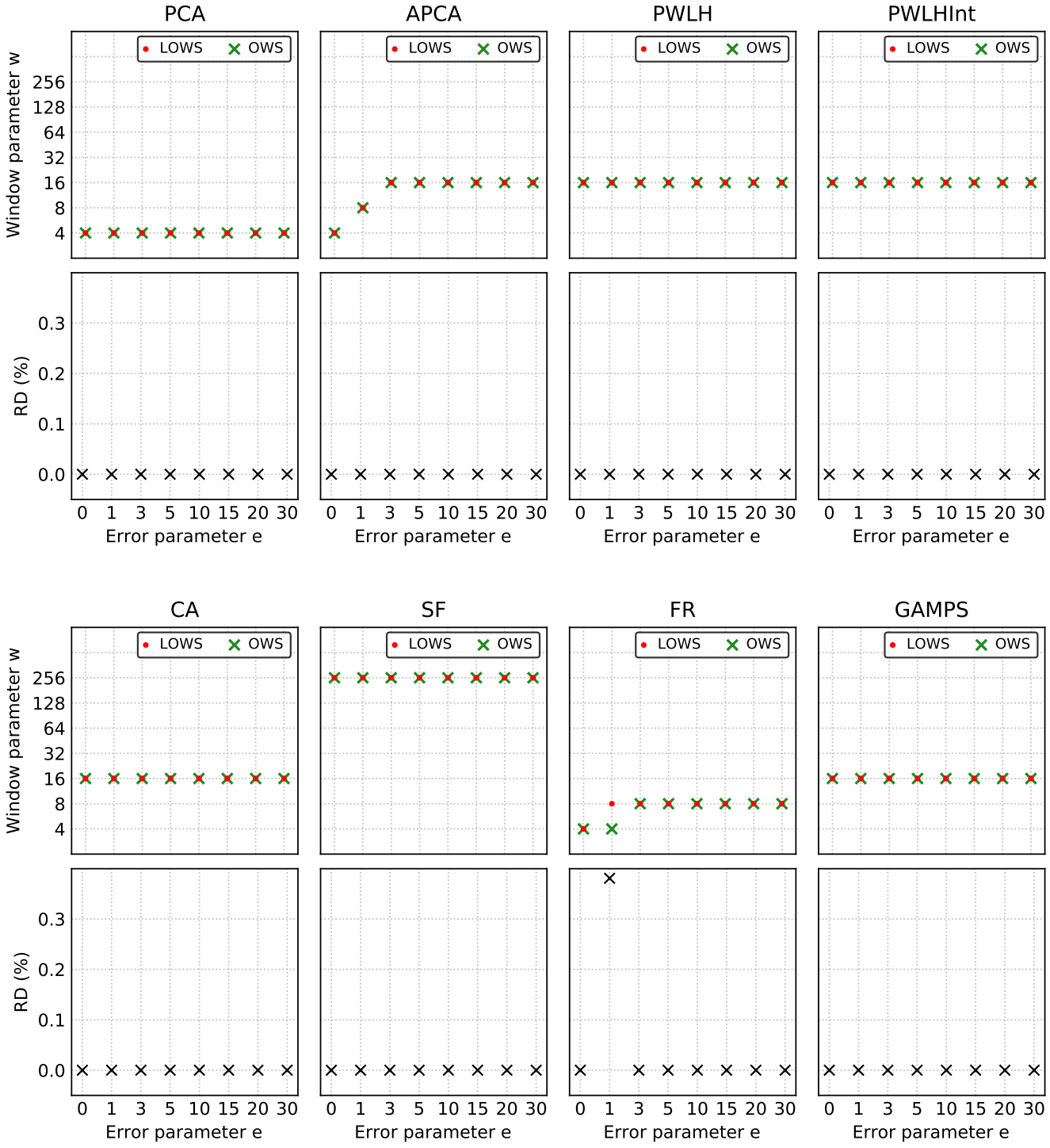

FIGURE B.14: Plots of w^*_{global}, w^*_{local}, and the RD between $c_{<a_v,w^*_{global},e>}$ and $c_{<a_v,w^*_{local},e>}$, as a function of the error parameter e, obtained for the data type "GHI" of the file "solar-2011.csv" of the dataset Solar.

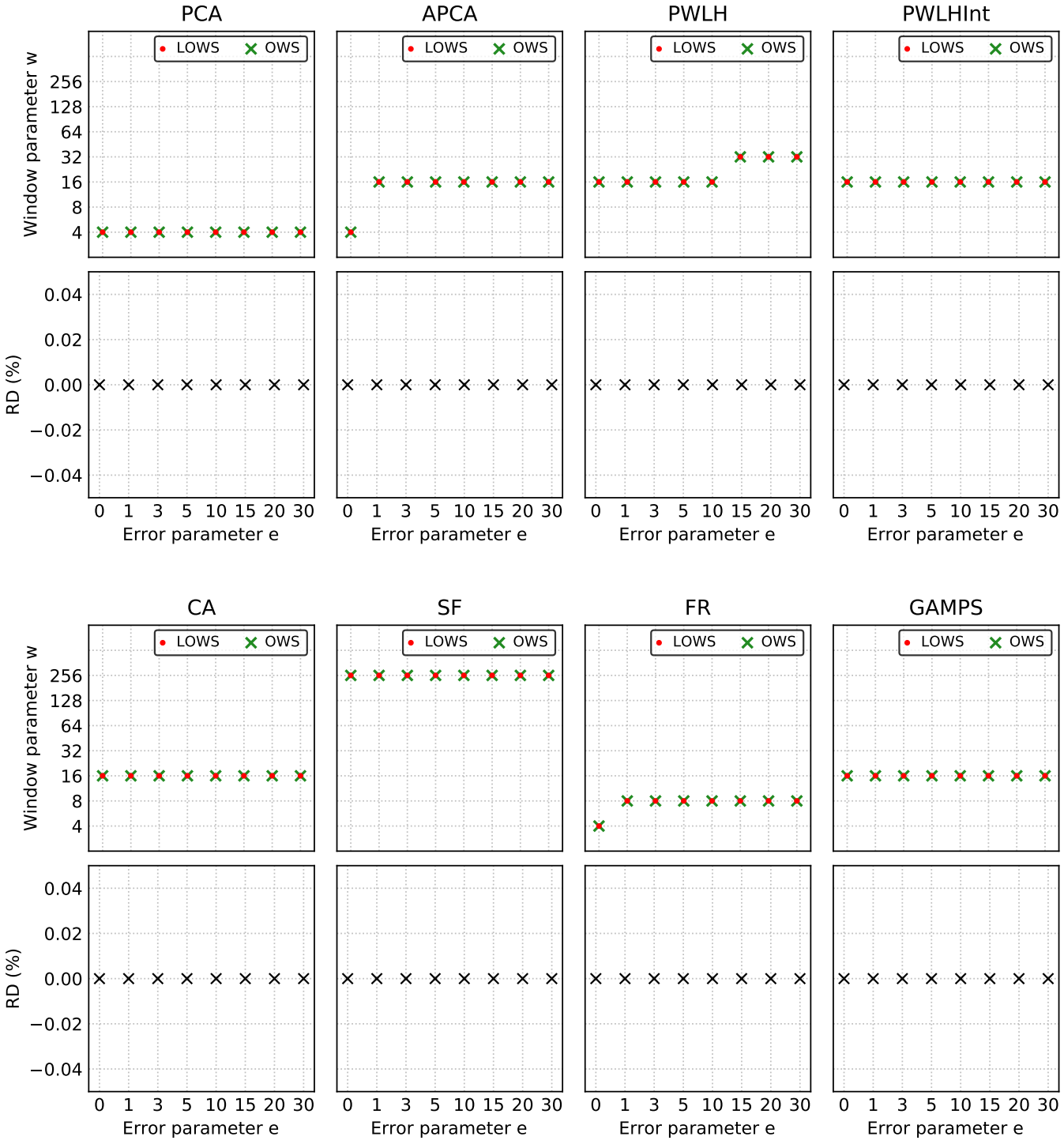

FIGURE B.15: Plots of w^*_{global}, w^*_{local}, and the RD between $c_{<a_v,w^*_{global},e>}$ and $c_{<a_v,w^*_{local},e>}$, as a function of the error parameter e, obtained for the data type "DNI" of the file "solar-2011.csv" of the dataset Solar.

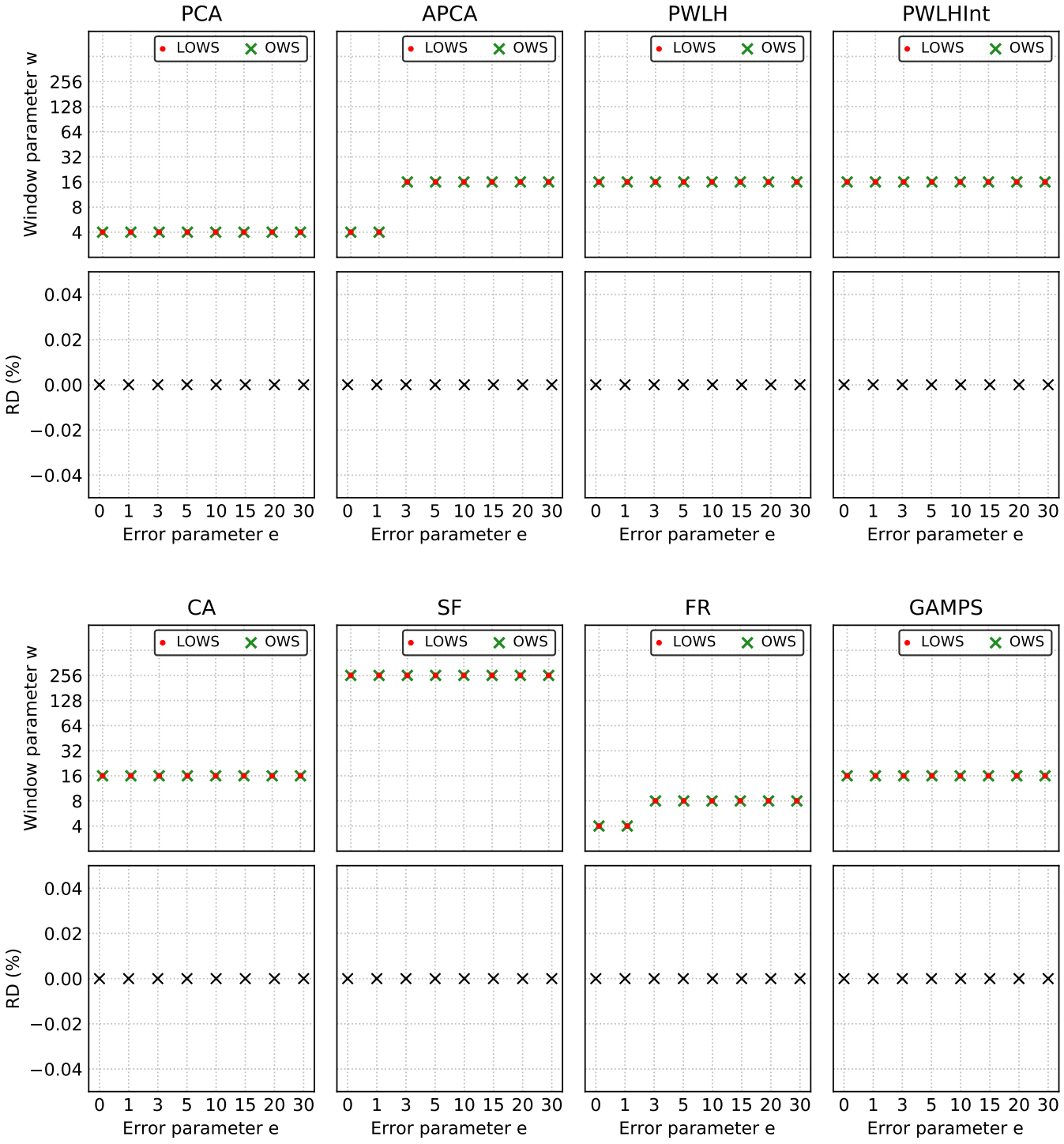

FIGURE B.16: Plots of w^*_{global}, w^*_{local}, and the RD between $c_{<a_v,w^*_{global},e>}$ and $c_{<a_v,w^*_{local},e>}$, as a function of the error parameter e, obtained for the data type "DHI" of the file "solar-2011.csv" of the dataset Solar.

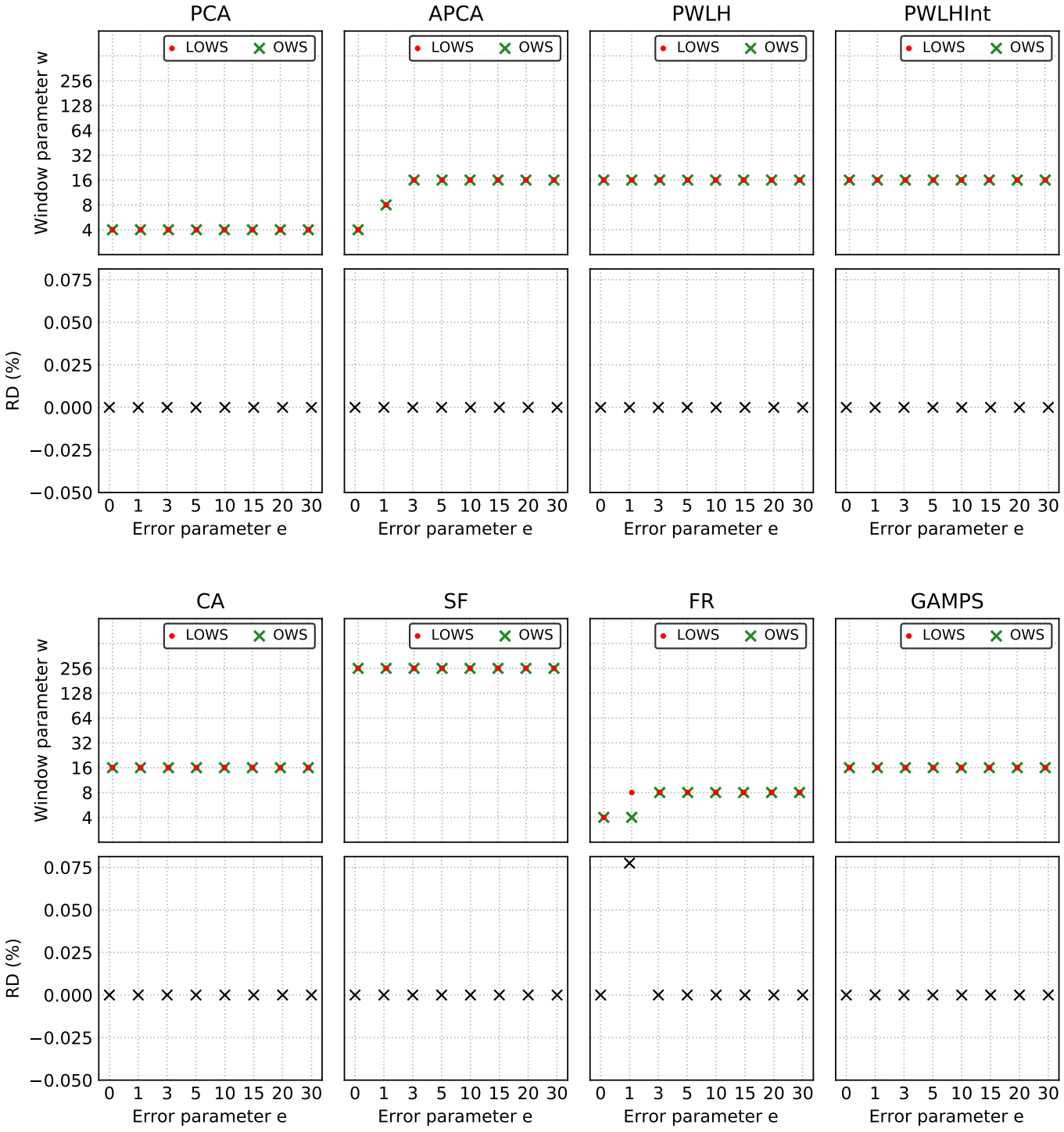

FIGURE B.17: Plots of w^*_{global}, w^*_{local}, and the RD between $c_{<a_v,w^*_{global},e>}$ and $c_{<a_v,w^*_{local},e>}$, as a function of the error parameter e, obtained for the data type "GHI" of the file "solar-2012.csv" of the dataset Solar.

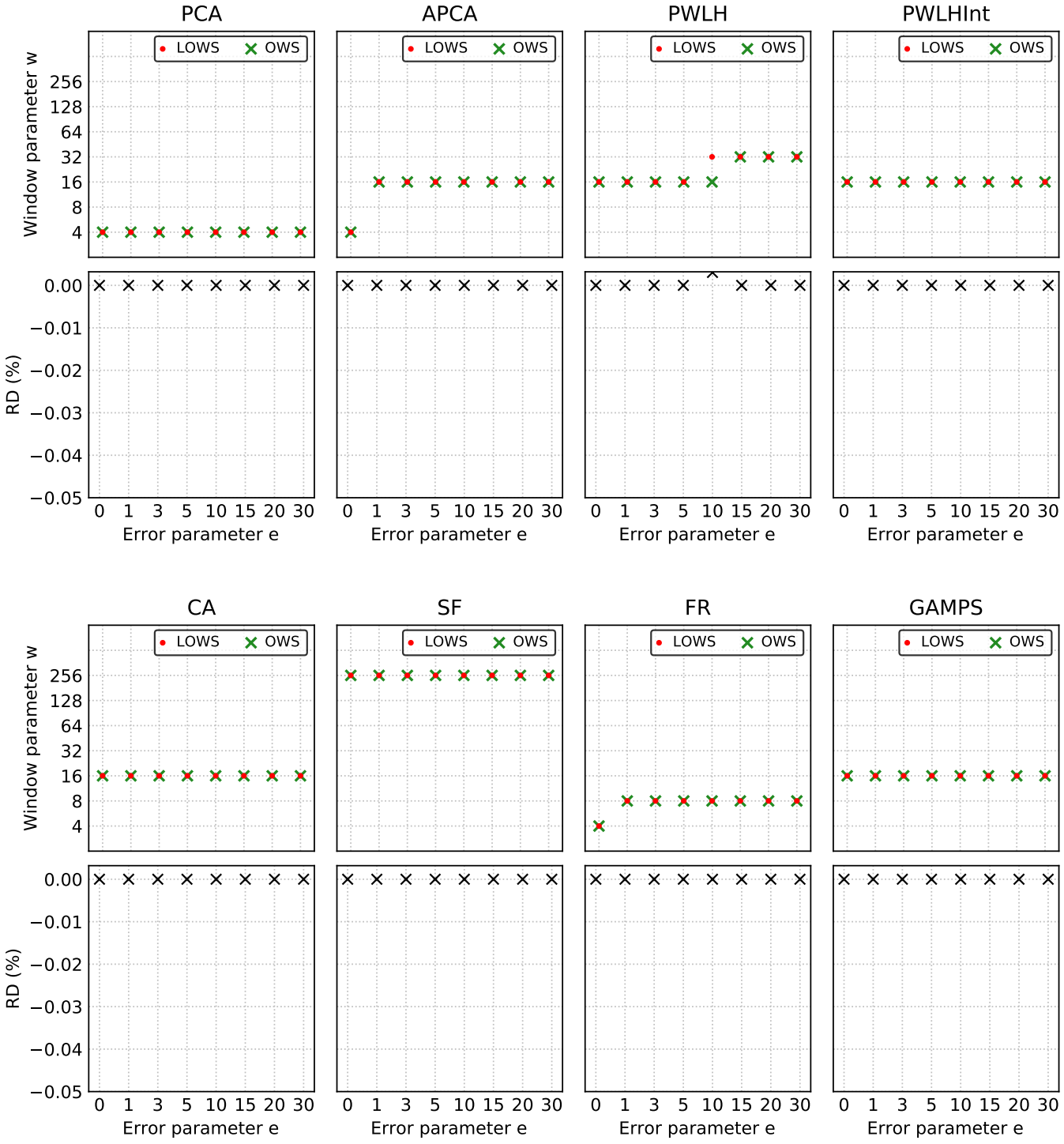

FIGURE B.18: Plots of w^*_{global}, w^*_{local}, and the RD between $c_{<a_v,w^*_{global},e>}$ and $c_{<a_v,w^*_{local},e>}$, as a function of the error parameter e, obtained for the data type "DNI" of the file "solar-2012.csv" of the dataset Solar.

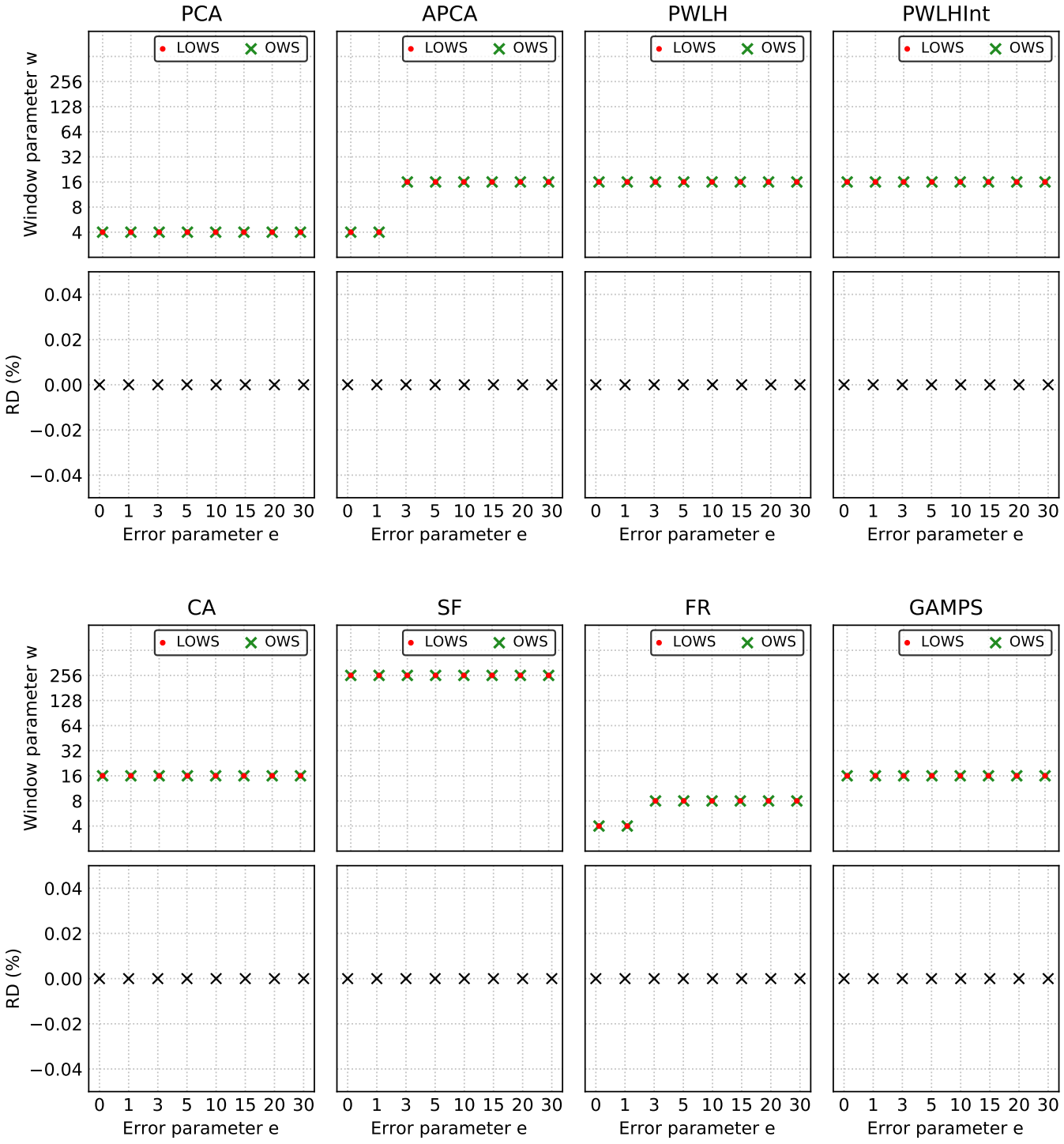

FIGURE B.19: Plots of w^*_{global}, w^*_{local}, and the RD between $c_{<a_v,w^*_{global},e>}$ and $c_{<a_v,w^*_{local},e>}$, as a function of the error parameter e, obtained for the data type "DHI" of the file "solar-2012.csv" of the dataset Solar.

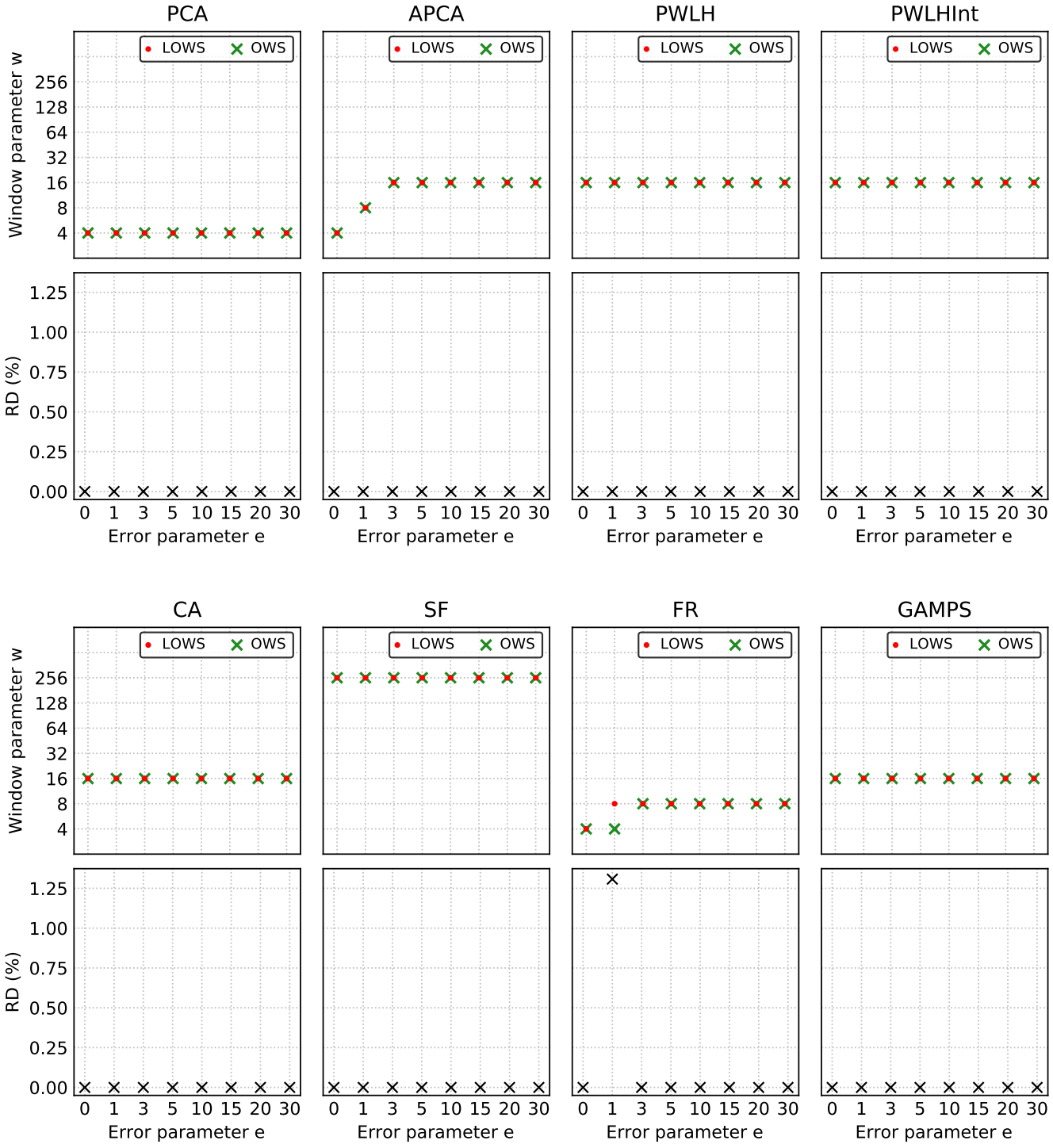

FIGURE B.20: Plots of w^*_{global}, w^*_{local}, and the RD between $c_{<a_v,w^*_{global},e>}$ and $c_{<a_v,w^*_{local},e>}$, as a function of the error parameter e, obtained for the data type "GHI" of the file "solar-2013.csv" of the dataset Solar.

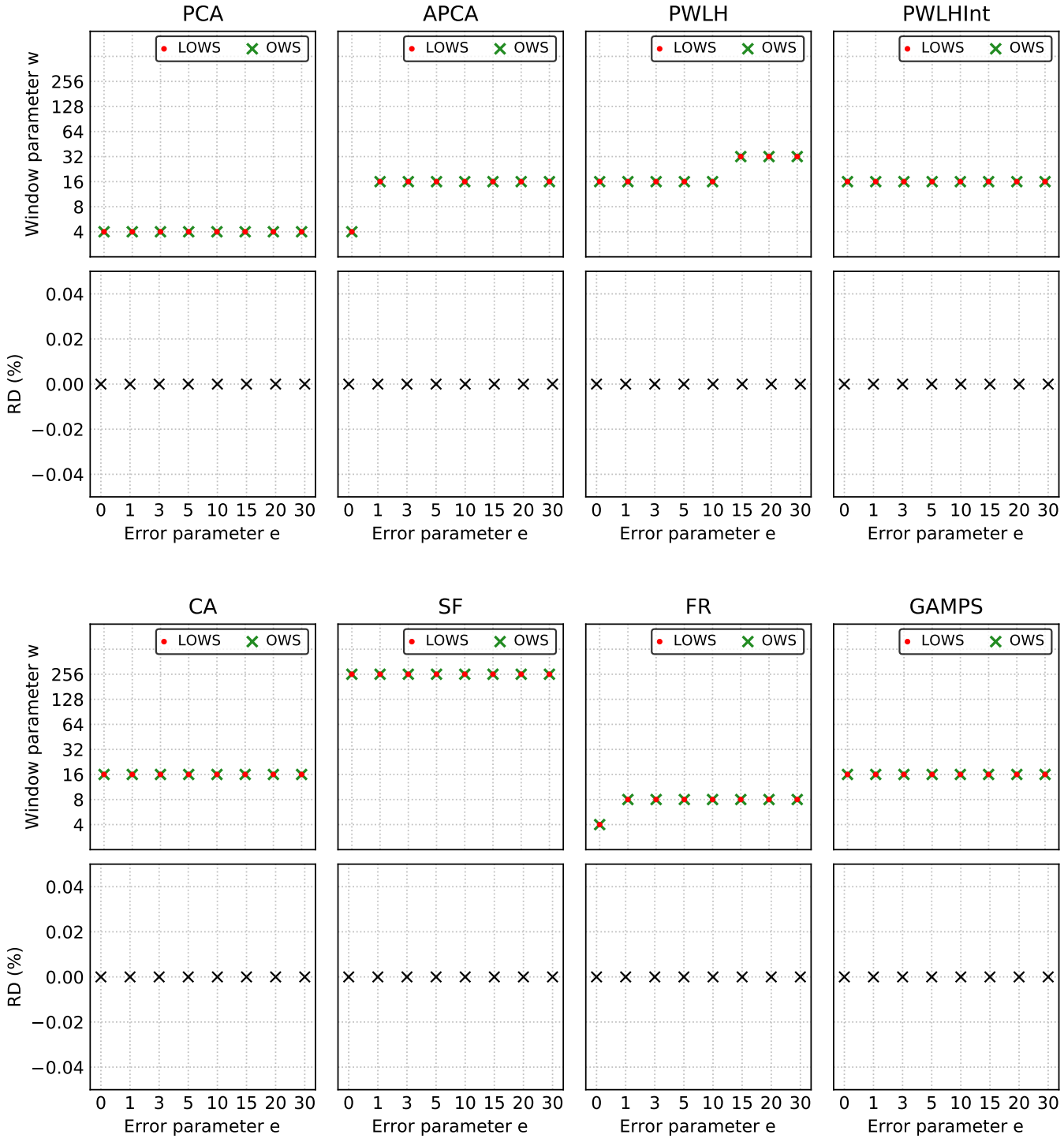

FIGURE B.21: Plots of w^*_{global}, w^*_{local}, and the RD between $c_{<a_v,w^*_{global},e>}$ and $c_{<a_v,w^*_{local},e>}$, as a function of the error parameter e, obtained for the data type "DNI" of the file "solar-2013.csv" of the dataset Solar.

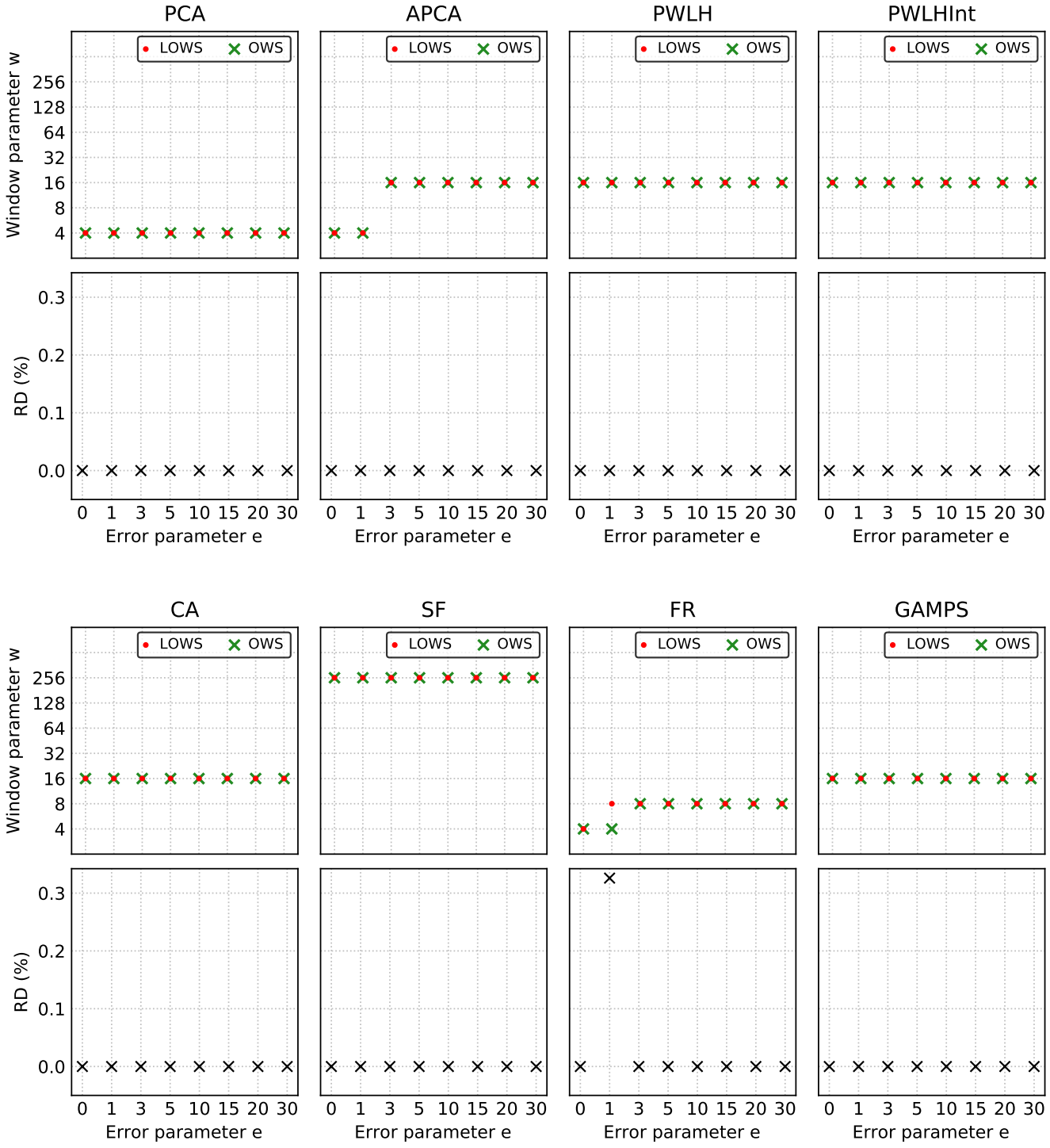

FIGURE B.22: Plots of w^*_{global}, w^*_{local}, and the RD between $c_{<a_v,w^*_{global},e>}$ and $c_{<a_v,w^*_{local},e>}$, as a function of the error parameter e, obtained for the data type "DHI" of the file "solar-2013.csv" of the dataset Solar.

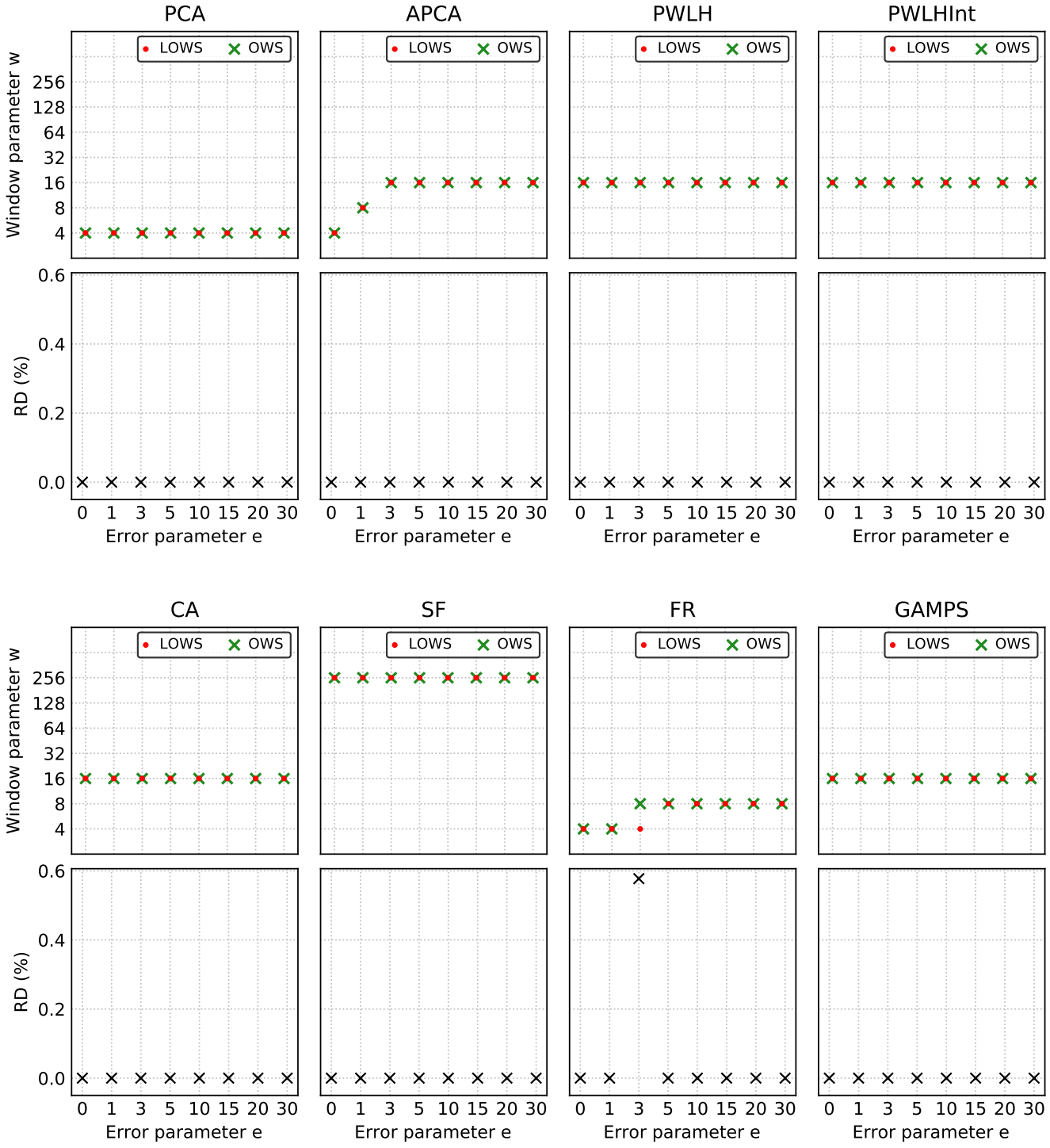

FIGURE B.23: Plots of w^*_{global}, w^*_{local}, and the RD between $c_{<a_v,w^*_{global},e>}$ and $c_{<a_v,w^*_{local},e>}$, as a function of the error parameter e, obtained for the data type "GHI" of the file "solar-2014.csv" of the dataset Solar.

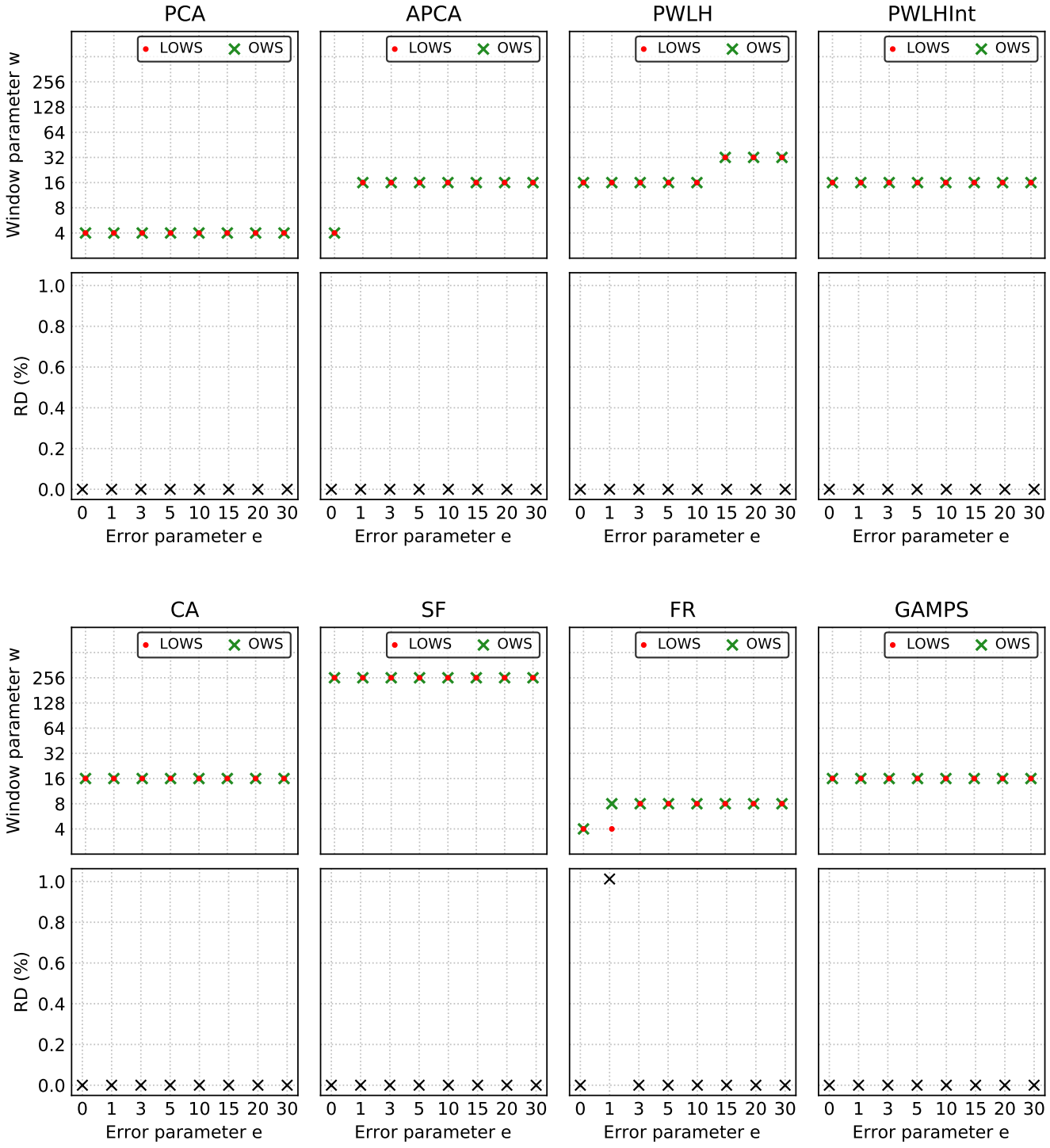

FIGURE B.24: Plots of w^*_{global}, w^*_{local}, and the RD between $c_{<a_v,w^*_{global},e>}$ and $c_{<a_v,w^*_{local},e>}$, as a function of the error parameter e, obtained for the data type "DNI" of the file "solar-2014.csv" of the dataset Solar.

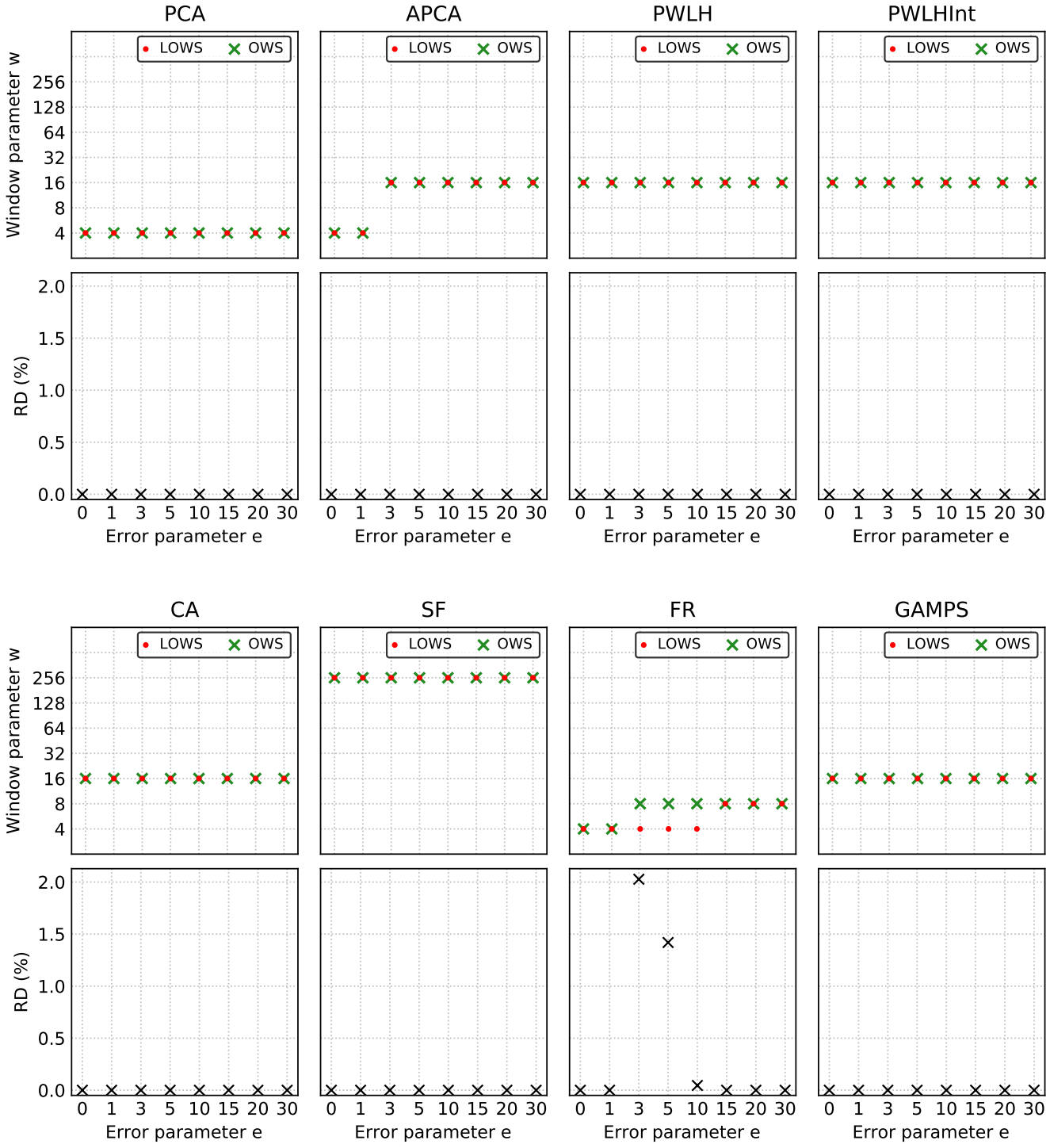

FIGURE B.25: Plots of w^*_{global}, w^*_{local}, and the RD between $c_{<a_v,w^*_{global},e>}$ and $c_{<a_v,w^*_{local},e>}$, as a function of the error parameter e, obtained for the data type "DHI" of the file "solar-2014.csv" of the dataset Solar.

Appendix C

Figures: Algorithm Compression Performance

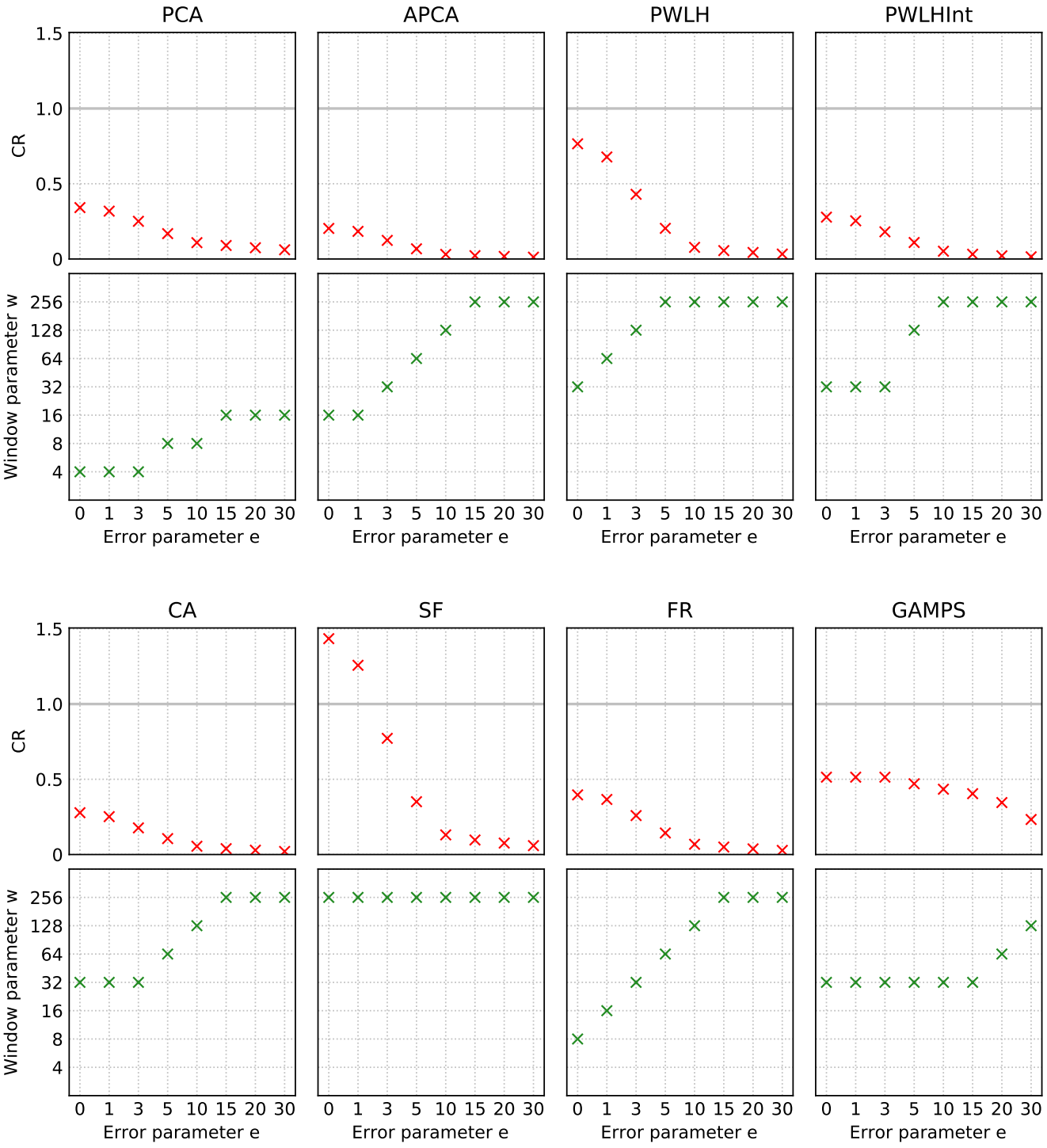

FIGURE C.1: CR and window size parameter plots for every evaluated algorithm, for the data type "VWC" of the dataset IRKIS.

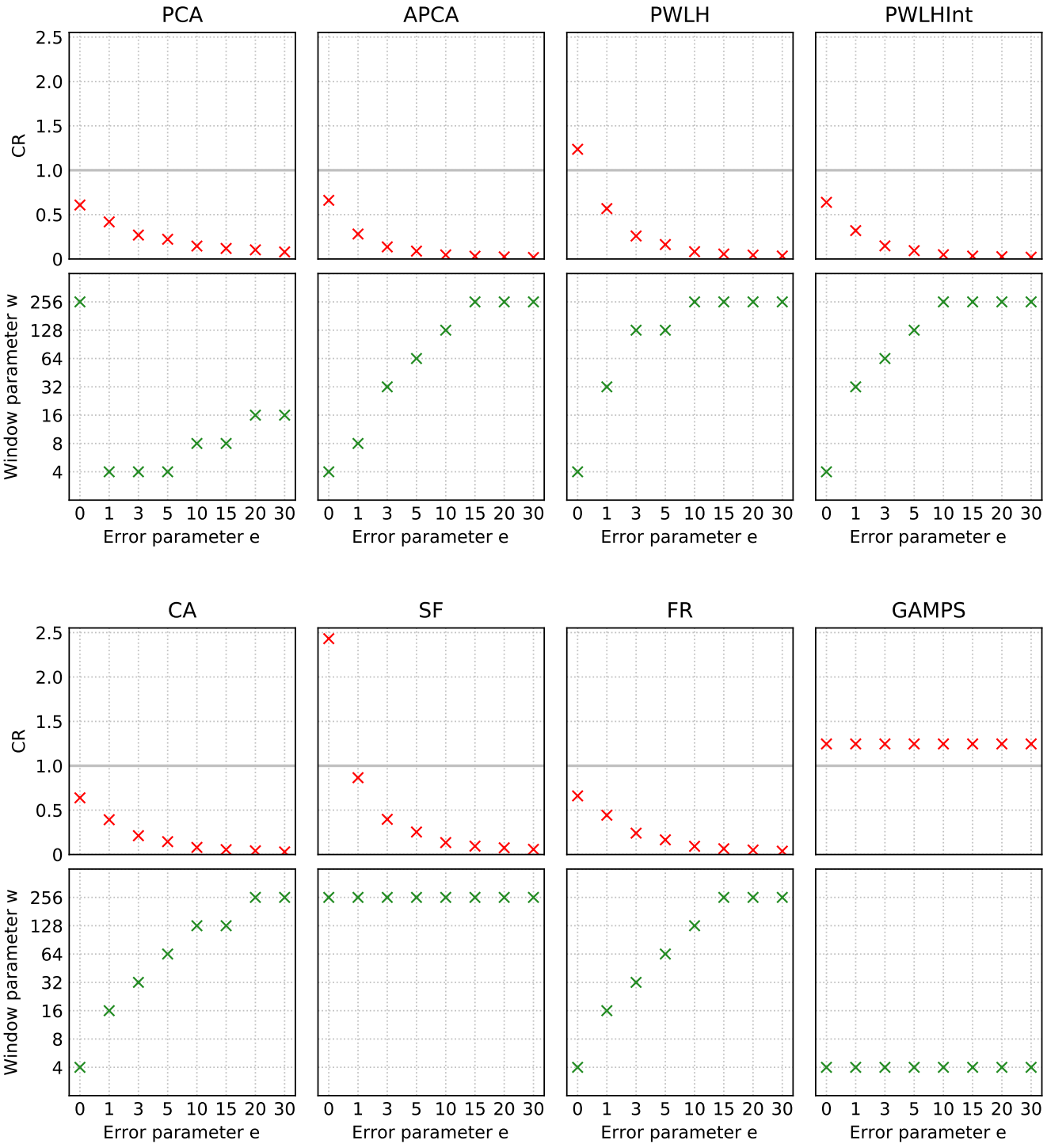

FIGURE C.2: CR and window size parameter plots for every evaluated algorithm, for the data type "SST" of the dataset SST.

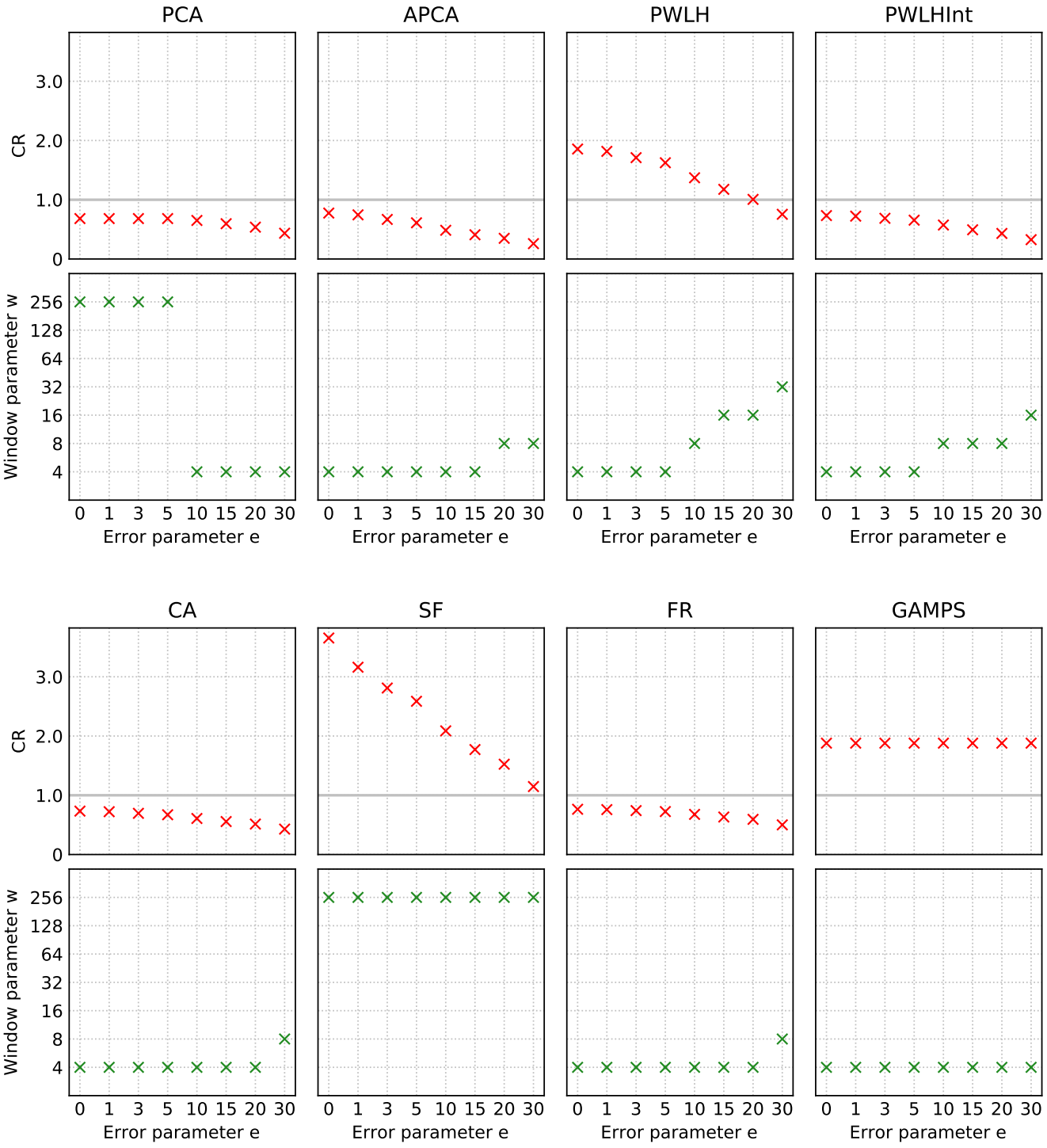

FIGURE C.3: CR and window size parameter plots for every evaluated algorithm, for the data type "Velocity" of the dataset ADCP.

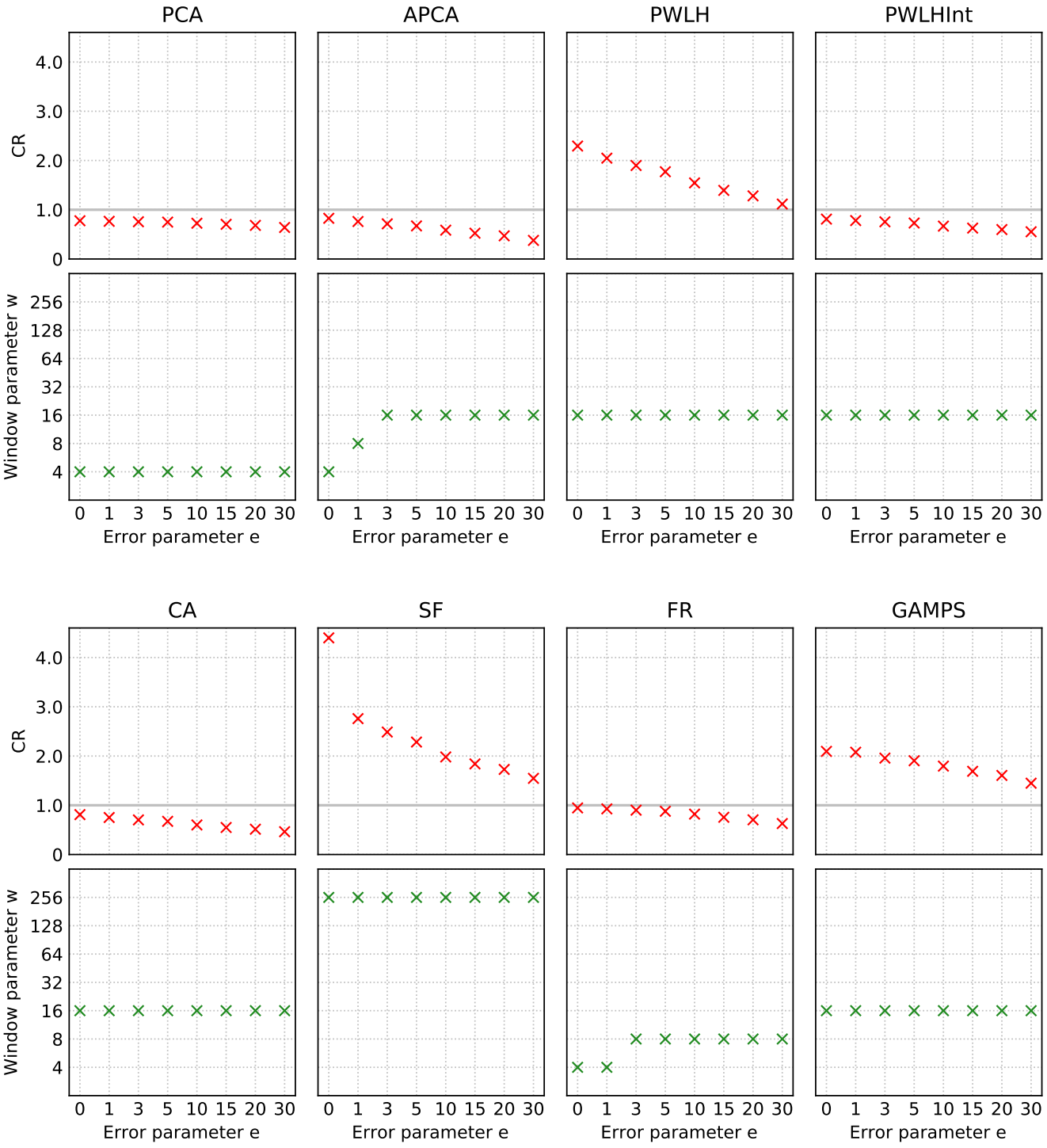

FIGURE C.4: CR and window size parameter plots for every evaluated algorithm, for the data type "GHI" of the dataset Solar.

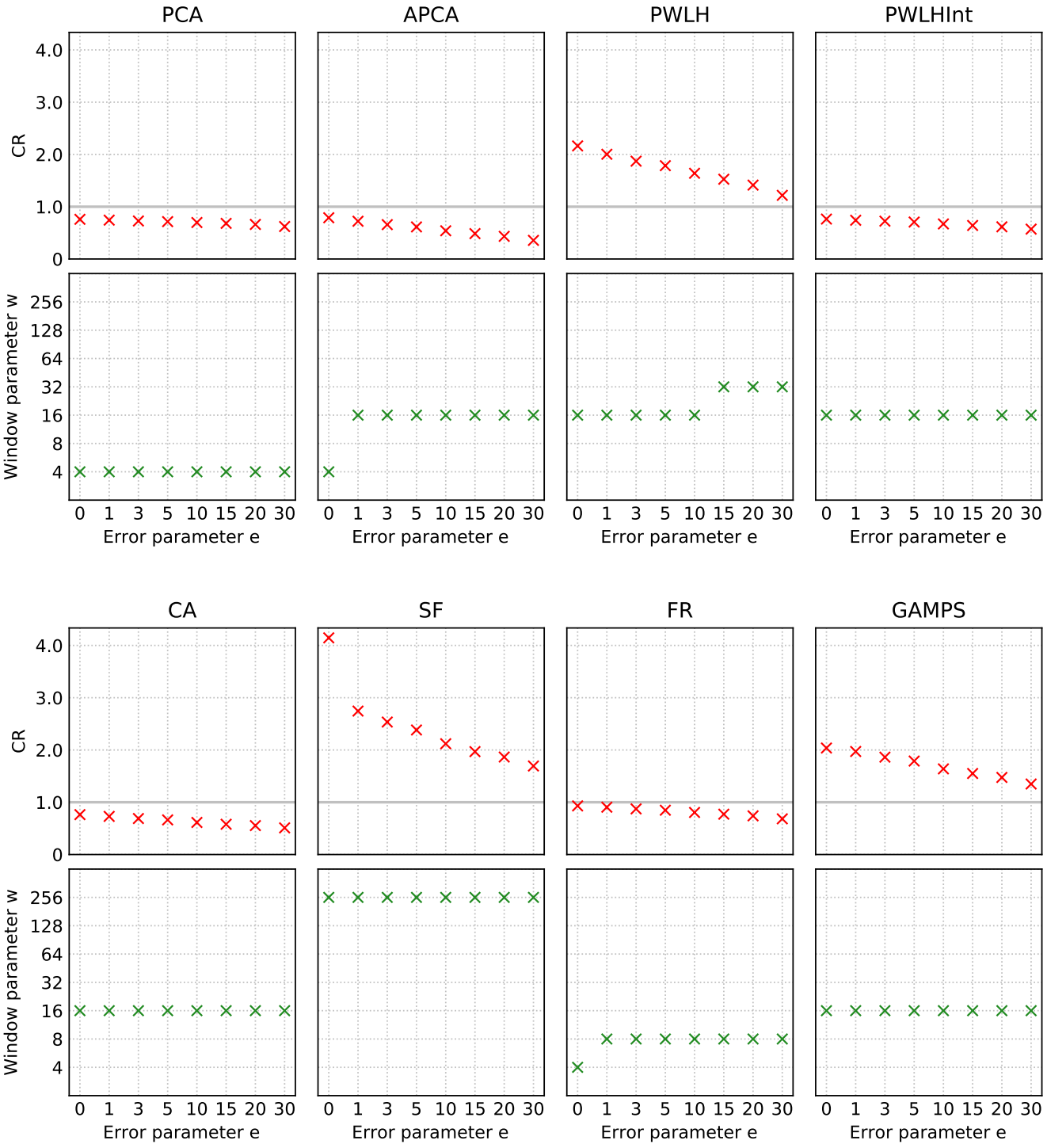

FIGURE C.5: CR and window size parameter plots for every evaluated algorithm, for the data type "DNI" of the dataset Solar.

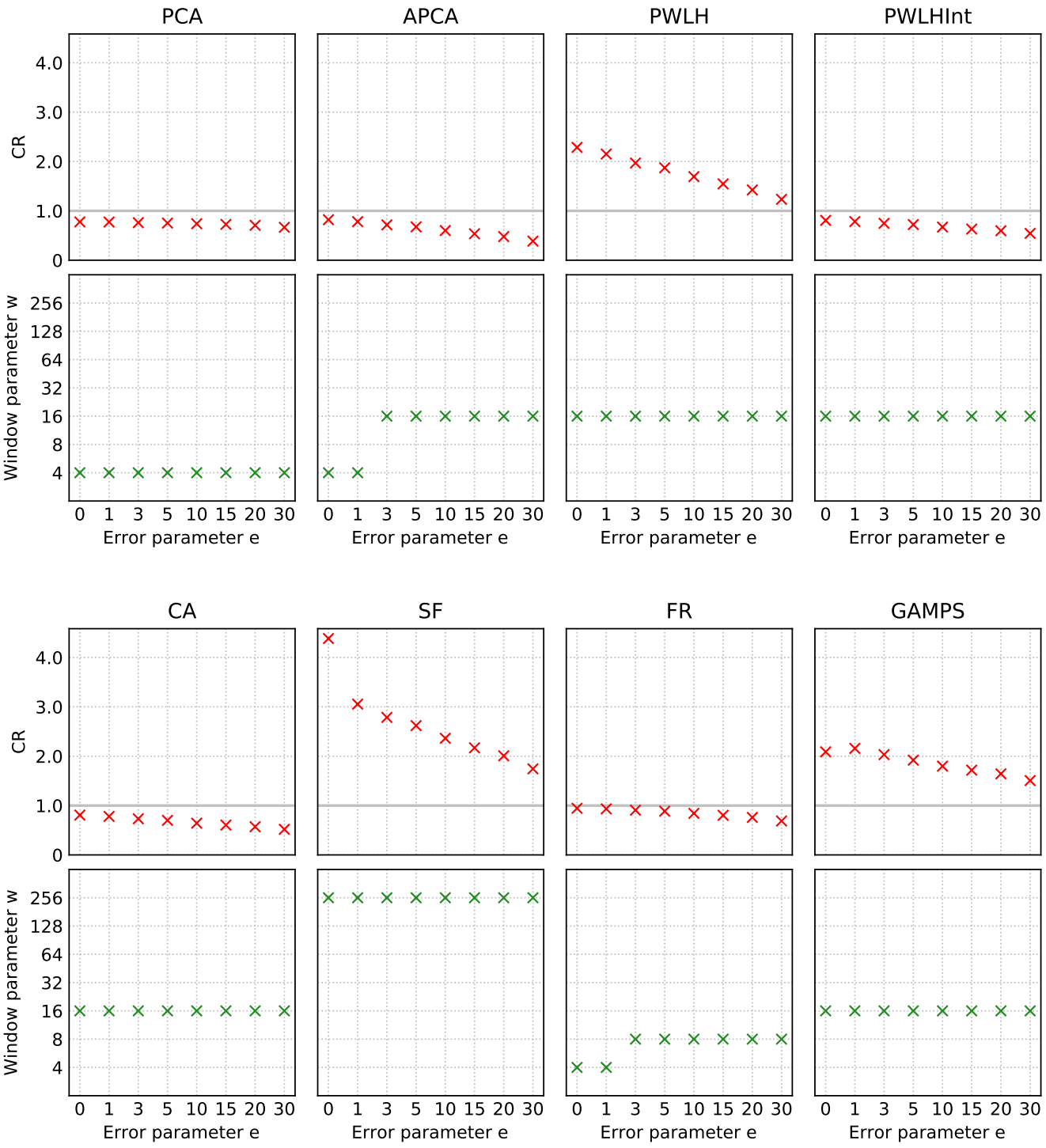

FIGURE C.6: CR and window size parameter plots for every evaluated algorithm, for the data type "DHI" of the dataset Solar.

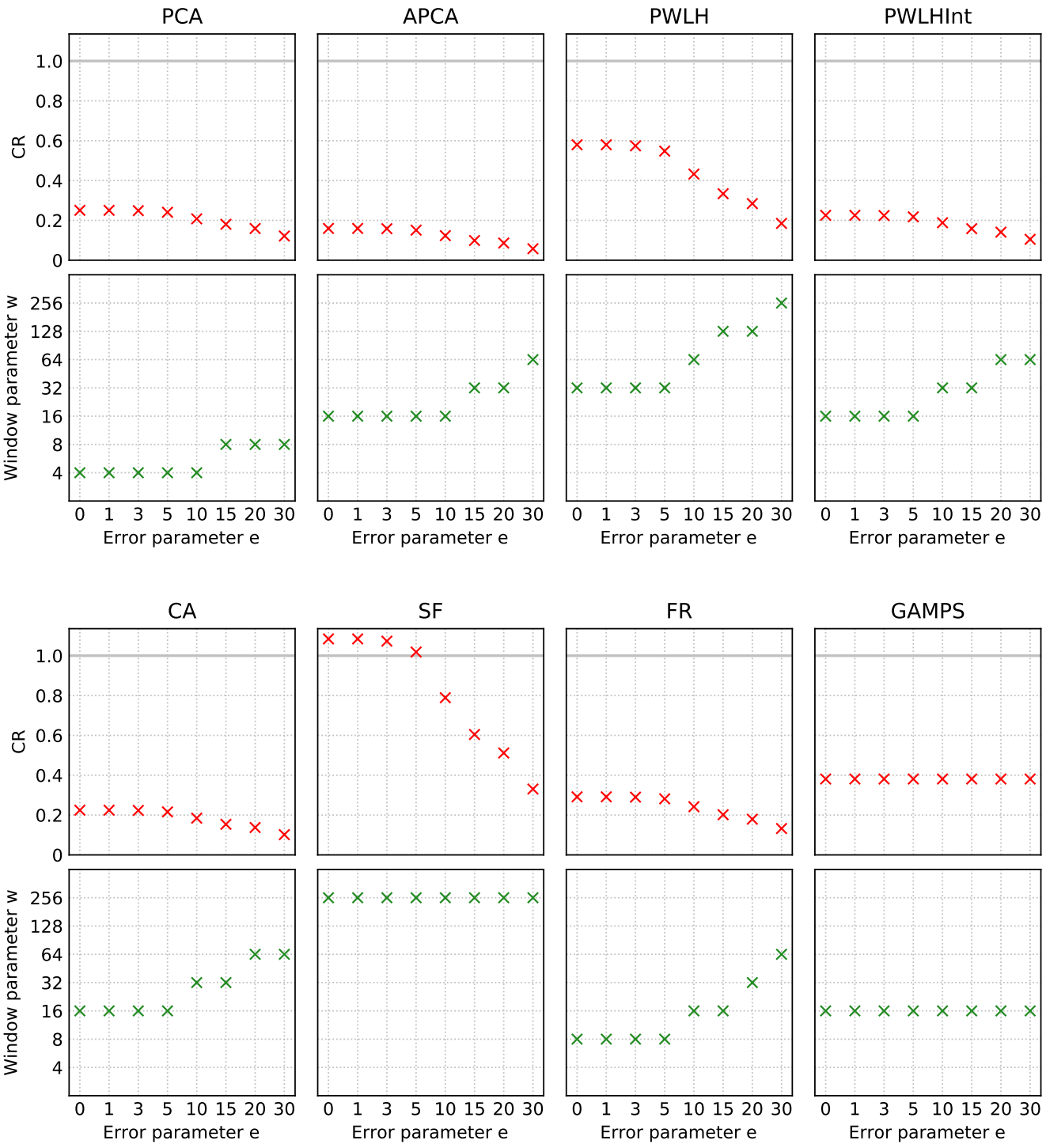

FIGURE C.7: CR and window size parameter plots for every evaluated algorithm, for the data type "Latitude" of the dataset ElNino.

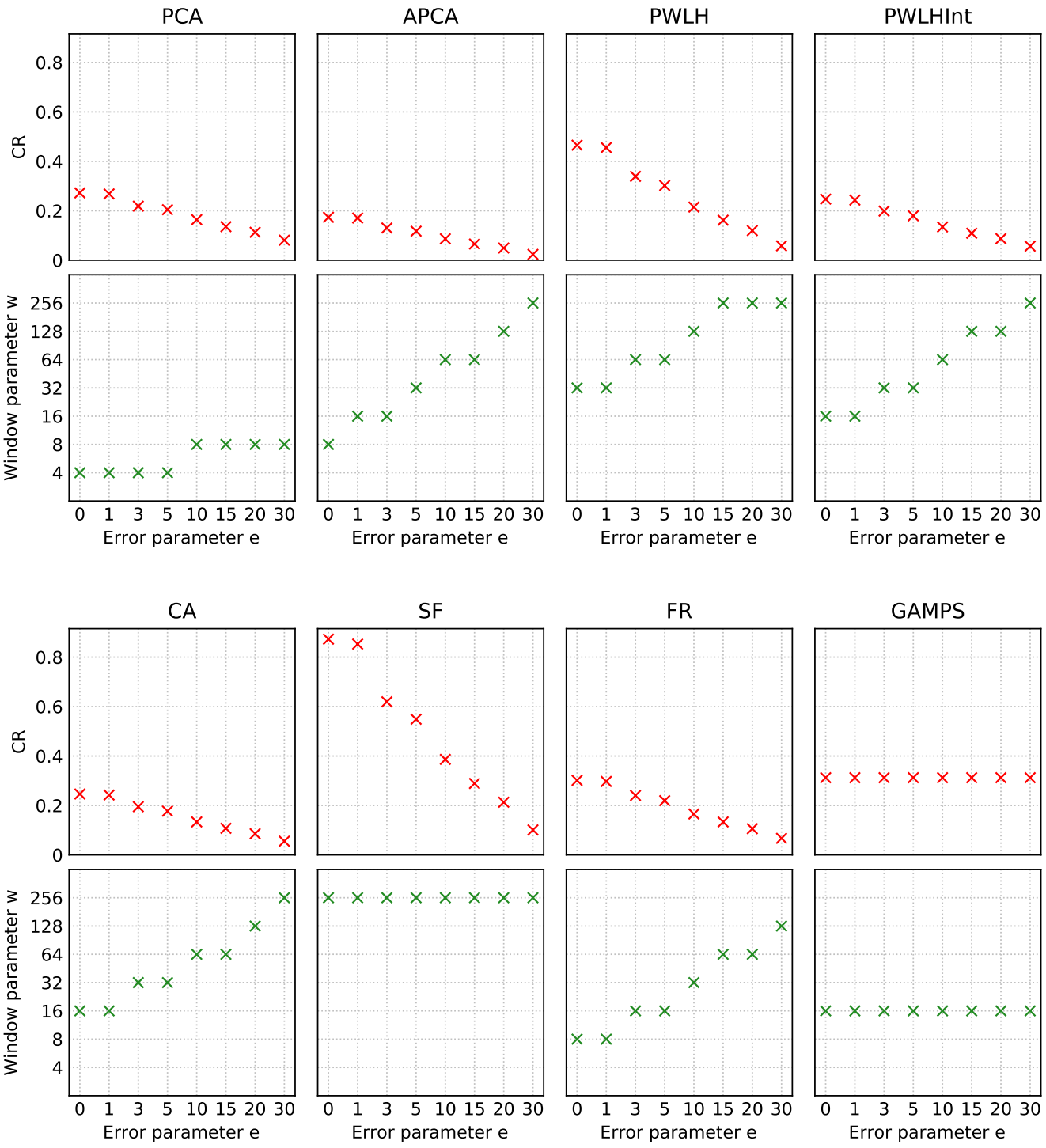

FIGURE C.8: CR and window size parameter plots for every evaluated algorithm, for the data type "Longitude" of the dataset ElNino.

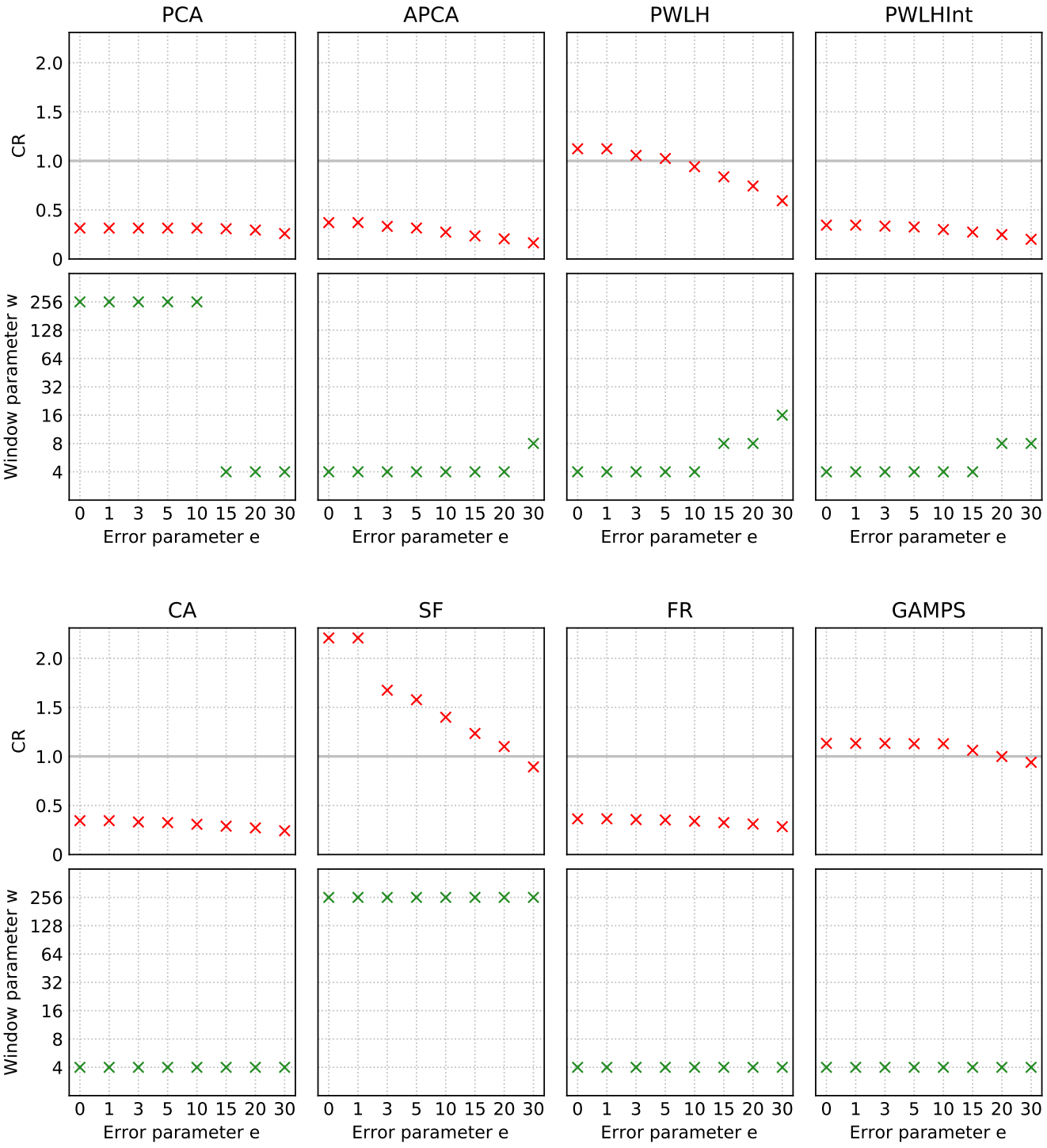

FIGURE C.9: CR and window size parameter plots for every evaluated algorithm, for the data type "Zon. Wind" of the dataset ElNino.

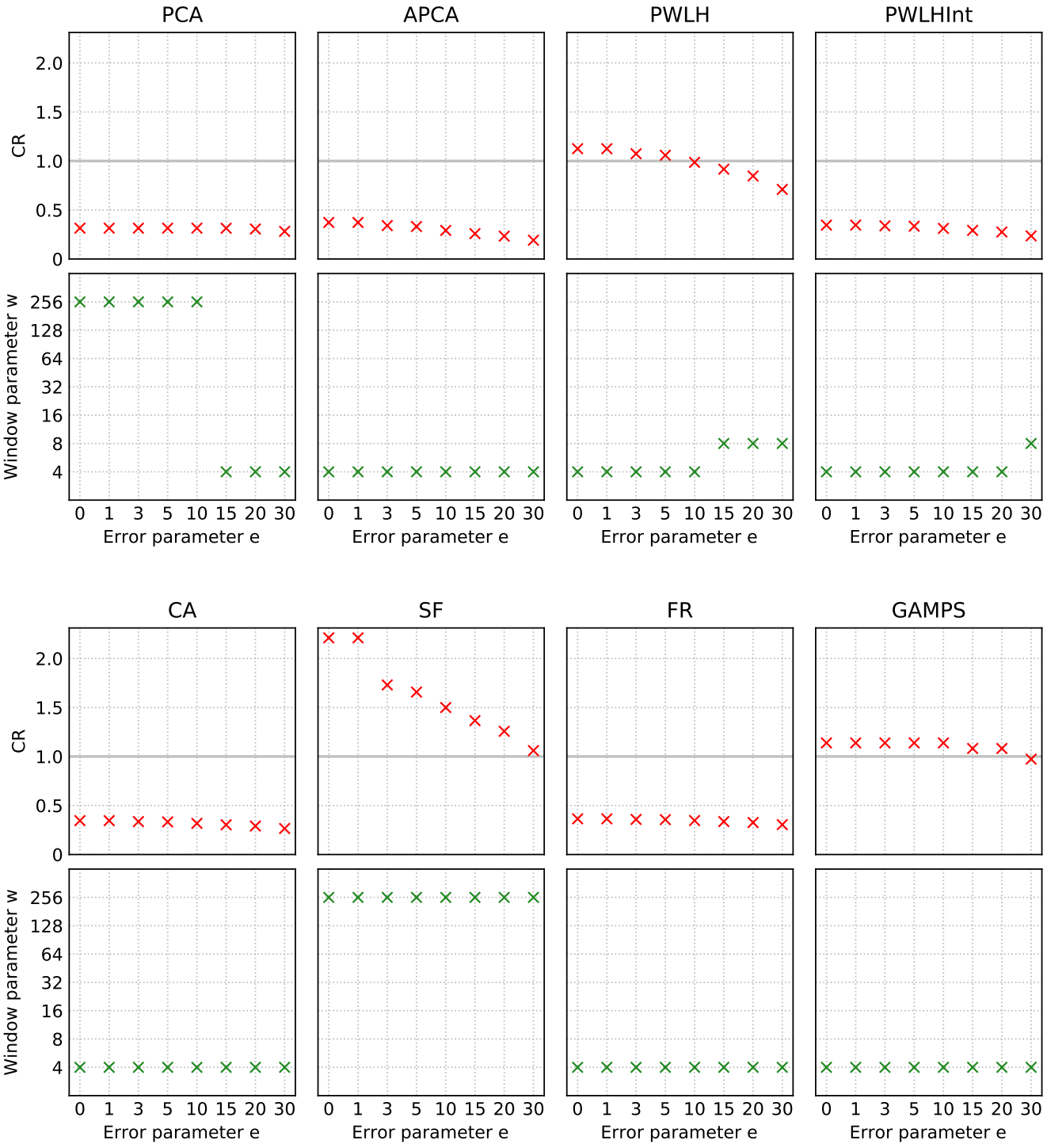

FIGURE C.10: CR and window size parameter plots for every evaluated algorithm, for the data type "Mer. Wind" of the dataset ElNino.

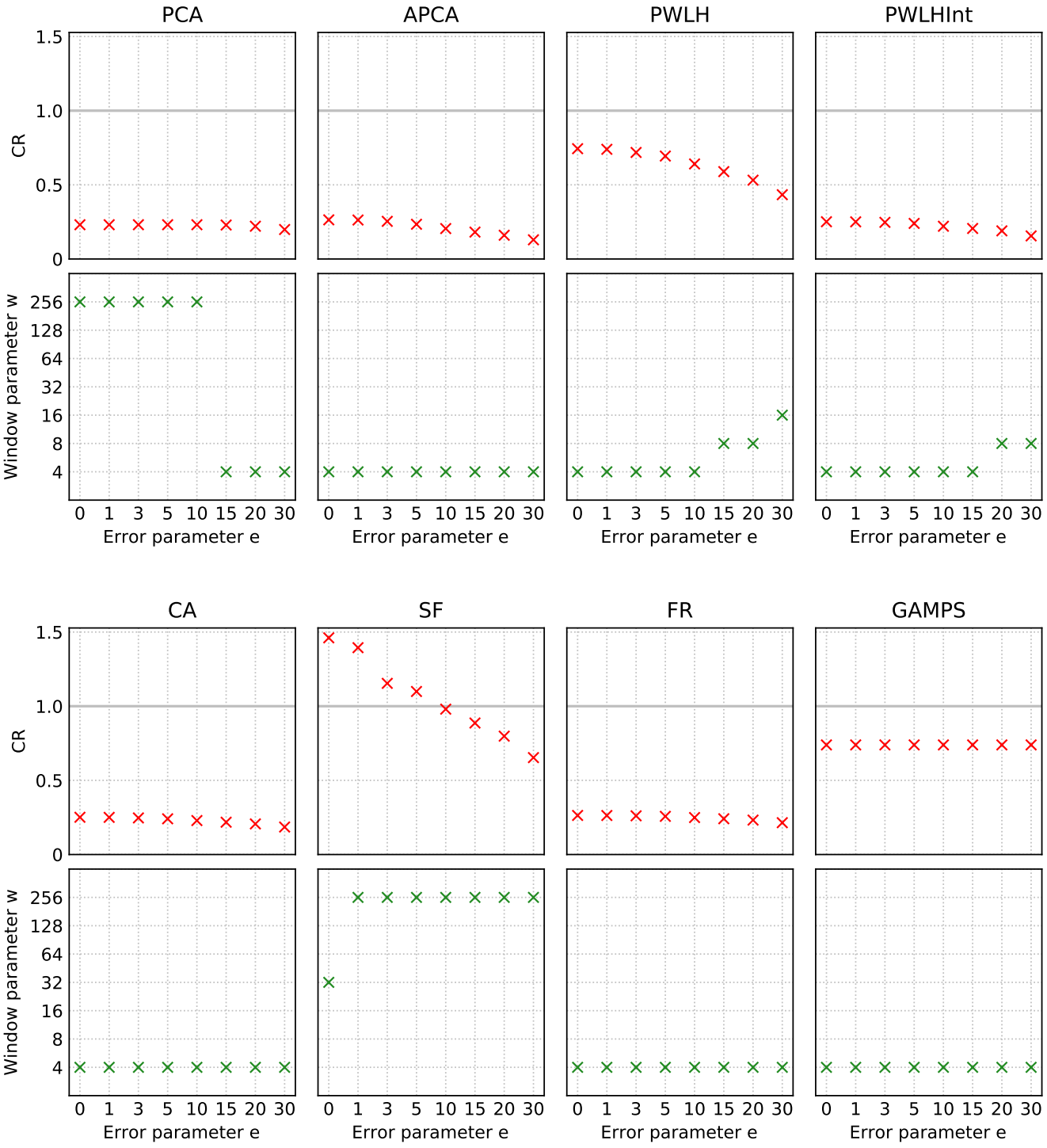

FIGURE C.11: CR and window size parameter plots for every evaluated algorithm, for the data type "Humidity" of the dataset ElNino.

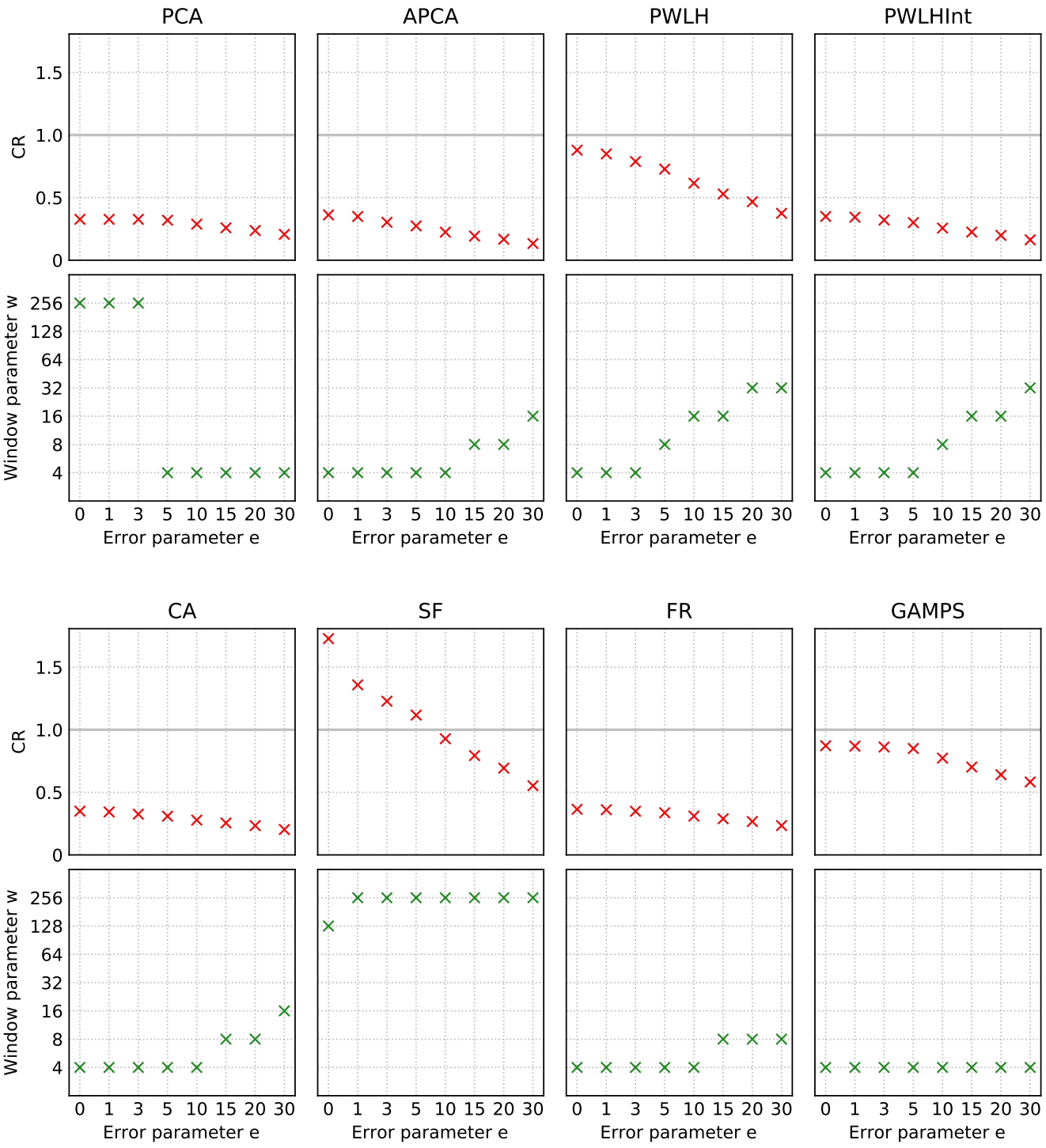

FIGURE C.12: CR and window size parameter plots for every evaluated algorithm, for the data type "Air Temp." of the dataset ElNino.

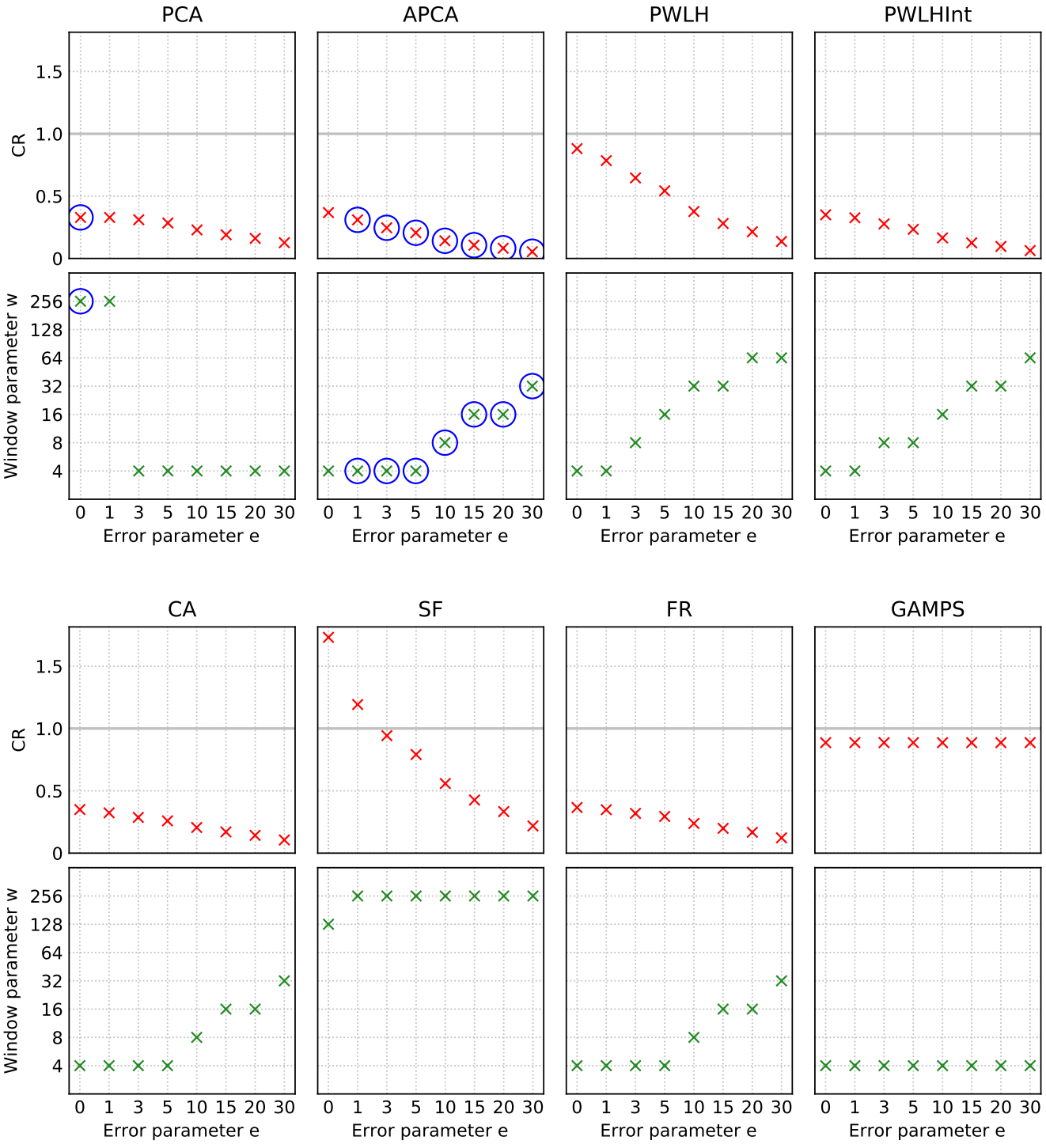

FIGURE C.13: CR and window size parameter plots for every evaluated algorithm, for the data type "Sea Temp." of the dataset ElNino. For each error parameter $e \in E$, we use blue circles to highlight the markers for the minimum CR value and the best window size (in the respective plots corresponding to the best coding variant).

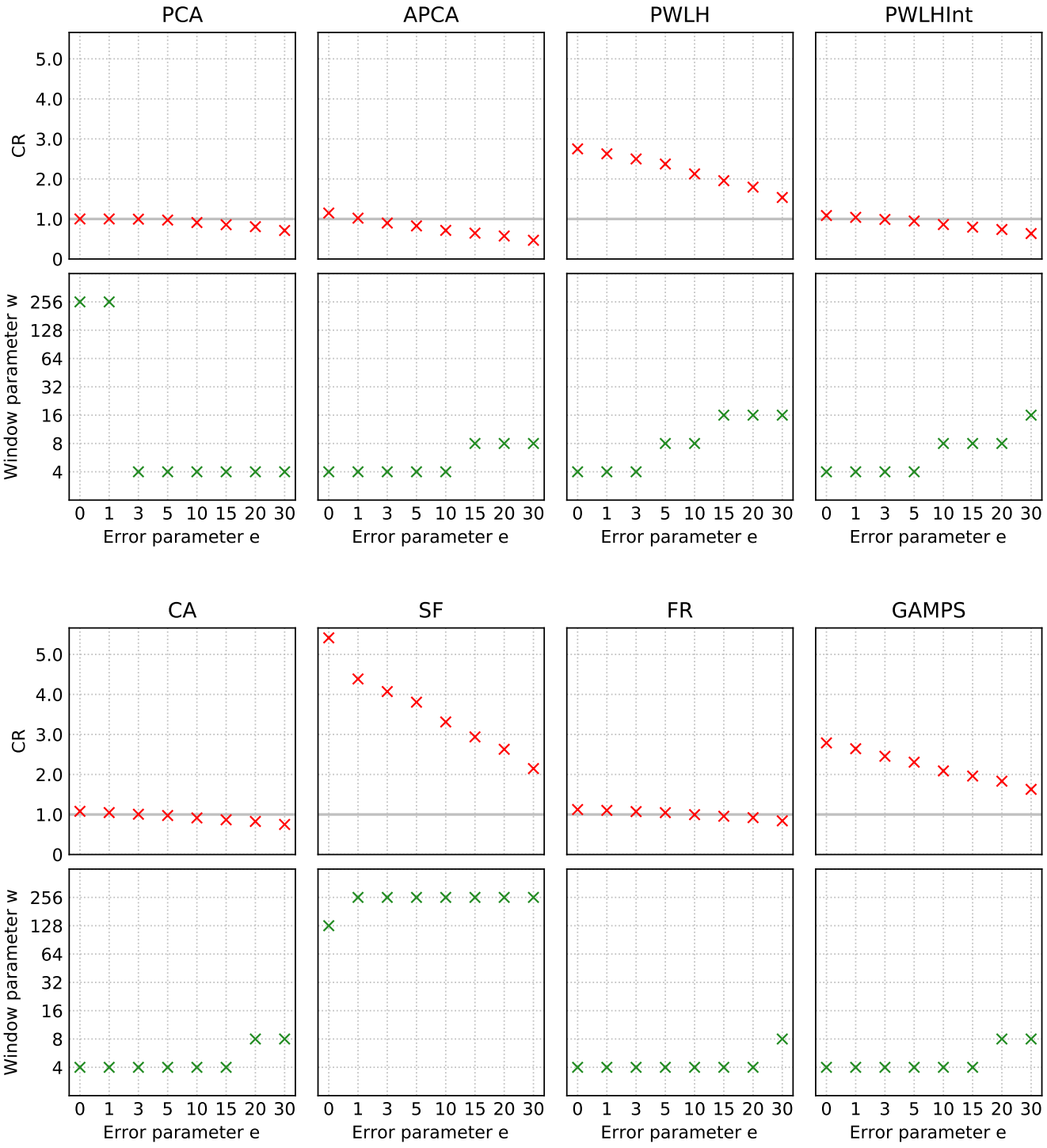

FIGURE C.14: CR and window size parameter plots for every evaluated algorithm, for the data type "Latitude" of the dataset Hail.

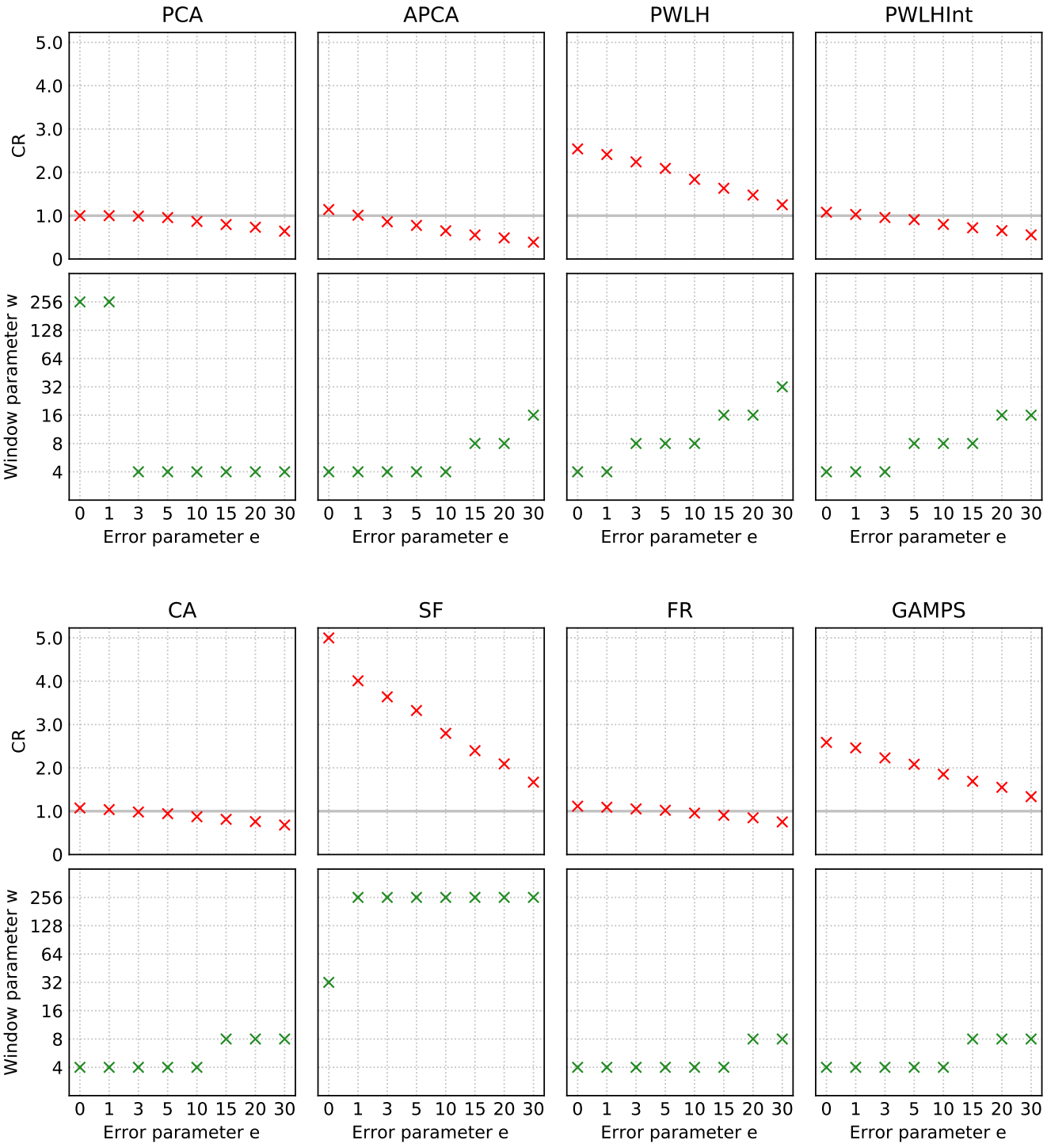

FIGURE C.15: CR and window size parameter plots for every evaluated algorithm, for the data type "Longitude" of the dataset Hail.

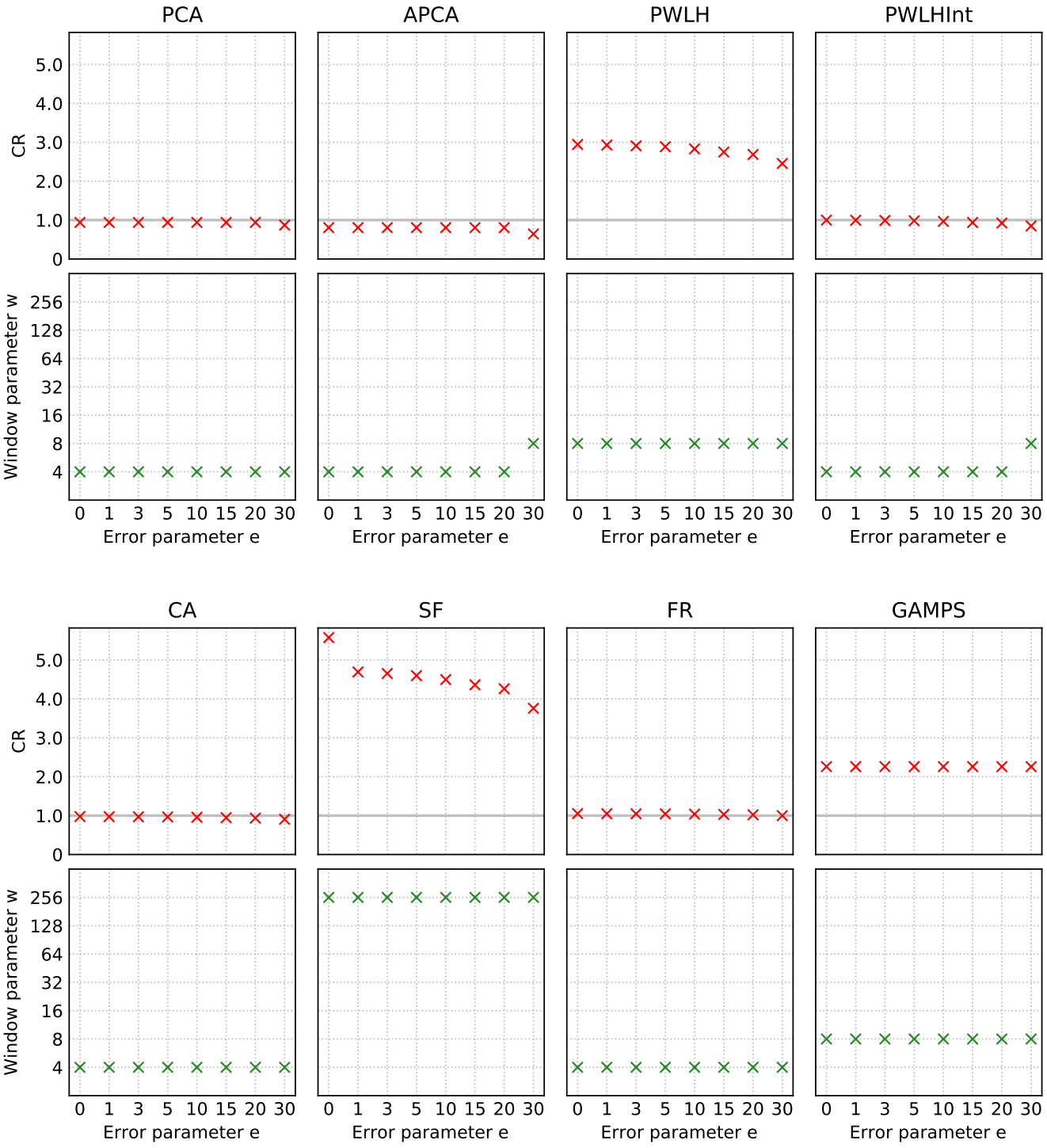

FIGURE C.16: CR and window size parameter plots for every evaluated algorithm, for the data type "Size" of the dataset Hail.

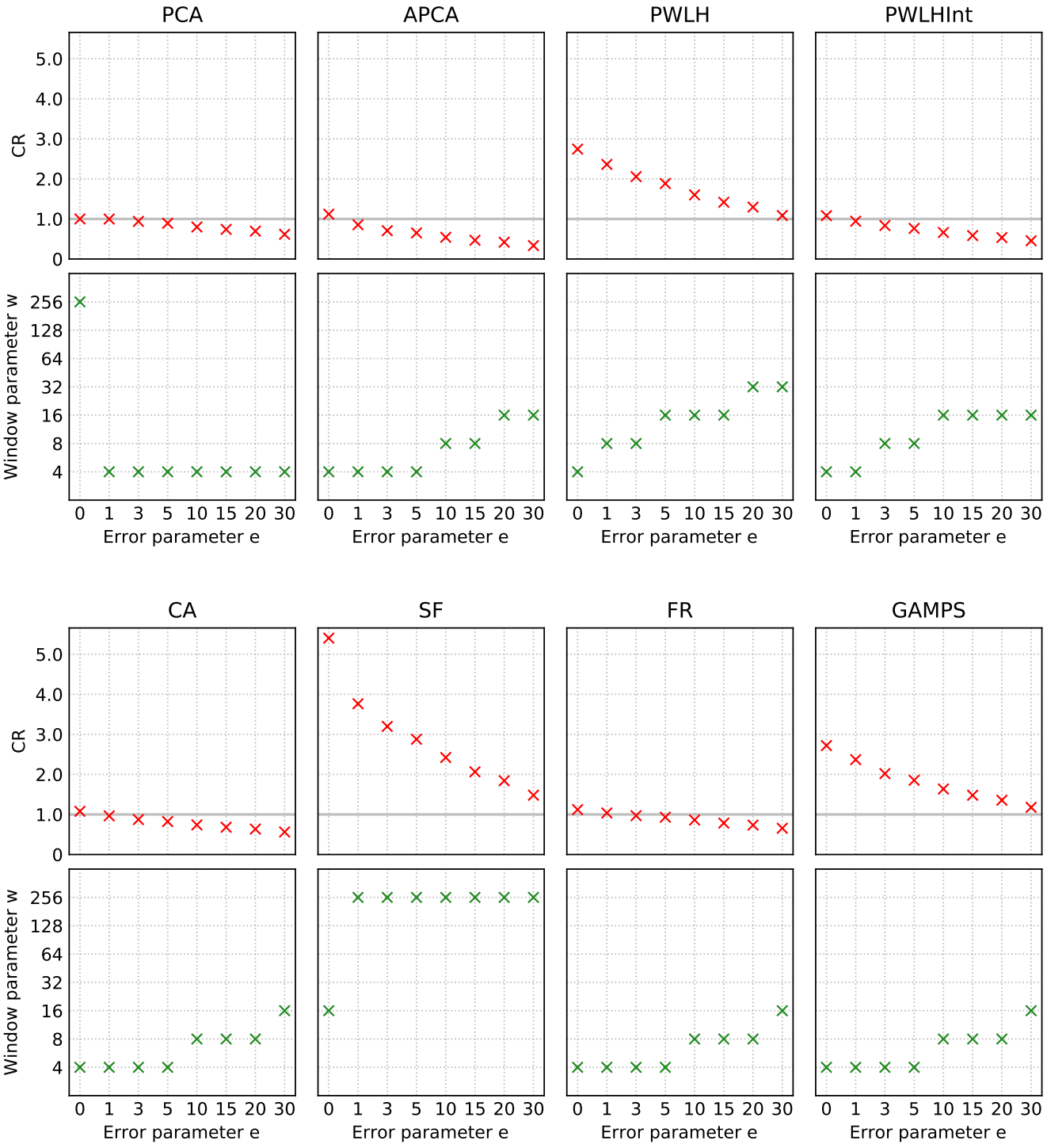

FIGURE C.17: CR and window size parameter plots for every evaluated algorithm, for the data type "Latitude" of the dataset Tornado.

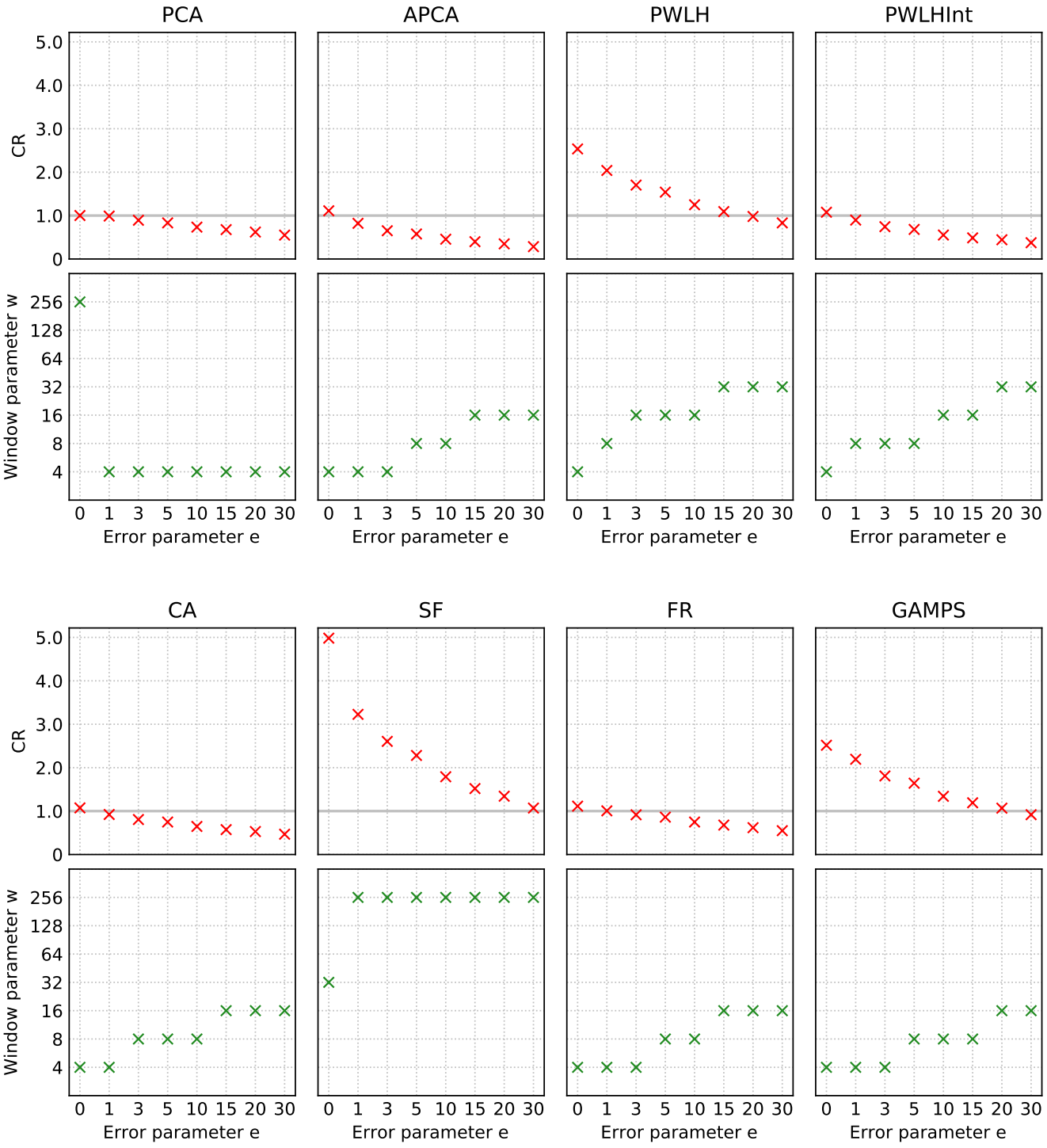

FIGURE C.18: CR and window size parameter plots for every evaluated algorithm, for the data type "Longitude" of the dataset Tornado.

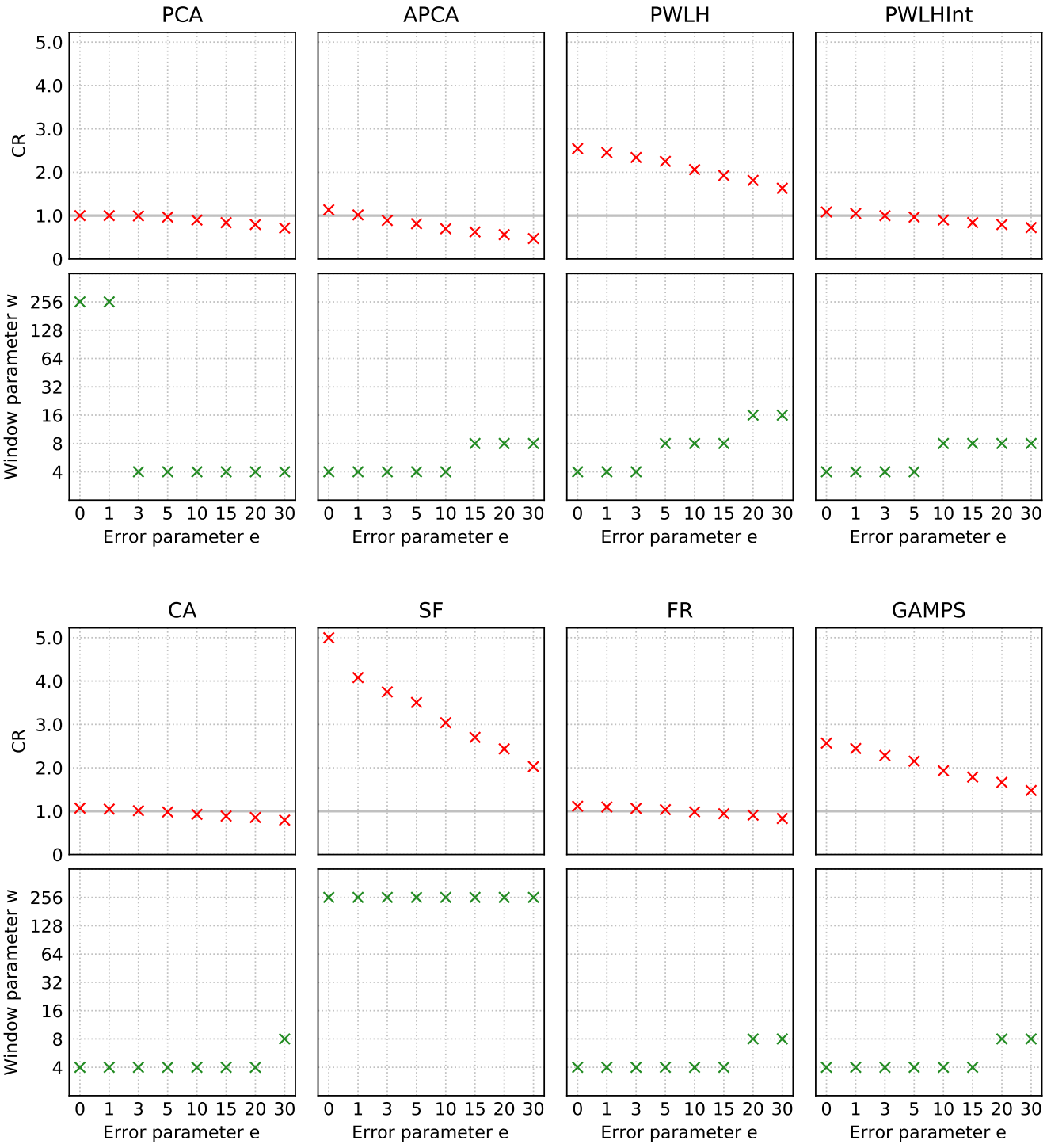

FIGURE C.19: CR and window size parameter plots for every evaluated algorithm, for the data type "Latitude" of the dataset Wind.

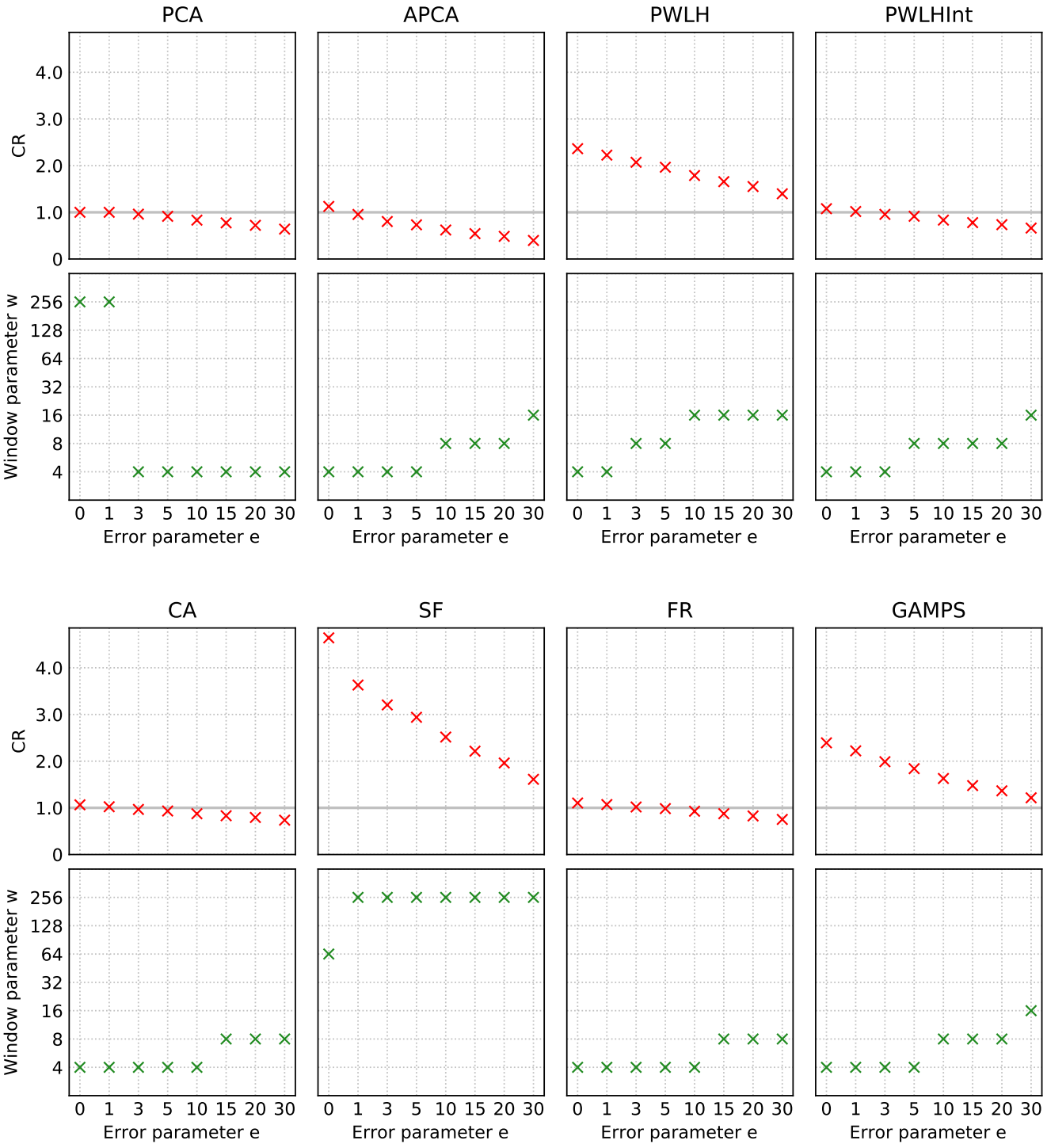

FIGURE C.20: CR and window size parameter plots for every evaluated algorithm, for the data type "Longitude" of the dataset Wind.

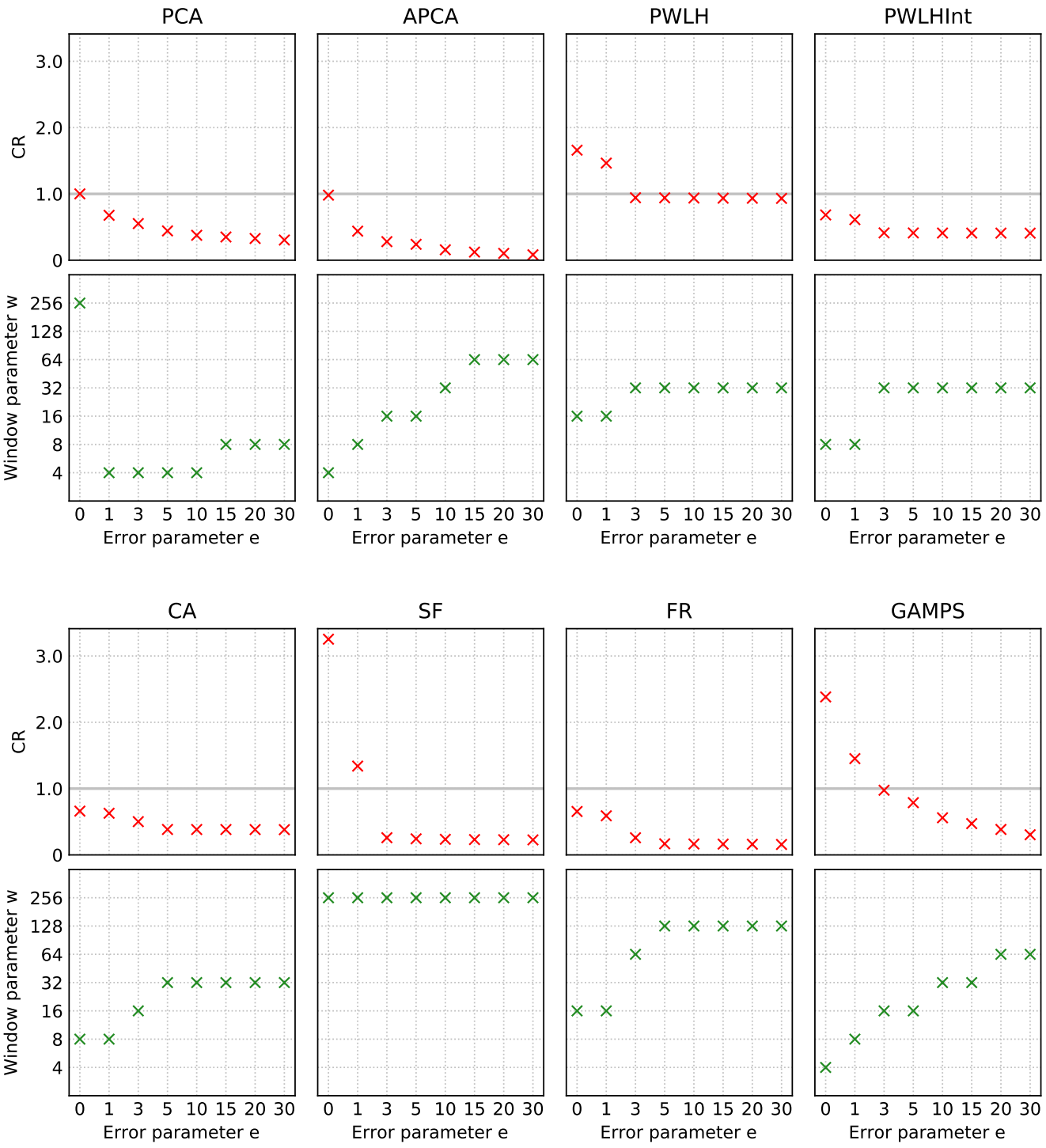

FIGURE C.21: CR and window size parameter plots for every evaluated algorithm, for the data type "Speed" of the dataset Wind.